Università degli Studi di Milano
Scuola di Dottorato in Medicina Molecolare

Curriculum in Genomica, Proteomica e Tecnologie Correlate

Ciclo XXV

Anno Accademico 2011/2012

Dottorando: Daniele PAROLINI

CALCIUM HANDLING IN MYOGENIC PROGENITORS AND SKELETAL MYOBLASTS: THE ROLE OF CD20

Direttore della Scuola: Chiar.mo Prof. Mario Clerici

Tutore: Prof. Giacomo P. COMI

Co-tutore: Dott. Yvan TORRENTE

SOMMARIO

Considerato il ruolo essenziale che lo ione calcio riveste nella fisiologia di tutte le cellule, diversi meccanismi intervengono nel preciso controllo della sua concentrazione intracellulare ($[Ca^{2+}]_i$). Nel muscolo scheletrico in particolare, l'efficiente regolazione del Ca^{2+} citosolico è cruciale per garantire la corretta funzionalità del tessuto. Anomalie a carico dell'omeostasi del Ca^{2+} contribuiscono infatti all'eziologia di patologie muscolari quali la distrofia muscolare di Duchenne (DMD). Sebbene un'alterazione della $[Ca^{2+}]_i$ sia stata più volte descritta in cellule muscolari distrofiche, i pathway coinvolti nel rilascio di Ca^{2+} ed il ruolo dei canali store-operati nei progenitori miogenici distrofici non sono noti. All'interno dell'eterogenea popolazione dei progenitori ematopoietici/endoteliali circolanti, abbiamo identificato una sottopopolazione di cellule $CD133^+$ dotata di proprietà miogeniche. Il riscontro dell'espressione di CD20 sulla membrana di tali cellule rappresenta un'evidenza inattesa, trattandosi di un antigene tipicamente associato ai linfociti B. La precisa funzionalità biologica di CD20 non è nota, sebbene diverse osservazioni suggeriscano un suo coinvolgimento nel regolare la concentrazione intracellulare di calcio ($[Ca^{2+}]_i$). I dati presentati nella prima parte della tesi descrivono la differente attivazione di un pathway legato a CD20 in cellule staminali $CD133^+$ normali e distrofiche, responsabile di un significativo incremento del calcio citosolico a carico delle cellule distrofiche. Nonostante CD20 possa influire sulla $[Ca^{2+}]_i$ attraverso un pathway specifico, diversi studi hanno dimostrato la sua localizzazione nei domini di membrana denominati lipid raft, dove CD20 sembra funzionare direttamente come canale Ca^{2+} store-operato. L'importanza dell'ingresso di Ca^{2+} store-operato (SOCE) nella fisiologia e nello sviluppo del muscolo scheletrico è stata riconosciuta solo di recente, e diversi interrogativi inerenti la modulazione del SOCE in questo tessuto rimangono aperti. Per tale motivo, unitamente alla comune origine mesodermica di sangue e muscolo, abbiamo ritenuto opportuno investigare il contributo di CD20 nella regolazione del calcio intracellulare in cellule muscolari. CD20 è risultato espresso nel muscolo scheletrico, mostrando una localizzazione di membrana in mioblasti e fibre muscolari. Inoltre l'inibizione di CD20 ha comportato la specifica compromissione del SOCE nella linea di mioblasti murini C2C12. Nel complesso le evidenze riportate hanno evidenziato l'alterazione di un pathway legato a CD20 in cellule staminali distrofiche, il cui ruolo nella patologia DMD può pertanto essere ipotizzato. I risultati prodotti dimostrano anche come la piena funzionalità di CD20 sia necessaria affinché l'ingresso di Ca^{2+} store-operato possa avvenire in mioblasti C2C12, contribuendo ad ampliare la comprensione dei meccanismi che regolano il SOCE nel muscolo scheletrico.

ABSTRACT

The calcium ion plays an essential role in the physiology of all living cells. Accordingly, multiple mechanisms contribute to the precise control of its intracellular concentration ($[Ca^{2+}]_i$). Particularly in skeletal muscle, the efficient regulation of cytosolic Ca^{2+} is crucial for tissue functionality and impairment of Ca^{2+} homeostasis has been shown to contribute to the etiology of muscular disorders such as Duchenne muscular dystrophy (DMD). Although the impairment of Ca^{2+} homeostasis affecting dystrophic muscular cells has been extensively reported, the pathways involved in calcium-release and the role of store-operated Ca^{2+} channels in dystrophic myogenic progenitors were not investigated before. Among the heterogeneous population of circulating hematopoietic and endothelial progenitors, we identified a subpopulation of $CD133^+$ cells displaying myogenic properties. Interestingly, expression of the B-cell marker CD20 was observed in blood-derived $CD133^+$ stem cells. Among the scarce available data about the biological role of the membrane protein CD20, there are some evidences of its involvement in the regulation of intracellular calcium concentration ($[Ca^{2+}]_i$). Here, we show that a CD20-related pathway leading to an increase of cytosolic calcium is differently activated in normal and dystrophic blood-derived $CD133^+$ stem cells, supporting the assumption of a CD20-related calcium impairment affecting dystrophic cells. Although CD20 can modulate cytosolic calcium through a specific signaling pathway, other studies demonstrated its association with lipid raft domains of the plasma membrane, where it probably functions directly as a store-operated Ca^{2+} channel. Recent works indicated that store-operated Ca^{2+} entry (SOCE) plays a central role in skeletal muscle physiology and development, but there remain a number of unresolved issues relating to SOCE modulation in this tissue. That being so, and considering that blood and muscle share common mesodermic origins, we were prompted to investigate whether CD20 contributes to calcium handling in committed muscular cells. Expression of CD20 was observed in skeletal muscle, displaying a membrane localization in myoblasts and adult muscle fibers. Additionally, we showed that inhibition of CD20 resulted in specific impairment of SOCE in C2C12 myoblasts. Together, reported findings contributed to identify deregulated pathways affecting dystrophic stem cells and potentially involved in DMD pathology. Moreover, our results suggested that functional CD20 is required for SOCE to consistently occur in C2C12 myoblasts, providing a novel insight to improve the understanding of store-operated Ca^{2+} entry regulation in skeletal muscle.

INDEX

INTRODUCTION

1. Origin, structure and physiology of skeletal muscle

Muscles can be categorized into three types based upon structure, function, and location in the body. The three types of muscle are skeletal, cardiac, and smooth muscle which have two common functions: (1) ensure movement and (2) produce force. In particular skeletal muscles also generate heat, thus participating to the thermoregulation of the body. Skeletal muscle is attached to the skeleton through tendons and thus it moves the body and its components. It appears striated under the microscope and is under voluntary control. Cardiac muscle is only located in the heart. It is also striated, but is not under voluntary control. Smooth muscle surrounds blood vessels and other passageways, regulates their size and propels material through body tubes. Smooth muscle is distributed throughout the body. It lacks striations and is involuntary. The respiratory and digestive tracts have layers of smooth muscle in their walls. Skeletal, cardiac and smooth muscle share common embryonic origins, being all derived from the middle germ layer: the mesoderm. Mesoderm lies between ectoderm and endoderm, the outermost and the innermost layer respectively. Together, they represent the first three tissue types to differentiate in an early stage of embryonic development, the gastrula, at approximately day sixteen, and from which all other more specialiazed tissues are later derived. Particularly, the epidermis and its derivatives, the nervous system and its sensory receptor cells derive from the ectoderm. The mesoderm develops into the connecitve tissues, bone, cartilage, dentin, cementum, all types of muscle, blood, endothelium of blood vessels, synovial membranes, serous membranes lining body cavities, the epithelium of the kidneys and urinary drainage system, the germinal epithelium of the gonads and the linings of the reproductive tracts. Endoderm develops into the epithelial linings of the gastrointestinal tract, the lungs, and associated structures (Table 1). A schematic representation of the events leading to the differentiation of the three primary embryonic germ layers is reported in Fig. 1.

Ectoderm	*Mesoderm*	*Endoderm*
All nervous tissue	Skeletal, smooth, and cardiac muscle	Epithelium of digestive tract (except that of oral and anal cavities)
Epidermis of skin and epidermal derivatives (hairs, hair follicles, sebaceous and sweat glands, nails)	Cartilage, bone, and other connective tissues	Glandular derivatives of digestive tract (liver, pancreas)
Cornea and lens of eye	Blood, bone marrow, and lymphoid tissues	Epithelium of respiratory tract, auditory tube, and tonsils
Epithelium of oral and nasal cavities, of paranasal sinuses, and of anal canal	Endothelium of blood vessels and lymphatics	Thyroid, parathyroid, and thymus glands
Tooth enamel	Serosae of ventral body cavity	Epithelium of reproductive ducts and glands
Epithelium of pineal and pituitary glands and adrenal medulla	Fibrous and vascular tunics of eyes	Epithelium of urethra and bladder
Melanocytes	Synovial membranes of joint cavities	
Some cranial bones and branchial cartilages (derived from neural crest)	Organs of urogenital system (ureters, kidneys, gonads, and reproductive ducts)	

Table 1: Derivatives of the primary germ layers
(Copyright 2004 Pearson Education, Inc.).

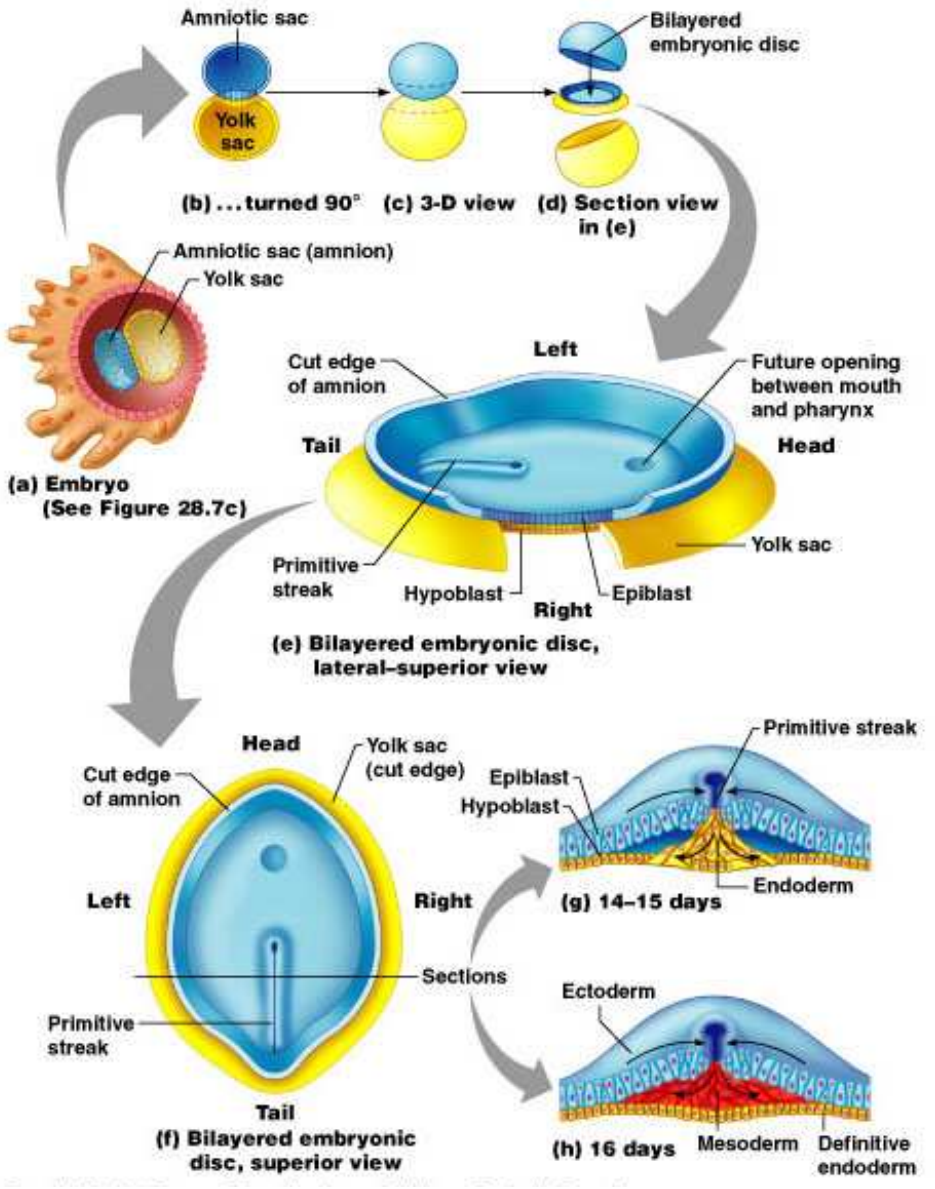

***Figure 1 (part 1)**: **Schematic representation of gastrulation in vetrebrates.** A gastrula develops from a blastula by the inward migration of cells by a complex and coordinated series of cellular movements which occur at the end of the cleavage stage of development. (Copyright 2004 Pearson Education, Inc.).*

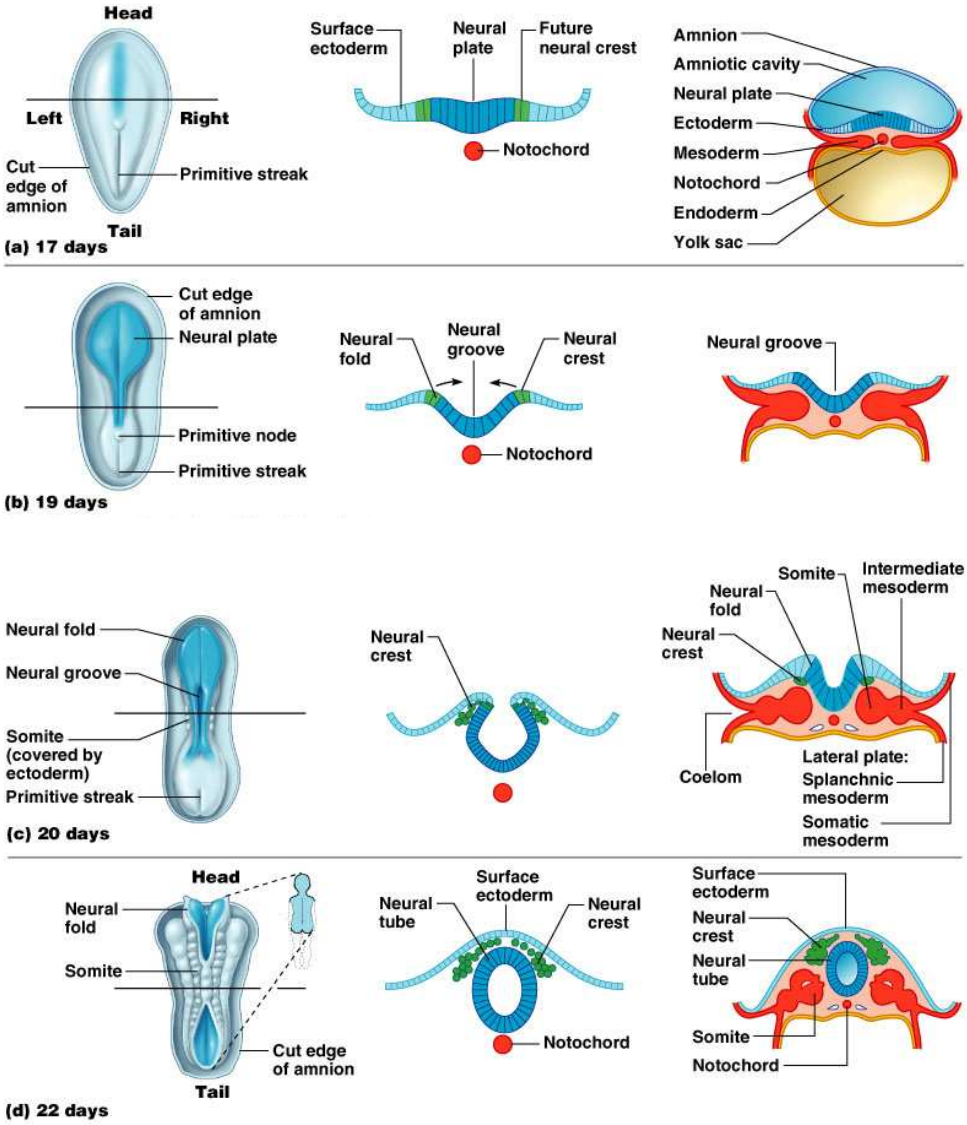

***Figure 1 (part 2)**: The cells begin to differentiate into the three primary embryonic germ layers, ectoderm and endoderm first, followed shortly thereafter by mesoderm (Copyright 2004 Pearson Education, Inc.).*

1.1 Specification of skeletal muscle from paraxial mesoderm

In vertebrate, skeletal muscle origins during embryonic development from somites, which are mesoderm paraxial masses, lateral to the neural tubes and the notochord [1]. Somites are divided into two components: the dermomyotome, which represents the dorsal part from which derm (comprising also endothelial and smooth muscle progenitors) and skeletal muscle origin, and the sclerotome, which is the ventral portion contributing to the formation of cartilage and bones of the spinal column and rib cage. The dermomyotome is subdivided in epiaxial, the inner part from which lumbar and vertebral muscles form, and ipoaxial, from which the remaining muscles origin (Fig. 2) [1].

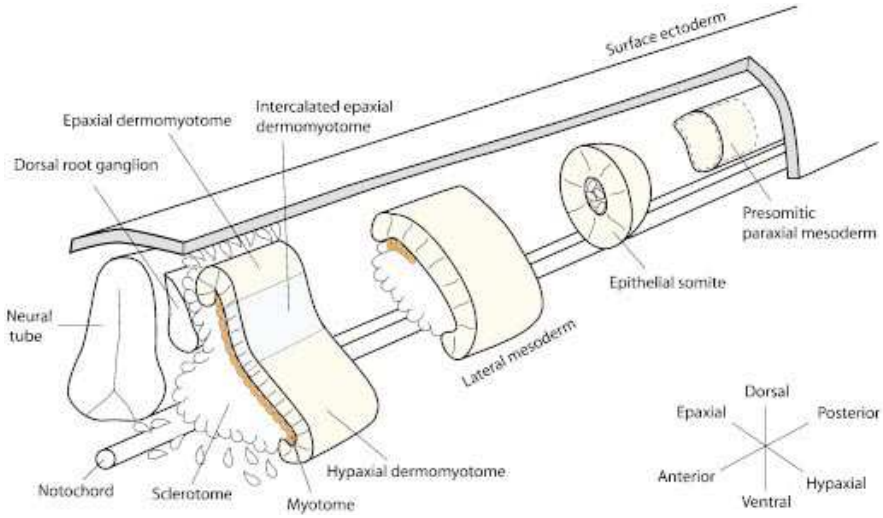

***Figure 2**: **Representation of somitogenesis.** Schematic representation of vertebrate somitogenesis as it occurs in the mouse embryo. Somites are formed and mature following a rostrocaudal gradient on either side of the axial structures.*

The progenitors of skeletal muscle are represented by the multi-potent stem cells which are localized in the hipoaxial dermomyotome and migrate after delamination from the dermamyotome towards developing limbs, tongue and diaphragm [2, 3]. The myogenic commitment is regulated by Wnts and sonic hedgehog (Shh) which are derived from axial structures [4] and activate either Paired Box (Pax) genes or directly MRFs (Myogenic Regulation Factors). Otherwise delamination to form migratory myoblasts is controlled by HGF (Hepatocyte Growth Factor) which is secreted by mesoderm cells and activating c-met, a tyrosin/kinasic receptor, expressed by lateral dermo-myotomal myoblasts, but not somites [5]. The expression of c-met is necessary for migration of muscle progenitors cells and is transcriptionally controlled by Pax3 a Pair Ruled gene that, together with the paralogue Pax7 (mainly expressed from the foetal stage onwards) regulate myogenic progenitors [6-8]. Transient activation of Notch, which is a factor produced by many cell types surrounding myoblasts, is necessary to promote proliferation and prevent premature differentiation of myoblasts. The differentiation of myogenic progenitors is a dynamic process controlled by the MRF genes, which

determine the formation of the myotome. Cells forming the myotome do not express Pax3 and Pax7 and directly activate MRFs (Myf5 and MyoD, and later MRF4 and Myogenin) differentiating into mononucleated, differentiated myocytes, that likely form a scaffold for the primitive epiaxial myofibers (Fig. 3A) [9-12]. MRFs belong to the family of bHLH (basic helix-loop-helix) proteins and include Myf5 (Myogenic factor 5), MyoD (Myoblast determination protein), MRF4 (Muscle specific regulatory factor 4) and Myog (myogenin) [13]. Myf5 and MyoD are the first factors to be induced during differentiation. Importantly, the absence of one of these factors does not preclude muscle-lineage differentiation. It was previously demonstrated that these factors are induced by Pax3 and Pax7, except than in the myotome, in all subsequent generations of myoblasts (embryonic, foetal and satellite cells [14-17]. Myog is a downstream target of MyoD and regulated the transition of myoblasts to myocytes and myotubes by direct transcriptional activation of structural muscle genes. MRF4 is essential in the final stages of differentiation [18, 19]. The analogies between the mechanisms regulating myogenesis and those that activates satellite cells, strongly suggest that regeneration of adult muscles somehow recapitulates embryonic development. Satellite cells (SCs) are an heterogeneous population of stem cells necessary for the growth, maintenance and regeneration of skeletal muscle [13, 20]. They are localized in niches between the basal lamina and the sarcolemma, and represent approximately 90% of post-natal muscle progenitors, which are already committed cells that express Pax7 and, after activation, Myf5. The remaining 10% is constituted by stem cells positive for Pax7 and negative for Myf5 [21]. During muscle regeneration, quiescent SCs activate and proliferate through a self-renewal process which includes either asymmetric division or stochastic differentiation. Symmetric expansion is particularly induced in the latest phases of muscle regeneration through the action of Wnt7a. Much as it happens to muscle progenitors during embryonic myogenesis, committed SCs positive for Pax7 and Myf5 initiate to express MyoD and become myoblasts. They proliferate and differentiate into myotubes by repressing Pax7 and activating MRF4. Newly formed myocytes form new myotubes or fuse with damaged fibers (Fig. 3B). However during this expansion phase, asymmetric divisions occur that generate a $Pax7^{+}/MyoD^{-}$ cells that return to quiescence and are required to maintain the “pool” of stem cells for subsequent regeneration cycles [22].

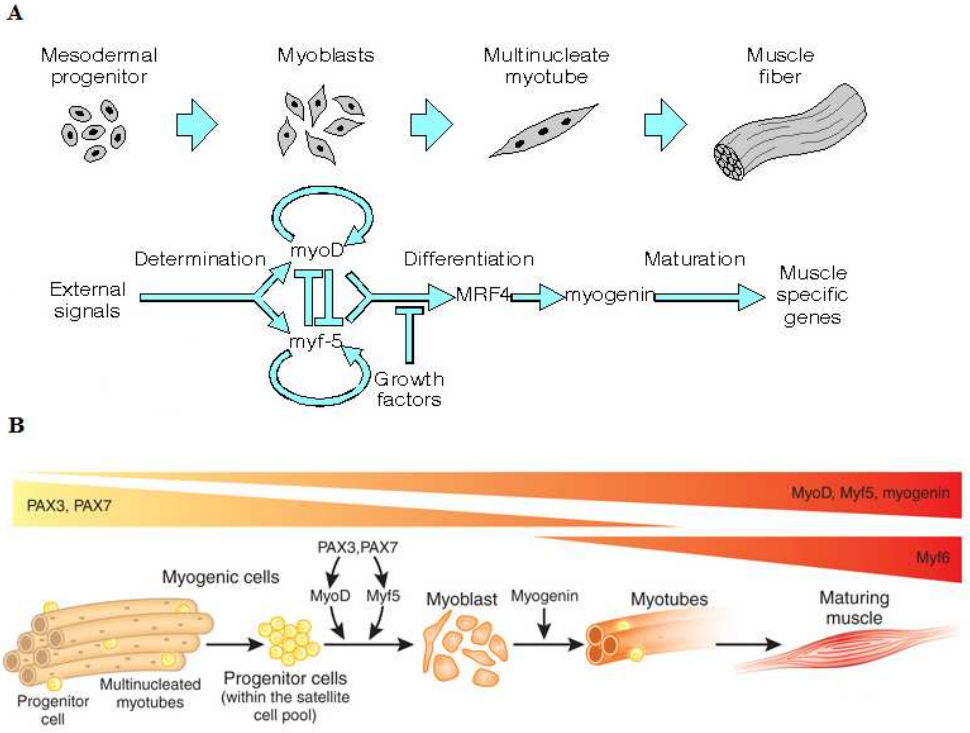

Figure 3: (A) Representation of myogenesis. (B) Representation of SCs differentation.

1.2 Skeletal muscle ultra-structure

Every skeletal muscle acts like an integrated unit of several muscle fibers (also called myofibers). The unit responsible for contraction is in fact made by a group of fibers and the motor neurons that innervate them. Inside a muscle, myofibers are oriented with the longitudinal axis parallel and are kept attached one to another by connective tissue called endomysium (the muscle fiber basal lamina) and perimysium, a ticker layer of connective that groups together several myofibers (Fig. 4). Between the bundles of fibers there are collagen, elastic fibers, nerves and blood vessels. Muscle is contained inside a connective sheath called epimysium. Every muscle fiber is a long cylindrical cell with up to hundreds of nuclei localized superficially. They are the biggest cell type since they originate from the fusion of several embryonic cells. The membrane of the muscle fiber is called sarcolemma and the cytoplasm is termed sarcoplasm. The muscle fibers are characterized by a small portion of cytosol since the principal intracellular structures are the myofibrilles, which are bundles of contractile and elastic proteins responsible of contraction. The myofibers also contain an extended sarcoplasmatic reticulum (SR), which is a modified form of the endoplasmatic reticulum (ER) that envelope myofibrilles. The role of SR is to concentrate and retain calcium ions. Strictly associated to SR is a branched network of the transversal tubules, known as T tubules. The membrane of T tubules is continuous with the surface of muscle fibers, so that the lumen of T tubules is in communication with the extracellular

liquid. They allow action potential, originating on the membrane at the level of the neuromuscular junction, to be rapidly transmitted inside the fiber. Without them, in fact, the action potential would reach the centre of the fibers just by the diffusion of positive charges into the sarcoplasm. Importantly, the sarcoplasm around the myofibrilles contains a lot of glycogen granules and mitochondria which provide energy during contraction. Glycogen is the molecule used by animals to store glucose and mitochondria provide ATP during muscle contraction.

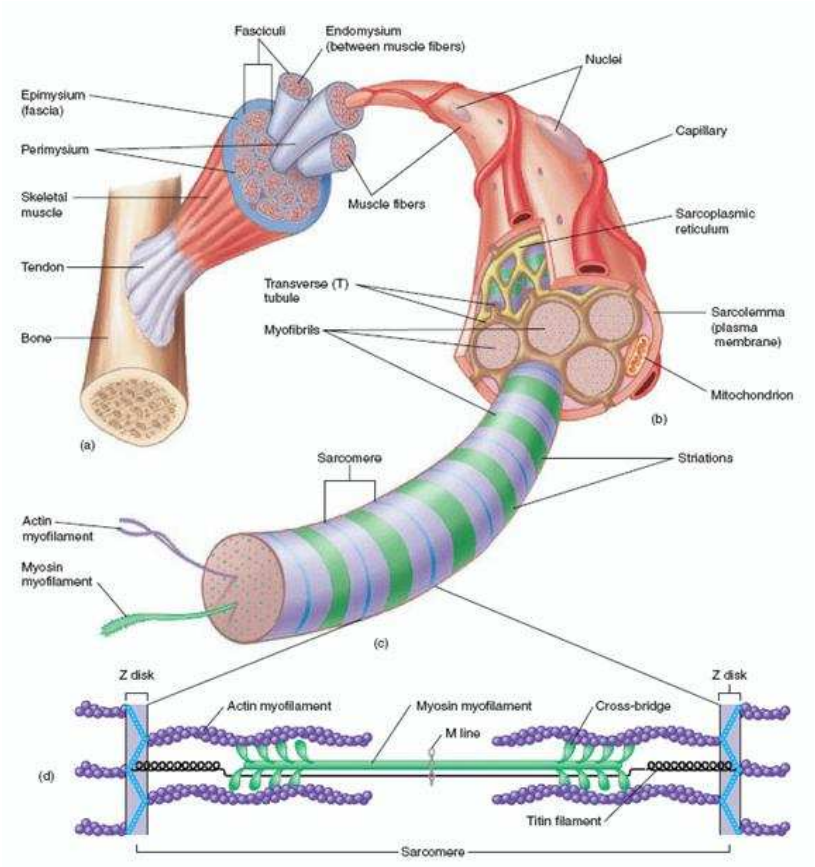

Figure 4: Skeletal muscle ultra-structure and sarcomere structure

1.3 Skeletal muscle contraction

Every muscle fiber results from the assembly of thousands myofibrils, which are composed by different type of proteins: the contractile proteins myosin and actin; the regulatory proteins tropomyosins and troponins and many proteins forming the scaffold of the sarcomere, including the accessory giant proteins titin and nebulin. The myosin (MyHCs) constitutes the thick filaments of myofibrils and different muscle types are characterized by the composition of different myosin isoforms. Every myosin is composed by two heavy chains that intertwine to form a long spiral tail with two globular heads, and four light chains (Fig. 5). The heavy and light chains of several myosins intercalate in order to form a tubular rigid structure with

the elastic heads on the extremity that protrude and function as an hinge during muscle contraction (Fig. 5). Actin is a globular protein (G-actin) that forms the thin filaments of the myofibril. Several molecules of actin polymerize to form long filaments (F-actin) and two polymers of F-actin wrap one on another to form the thin filaments (Fig. 5 and 6). The thick and thin filaments are parallel one to another and are interconnected by transversal bridges represented by the heads of the myosins. Every G-actin as a single binding site on one head of the myosin. The disposal of thin and thick filaments in the myofibril gives origin to the alternation of light and darks band from which derives the term “striated muscle”. Every single repetition of band constitutes the sarcomere which is composed by (Fig. 6):

- Z disks: these are zigzag protein structures to which thin filaments attach. A sarcomere is made up of two Z disks e the thin filaments attached to them.
- I bands: these are the light bands and are composed by thin filaments.
- A bands: these are the dark bands and covers the entire length of one thick filament. At the extremity of this band, the thin and thick filaments overlap while the centre is occupied only by the thick filaments.
- H zone: this is the central region of A band.
- M line: this band represents the site of attachment of thick filaments. It is the equivalent of Z disk for the thin filaments.

The titin is a giant elastic protein which extends from a Z disk to the next M line. It has two functions: (1) it stabilizes the position of contractile filaments; (2) its elasticity aloud the muscle to maintain is length constant after contraction. Titin collaborates with the giant non-elastic protein nebulina that guarantees the alignment of actin filaments in the sarcomere.

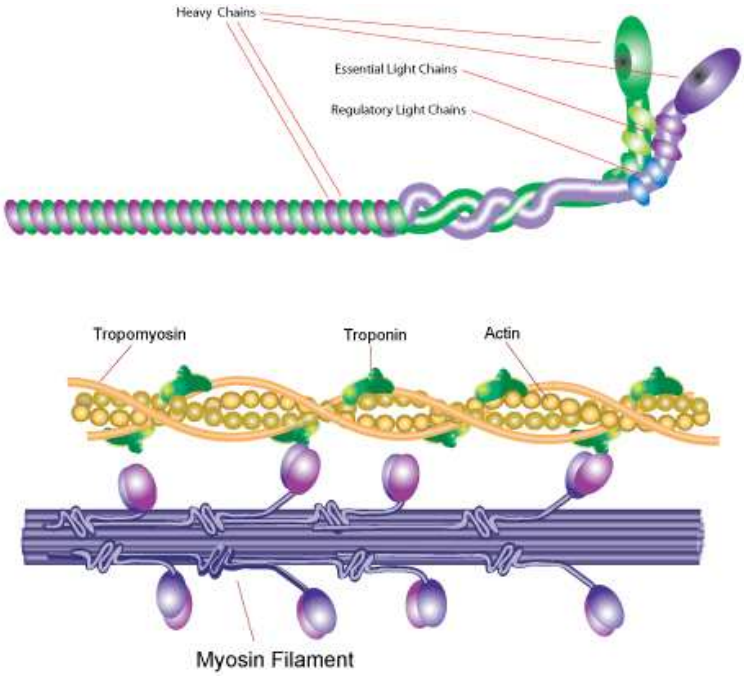

Figure 5: The contracting and regulating proteins of skeletal muscle

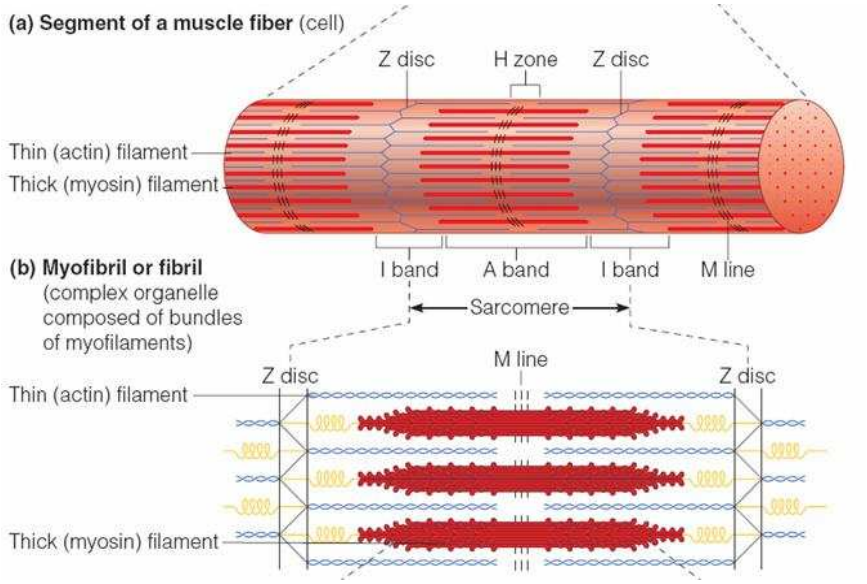

Figure 6: The structure of sarcomere

The contraction of muscle fibers generates force necessary to produce movement or to resist a load. The strength developed by muscular contraction is defined tension. In the past centuries, scientists believed that during contraction, the muscle shortens since it is made of molecules that shorten when active and elongate at rest. However, in 1954 Andrew Huxley and Rolf Niedeigerke discovered that the length of A bands does not change during muscle contraction and proposed a different model to explain muscle contraction: the theory of the scroll of the filaments. In this model the length of the filaments does not vary but they simply overlap slipping one on another. This model includes either that the muscle shorten during contraction in order to make a movement either that the muscle does not shorten when it generates a tension without making a movement. According to this theory, when the myofibril is at rest, thin and thick filaments overlap for a small region in the extremities. When the muscle contracts, the actin and myosin filaments slip one onto another so that the sarcomere shortens: the extremities of 2 Z disks get closer, the I band and H zone disappear while the length of the A band remains constant. The strength that drives the actin filaments is the movement of the transversal bridges of myosin that link actin and myosin. Myosin is a motor protein that converts the binding of ATP into mechanical energy: every molecule of myosin hydrolyses ATP into ADP and inorganic phosphate; the energy released modifies the angle between the head of myosin and the axis of its filament. In this model, the actin filament functions as a guide for the heads of myosin and has a single binding site for one myosin-head and single binding site for a molecule of ATP. During every rotation of the myosin-head, myosin releases actin, retracts and binds to a new molecule of actin, in order to start a new cycle of contraction.

In conclusion the contraction-cycle can be summarized as follows (Fig. 7):

(1) It starts with the myosin-head bound to a molecule of G-actin. In this phase there is no ATP associated to the myosin.
(2) A molecule of ATP binds to the myosin-head and the myosin detaches from actin.
(3) ATP is hydrolyzed in ADP and inorganic phosphate that remain associated to myosin.
(4) Head-myosin rotates and bind to a new molecule of G-actin.
(5) The rotation of the head-myosin starts when the inorganic phosphate dissociates.

When the myosin-head moves, it drives the F-actin to the centre of the sarcomere. Myosin releases ADP and returns to be strictly linked to actin. The cycle is ready to start again.

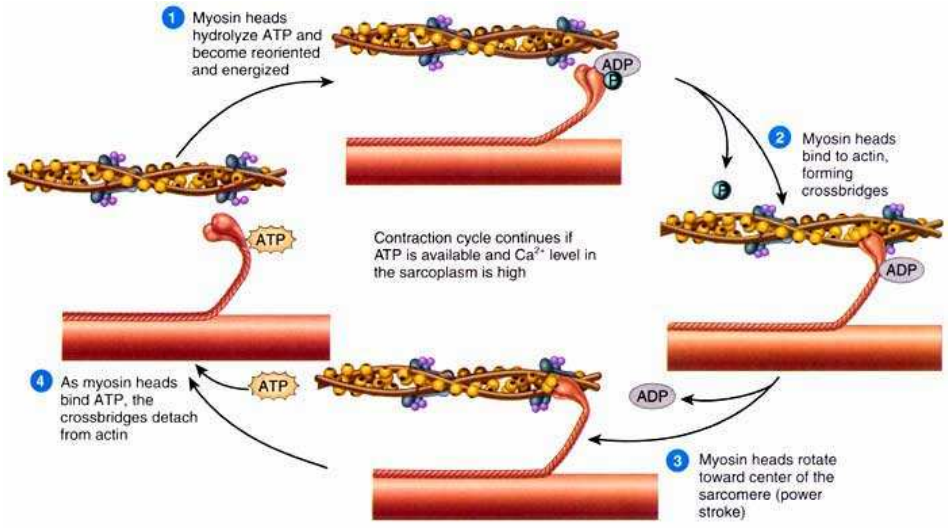

Figure 7: The contraction-cycle

The thin filaments of actin are associated to two regulatory proteins that avoid the myosin-head to complete their cycle. The tropomyosin is an elongated polymer that wrap over the F-actin, blocking part of the site for the myosin on each molecule of actin (Fig. 7). In order to perform the contraction, tropomyosin needs to completely release the binding site for myosin allowing the rotation of the myosin-heads. The capacity of the tropomyosin to release this binding site depends on the regulatory protein troponin, a complex of three proteins associated to tropomyosin (troponin I, C and T). When a contraction starts, troponin C reversible binds to Ca^{2+}. This binding makes tropomyosin to retract, freeing the binding sites of myosin. In order to have muscle relaxation, the concentration of calcium needs to slow down. During the relaxation time when actin and myosin are not bound one to another, the filaments of the sarcomere slip back to the original position with the help of elastic connective tissue in the muscle. The stimulus for contraction comes from the central nervous system to the skeletal muscle via the motoneurons. The

acetylcholine coming from the motoneurons induce an action potential in the muscle fiber, inducing contraction. The combination of these electric and mechanic events is called excitation-contraction coupling. The acetylcholine from the synapsis at the neuromuscular junction binds to the receptor of the motor plaque. The colynergic receptors are cationic channels that allow the movement of Na^+ and K^+ across the sarcolemma. When the channels are open, the entrance of Na^+ exceeds the exit of K^+ because the electrochemical gradient is higher for Na^+. In this way the membrane of the muscle fiber depolarizes, originating the potential plaque (PP). The PP gives origin to an action potential in the muscle that is conducted on the surface of the cell and in the tubuli T through the opening of the voltage-dependent Na^+-channels. The potential of action that moves along the membrane and the tubuli T is responsible for the release of Ca^{2+} from the SR. The membrane of the tubuli T contains voltage-sensible receptors (VSR) mechanically linked to Ca^{2+} channel in the membrane adjacent to the SR. When a depolarisation wave reaches the VSRs, their conformation change: this variation open the Ca^{2+}-channels in the SR and the Ca^{2+} diffuse in the cytosol. As a consequence the cytoplasmatic concentration of calcium augments to 100 folds and in these conditions Ca^{2+} can bind to troponin and the tropomyosin frees the binding site of the F-actin for myosin. The muscle relaxation begins when the SR absorbs Ca^{2+} via a Ca^{2+}-ATPase. There is a little period of latency between the muscular-action potential and the development of the muscular tension. This interval represents the time necessary for the excitation-contraction coupling. A single potential of action provokes a single shock in a muscle. The shocks differ among different muscle fibers because of the velocity required for the generation of the tension, maximum tension reached and duration of the shock. The contraction of muscle fibers requires a large amount of energy in the form of adenosine triphosphate (ATP). ATP is made available through various mechanisms. A limited amount of ATP is stored in the muscle cell (granules of glycogen). ATP is also produced by a phosphate transfer from creatine phosphate to ADP and muscle does store larger amounts of creatine phosphate. The stored ATP and the ATP created from creatine phosphate are available for immediate use and provide approximately enough ATP for about six seconds of exercise. Additional ATP can be produced through anaerobic and aerobic metabolism. Aerobic respiration provides a larger production of ATP but depends on sufficient oxygen delivery. Myoglobin, a protein in muscle cells that binds oxygen, contributes to some of the oxygen for aerobic respiration. Aerobic ATP production also requires mitochondria. Muscles packed with mitochondria give meat a darker colour ("dark meat") than muscles with fewer mitochondria ("white meat"). Anaerobic fermentation provides less energy but can produce ATP in the absence of oxygen. A serious drawback of anaerobic fermentation is the production of lactic acid, a product that can alter cell pH. Both processes can use glucose released from glycogen, which is stored in muscles as a reserve fuel.

1.4 Classification of skeletal muscle fibers

Skeletal muscle fibers can be classified in three groups depending on resistance to fatigue upon several stimulations and on the contraction-velocity: rapidly-contracting glycolytic-fibers; rapidly-contracting oxidative-fibers; slowly-contracting oxidative-fibers. A decrease in the ability of muscle to contract is muscle fatigue. The fatigue is highly variable and is influenced by the intensity and duration of the

contractile activity, from the metabolism used, from the composition of the muscle and the degree of training. Otherwise the contraction velocity of a muscle is determined by the myosin isoform that constitutes the thick filaments. The various isoforms of myosin, in fact, differ in the ATPase activity and rapidly-contracting fibers are characterized by a higher velocity of ATP-hydrolysis. Also the duration of muscle contraction depends on the type of fibers constituting the muscle. More in detail, the time of shock persistence depends on the velocity of Ca^{2+}-removal from the cytosol by the SR: when the Ca^{2+}-concentration slows down, calcium dissociates from troponin so that tropomyosin partially blocks the binding sites for myosins. When the movement of the head-myosin is inhibited, muscle fibers relax. The efficiency of a muscle fiber to extract oxygen contributes in determining its metabolism. Slow fibers are also termed “red fibers” due to a big quantity of myoglobin, a red pigment that binds oxygen. They are also characterized by a smaller diameter, enabling a shorter route for the oxygen to reach mitochondria. Slow fibers major depends on oxidative phosphorylation. For these reasons, they are characterized by more mitochondria and more blood vessels. Fast fibers are also called “white fibers” because they are characterized by a minor content of myoglobin and vessels, and have a greater diameter. All these characteristics are responsible for the anaerobic metabolism of these fibers. They are subgrouped into other categories based upon their diameter and resistance to fatigue. In conclusion, there are two principal ways to classify muscle fibers: the type of myosin (fast or slow) present, and the degree of oxidative phosphorylation that the fiber undergoes. Skeletal muscle can thus be broken down into two broad categories: Type I and Type II. Type I fibers appear red due to the presence of the oxygen binding protein myoglobin. These fibers are suited for endurance and are slow to fatigue because they use oxidative metabolism to generate ATP. Type II fibers are white due to the absence of myoglobin and a reliance on glycolytic enzymes. These fibers are efficient for short bursts of speed and power and use both oxidative metabolism and anaerobic metabolism depending on the particular sub-type. These fibers are quicker to fatigue. A summary of fibre types and their features is reported in Table 2.

	Type I fibers	Type II a fibers	Type II x fibers	Type II b fibers
Contraction time	Slow	Moderately Fast	Fast	Very fast
Size of motor neuron	Small	Medium	Large	Very large
Resistance to fatigue	High	Fairly high	Intermediate	Low
Activity Used for	Aerobic	Long-term anaerobic	Short-term anaerobic	Short-term anaerobic
Maximum duration of use	Hours	<30 minutes	<5 minutes	<1 minute
Power produced	Low	Medium	High	Very high
Mitochondrial density	Very High	High	Medium	Low
Capillary density	High	Intermediate	Low	Low
Oxidative capacity	High	High	Intermediate	Low
Glycolytic capacity	Low	High	High	High
Major storage fuel	Triglycerides	Creatine phosphate, glycogen	ATP, Creatine phosphate, glycogen (little)	ATP, Creatine phosphate
Note	Consume lactic acid	Produce lactic acid and Creatine phosphate	Consume Creatine phosphate	Consume Creatine phosphate
Myosin heavy chain, human genes	MYH7	MYH2	MYH1	MYH4

Table 2: Muscle fibers type

1.5 Muscle regeneration

Adult skeletal muscle is a stable tissue with limited nuclear turnover [23], but it has the ability to rapidly regenerate in response to damage. The regeneration of skeletal muscle depends on the balance between pro- and anti-inflammatory factors that determine whether the damage will be repaired with muscle fiber replacement and functional contractility or with scar tissue formation [24, 25]. Skeletal muscle regeneration includes three distinct stages: degeneration, muscle repair and maturation, and follows a fairly consistent pattern irrespective of the underlying cause of injury (direct trauma, tissue ischemia, old age or genetic defects) [23]. If the muscle repair mechanisms are inadequate, the consequence might be reduced muscle function and muscle wasting [24]. The well-orchestrated course of satellite cell activation and differentiation is largely similar to the gene

expression during embryonic development of muscle while in myopathic patients the main difference is the presence of immune cells during muscle regeneration. The initial event in the degeneration of muscle, necrosis of muscle fibers, is triggered by disruption of the sarcolemma followed by increased serum levels of proteins such as creatine kinase and myoglobin [26, 27]. In the early phase of muscle damage, the injured muscle activates an inflammatory response driven by T helper (Th)1 cytokines, such as interferon (IFN) and tumour necrosis factor (TNF). Neutrophils are rapid responders within the first hours, followed by CD68-expressing M1 phenotype macrophages during the first 24 h. These two cell types contribute to further muscle membrane lysis by production of free radicals but also clear the cellular debris by phagocytic removal [23]. Whether this elimination of debris is of importance for further regeneration is not fully understood. After the pro-inflammatory phase, quiescent Pax7- expressing muscle SCs are exposed to signals such as insulin-like growth factor 1 (IGF-1), fibroblast growth factor 2, and hepatocyte growth factor promoting activation, proliferation and migration to the site of injury [28]. During this stage, the cells become MyoD- and Myf5-expressing myoblasts. Throughout the shift from the proliferative stage to the differentiation phase, the M1 macrophages are replaced by $CD163^+$ M2 macrophages, activated by Th2 cytokines such as interleukin-4 (IL-4), interleukin-10 (IL-10) and interleukin-13 (IL-13) [29]. The M2 macrophages display a more anti-inflammatory phenotype and are found during the healing phase of acute inflammation, in wound-healing tissue and in chronic inflammation [23, 30]. Following the proliferation stage, expression of Myog and MRF4 is up-regulated, myoblasts exit the cell cycle and become terminally differentiated. These muscle progenitor cells fuse together or with the existing fibers to replace the damaged muscle cells [23].

1.6 Myogenic stem cells

Although SCs represent the proper muscular resident stem cells (see section 1.1 for details), other cell types able to differentiate into skeletal muscle can be recruited to support muscle regeneration under physiological or pathological conditions.

1.6.1 Muscle-derived cells

Qu-Petersen and colleagues isolated three populations of *muscle-derived cells (MDSC)* according to their adhesion characteristics and proliferation behaviours [31]. Two of them - the early preplate cells (EP) and the late preplate cells (LP) - are populations of satellite cells based on their patterns of myogenic marker expression and their behavior *in vitro*. The majority of the EP cells expressed the myogenic markers desmin, m-cadherin and myogenin [32], suggesting that EP cells represent a late myogenic precursor. Similarly to satellite cells [33, 34], the EP cells exhibited a very fast but limited ability to proliferate and a strong capacity to differentiate into myotubes. Unfortunately, they showed a limited capacity to regenerate skeletal muscle after transplantation. The LP population represented 1% of satellite cells: they demonstrated a very limited capacity to proliferate and differentiate and so that their function in skeletal muscle remains unclear. The last population, called MDSC, derived from primary LP cultures and represented highly proliferating cells: they maintained the same phenotype for a long period of time *in vitro*, indicating they were capable of self-renewal *in vitro*. Moreover, the detection of donor-derived cells in myofibers, peripheral nerves, and blood vessels within the

MDSC-injected muscle demonstrated the multipotent nature of MDSC *in vivo,* when appropriately stimulated with growth factors [31]. According to several features such as their differentiation potential, their ability to express myogenic markers, and their similarity in phenotype to a subpopulation of cells that were identified within the basal lamina of myofibers [35], it was suggested that MDSC derived from skeletal myofibers [31].

1.6.2 Myo-endothelial cells

Few years ago, Nishikawa et al. demonstrated that endothelial cells could give rise to hematopoietic stem cells, suggesting as endothelial cells may have additional differentiation potential [36-38]. At the same time, other groups showed that MDSCs could express endothelial cell markers and differentiate into endothelial cells after muscular injection and promote angiogenesis [31, 39, 40]. According to these observations, Zheng and colleagues provided evidence for the existence of myogenic cells related to the endothelial cell lineage in human skeletal muscle [41]. They were able to isolate between muscle fibers a subpopulation of cells that co-expressed Pax7 and endothelial cell markers; they purified by flow cytometry rare muscle cells co-expressing the myogenic cell antigen CD56 and the endothelial cell markers CD34 and CD144; and, starting from $CD56^+$ myogenic cells, they identified several cells that expressed both myogenic and endothelial cell markers. The main conclusion of this study was that human muscle–derived endothelial cells ($CD56^-CD34^+CD144^+$) and *myo-endothelial cells* ($CD56^+CD34^+CD144^+$) regenerated skeletal muscle more efficiently compared with myogenic cells ($CD56^+CD34^-CD144^-$). Furthermore they demonstrated that myo-endothelial cells possessed good myogenic potential, due to fast proliferation rate and high resistance to oxidative stress.

1.6.3 Mesoangioblasts

Mesoangioblasts are multipotent progenitors of mesodermal tissues, physically associated with the embryonic dorsal aorta in avian and mammalian species. Cossu and Bianco [42] demonstrated the capacity of mesoangioblasts to differentiate in various mesodermal phenotypes so that these progenitors were considered as a novel class of stem cells. These cells expressed Flk-1, stem cell antigen 1, CD34 - known to be early endothelial markers [42] - and many of the leukocyte molecules implicated in transmigration [43]. Moreover, they differentiated into mature smooth muscle that expressed smooth muscle myosin upon treatment with TGF-β [44].

1.6.4 Perycites

Among the various cells that constituted the bone marrow - $CD34^+$ and $CD34^-$ haematopoietic and mesenchymal stem, progenitors cells - putative muscle-specific progenitors [45], distinct from satellite cells [46], were identified. These cells were identified as *pericytes*: they wrapped around the vascular tube and interdigitated with the endothelial cells in the basement membrane of the vessels. Pericytes played a fundamental role in the maintenance of microcirculation functionality and they can be also mobilized from adult bone marrow under ischemic conditions and utilized for their contractile capabilities and their multiple cytoplasmic processes [47]. They seemed to be progenitor cells for mesenchymal cells such as osteoblasts and adipocytes; however Dellavalle and colleagues demonstrated that pericytes had good capacity of myogenic differentiation [46]. Moreover, it was proposed that the pericytes could be released from its position on

a vascular tube in the case of a focal injury and functioned as immunomodulatory and trophic mesenchymal stem cell [48]. According to these evidences, the activity of pericytes ensured that the field of damage remained limited and that tissue-intrinsic progenitors replaced the expired cells.

1.6.5 CD133^{+} cells

In 2003, Stamm and colleagues demonstrated that autologous bone marrow-derived CD133+ cells could induce angiogenesis and restore myocardial tissue viability after infarction [49]. In 2004, Torrente et al. published the stem cell characteristics of human *circulating CD133^{+} cells* and their ability to restore skeletal muscle and eventually regenerate the satellite cell pool after intra-muscular and intra-arterial delivery [50]. Few years after, the same group isolated *CD133^{+} cells from muscle* also co-expressing CD34, CD45, Thy-1 and KDR. The ability of these cells to express myogenic markers and/or to undergo myogenic differentiation was consistently evaluated *in vitro* [51]. RT-PCR analysis revealed the expression of Pax-7, Myf-5, MyoD, m-cadherin, MRF-4, and myogenin after 24 days of culture into proliferative medium. In addition, CD133^{+} cells differentiated into multinucleated myotubes expressing MyHCs.

1.6.6 PW1^{+}/Pax7^{-} interstitial cells

Although the contribution to myogenesis of non-satellite cell progenitors has been extensively reported [52, 53], as a consequence of the methods used to isolate these myogenic progenitors, critical information is missing regarding the precise anatomical localization of these cells, as well as their physiological contribution to muscle growth and repair [54-56]. Trying to overcome these limitations, Mitchell et al. described a new population of muscle-resident stem cells located in the interstitium and expressing the cell stress mediator PW1 [57]. These so-called *PW1^{+}/Pax7^{-} interstitial cells* (PICs) were more abundant at birth and declined until about 2–3 weeks after birth, maintaining a 1:1 ratio with satellite cells. It was demonstrated that PICs were a significant myogenic progenitor population as they participated in myogenesis *in vivo* at levels comparable to those obtained with freshly isolated satellite cells. PICs required *Pax7* for myogenic specification and expressed Pax3 during myogenic commitment. Notably, PICs re-populated their niche at high levels (as a stem cell) however only PICs gave rise to more PICs in addition to satellite cells and myofibers [57]. Furthermore, it had to be determined whether PICs are a source of satellite cells during normal postnatal development.

1.6.7 Mesenchymal stem cells

Mesenchymal stem cells (MSCs) reside within the stromal compartment of bone marrow. They play a fundamental role in providing the support system for haematopoietic stem cells in the marrow and constitute a very small fraction, 0.001–0.01% of the total population of nucleated cells in marrow [58]. Importantly they have the capacity to differentiate into several tissues, included skeletal muscle. Moreover, MSC-like cells were recently isolated from human healthy muscle tissue biopsies [41] an/or surgical waste tissues [59]. As these cells could be obtained with non- or minimally invasive-biopsy procedures, skeletal muscle could be an important clinical source of MSCs for use in therapeutic applications. However even if MSCs do not con tribute massively to muscle regeneration, they could have a therapeutic effect by either producing extracellular matrix molecules [60], or reducing inflammation [61]. MSCs played multifactorial roles in controlling inflammation as selectively home towards damaged tissue via expression of

receptors for SDF-1, lysophosphatidic acid [62], and CCL2 [63]. Di Bari and collaborators described the myogenic potential of adult human synovial membrane-derived mesenchymal stem cells (hSM-MSCs) [64]. They also demonstrated their myogenic differentiation in a nude mouse model of skeletal muscle regeneration: when implanted into regenerating nude mouse muscle, hSM-MSCs contributed to myofibers and to long term persisting functional satellite cells [64]. MSCs were also isolated from adipose tissue: these cells, called adipose-derived stem cells (ASCs), transplanted in a rat ischemic model, improved the vascular compartments [65, 66], ameliorating myocardial regeneration [67, 68].

2. Calcium ion in skeletal muscle

The calcium ion is an ubiquitous intracellular signal responsible for controlling numerous cellular processes including growth and differentiation, metabolism, and regulation of gene expression. Free Ca^{2+} concentration in the cytoplasm is modulated by two different mechanisms, the entry of external calcium (influx of calcium) and the release of calcium from internal stores. Since prolonged high intracellular calcium levels are highly toxic and lead to cell death, once calcium has carried out its signaling functions, the initial concentration is rapidly restored in the cytoplasm, principally by the calcium pump [69-71].

2.1 Calcium signaling in muscle development

Changes in cytosolic Ca^{2+} in muscle can be converted into biochemical changes through activation of signal transduction cascades that are require Ca^{2+}/calmodulin for activation. Examples of these cascades include signaling through calmodulin kinases (CamK) or the Ca^{2+}/calmodulin-activated serine-threonine phosphatase, calcineurin, where changes in Ca^{2+} concentration can influence the phosphorylation state of key target proteins [72, 73]. It is through these signaling cascades that Ca^{2+} can influence skeletal muscle development and differentiation. During muscle development and muscle regeneration, myoblasts proliferate and then undergo a highly ordered process of myogenic commitment in which they leave the cell cycle and express muscle specific proteins [74]. Myoblasts then migrate and align with each other, and ultimately undergo fusion with one another to form primary myotubes. Myoblasts then fuse with the primary myotubes generated in this manner to form secondary myotubes. A multitude of elements are critical for the process of myoblast fusion including membrane-associated proteins, signaling complexes, and extracellular/secreted molecules [75]. Calcium plays a critical role in multiple steps involved in myotube formation. Calcium activates intracellular cysteine proteases, calpains, which are required for cytoskeletal re-organization during migration and cell fusion [76]. Increased intracellular calcium also activates calcineurin, a serine-threonine phosphatase, involved in the downstream activation of MEF-2 and the NFAT family of transcription factors which have been shown to regulate myotube development [77-80]. Ca^{2+}-calmodulin can also influence muscle specific gene expression through the activation of the CamKII pathway [81]. Here, CamKII can influence MEF2 signaling by altering the actions of class II histone deacetylases (HDAC) [82]. In addition CamKII can stimulate the expression of peroxisome proliferator-activated receptor gamma coactivator 1 (PGC-1), a master regulator of mitochondrial biogenesis [73]. Finally, calmodulin can also influence the actions of a transcriptional coactivator called

calmodulin binding transcriptional activator (CAMTA). CAMTAs are known to activate cardiac transcription through a mechanism that involves class II HDACs [83]. Interestingly, dCAMTAs have been implicated in phototransduction of the drosophila eye [84]. Here, mutants of CAMTA signaling reveal a defect in the deactivation of rhodopsin. Given the critical importance of TRP channels in phototransduction, it is likely that Ca^{2+}/calmodulin from TRP channels are required to activate CAMTA dependent transcription. Interestingly, several recent studies have demonstrated the importance of TRPC channels to striated muscle development, degeneration and performance [85-87]. It will be important to determine if CAMTAs have a role in the TRPC response of Ca^{2+} dependent gene expression in skeletal muscle. Furthermore, a deeper knowledge of the specific pathways by which Ca^{2+} signaling influences gene expression in muscle will be important in our understanding of how these events occur during muscle development and are altered during the adaptation response to exercise or in the pathogenesis of myopathies. Transient receptor potential (TRP) channels have previously been shown to function in axonal pathfinding during neuronal development [88]. TRP channel activation by local growth factor concentrations allows for extension or retraction of axonal processes [89]. Recent studies have also implicated transient receptor potential channels in myotube development. Rosenberg and colleagues previously showed that overexpression of TRPC3 in C2C12 myotubes resulted in increased NFAT transactivation: a process involving activation of calcineurin by Ca^{2+} influx, dephosphorylation of NFAT by calcineurin, translocation of NFAT to the nucleus, and DNA binding by NFAT resulting in altered gene expression [85]. Similarly the scaffolding protein Homer, which has been shown to bind to multiple members of the TRP channel family, is expressed as part of the myogenic differentiation program and promotes myotube differentiation through modulation of calcium-dependent gene expression [90]. Homer enhanced calcium signaling via the calcineurin/NFAT pathway resulting in greater activation of a muscle-specific transcriptional program [91]. Evidence also suggests that TRPC1 may be a route for calcium influx required for calpain activation during myoblast migration and fusion. Migration of C2C12 myoblasts was inhibited by GsMTx-4 peptide, an inhibitor of mechanosensitive channels, and Z-Leu-Leu, an inhibitor of calpains. Knockdown of TRPC1 in C2C12 myoblasts resulted in decreased calpain activity, reduced cell migration, and a reduction in myotube fusion [92]. Growth factor stimulation resulted in increased calcium influx, calpain activity, and accelerated migration which was blocked by TRPC1 knockdown [92]. TRPC1 has also been shown to play a role in mechanotransduction during myotube development. TRPC1 knockdown inhibited stretch-activated calcium influx in C2C12 myoblasts in response to atomic force microscopic pulling and blocked stretch-activated current assessed by the whole-cell patch clamp technique [93]. TRPC1 activity was negatively regulated by cholesterol depletion, suggesting that TRPC1 was functionally assembled in lipid rafts, but enhanced by sphingosine-1-phosphate suggesting a role for stress fibers and cytoskeleton in TRPC1 recruitment [93].

2.2 Calcium and skeletal muscle function: excitation-contraction coupling

Skeletal muscle fibers are unique cells. They are large, elongated and specialized for the rapid delivery of large amounts of Ca^{2+} to the contractile apparatus for periods of work. Their membrane architecture has evolved to create a signaling microdomain between the invaginations of the surface membrane, the transverse (t–) tubules and the sarcoplasmic reticulum (SR). The t–tubules and their junction with the terminal cisternae of the SR are specifically aligned along the A–I bands in the sarcomere of mammalian skeletal muscle. This region is referred to as the junctional membranes, and there is only a 10–15-nm gap between them, which is spanned by the dihydropyridine receptor (DHPR)/voltage sensor on the t–tubule and the ryanodine receptor (RyR)/Ca^{2+} release channel on the SR membranes [94, 95]. Note that the SR is a specialization of the ER in muscle cells. Via the process known as excitation–contraction coupling (EC coupling), these proteins convert the electrical signal propagating (action potential) from the surface membrane down through the t–tubules to a mechanical signal that activates the opening of the SR Ca^{2+} release channels. Ca^{2+} is released rapidly from the SR to the cytoplasm, and the increase in $[Ca^{2+}]_{cyto}$ causes Ca^{2+} to bind to troponin C (TnC) on the contractile proteins to initiate contraction. The muscle fiber relaxes as Ca^{2+} is pumped back into the SR via Ca^{2+} pumps located on the SR, returning $[Ca^{2+}]_{cyto}$ to resting levels [95] (Fig. 8). This re-sequestration is performed by the actions of the sarco/endoplasmic Ca^{2+}-ATPase pump (SERCA1) and mitochondrial calcium buffering and is critical for relaxation of skeletal muscle fibers [96]. SERCA1 can refill calcium stores faster than the other SERCA isoforms: SERCA2a and SERCA3 [97]. Other plasma membrane calcium pumps such as the plasma membrane Ca^{2+}-ATPase (PMCA) and Na^{+}/Ca^{2+} exchanger (NCX) are known to exist in the sarcolemma and work to rapidly lower cytosolic Ca^{2+} levels in order to relax the myofiber [98-100]. ATP is hydrolyzed by the Ca^{2+} pumps and contractile proteins during these processes, increasing the concentrations of ADP, Mg^{2+} and inorganic phosphate, which has implications for the regulation of Ca^{2+} during EC coupling [101]. In the EC coupling cycle, $[Ca^{2+}]_{SR}$ is buffered by a dynamic Ca^{2+} buffer, calsequestrin (CSQ) [102, 103]. Indeed as $[Ca^{2+}]_{SR}$ drops the aggregation state of CSQ is reduced from polymers to dimers and monomers. This reduces the Ca^{2+}–buffering ability of CSQ as the affinity of Ca^{2+} for CSQ changes with the changing aggregation state of CSQ [104-107].

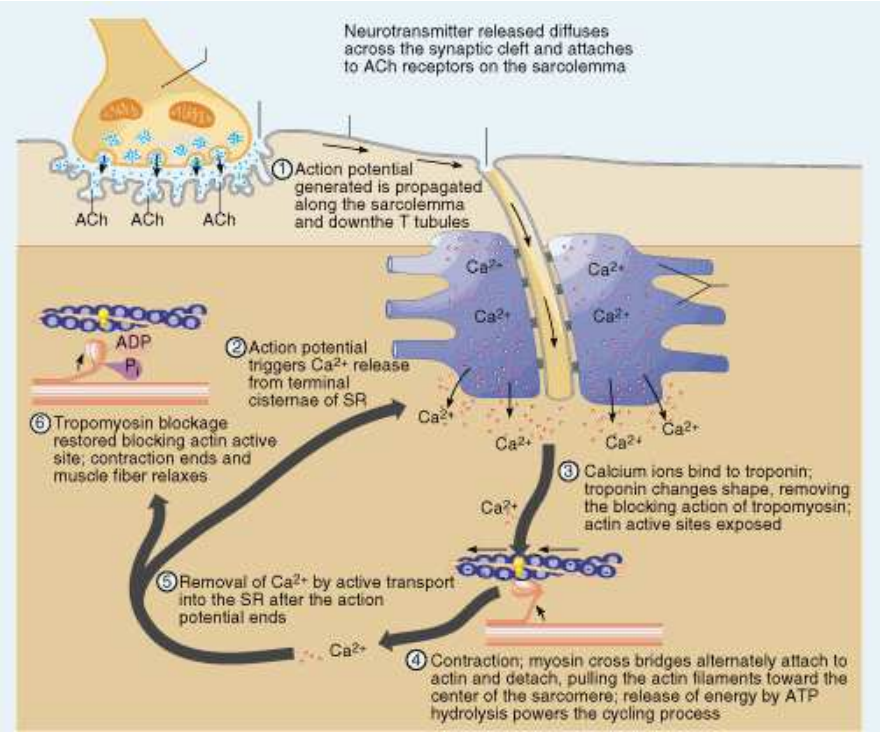

Figure 8: Schematic summary of excitation-contraction phases
(Copyright 2001 Benjamin Cummings, an imprint of Addison Wesley Longman, Inc.)

2.3 Store-operated calcium entry in skeletal muscle

The concept of store-operated calcium entry (SOCE) was first introduced in 1986 when series of experiments suggested that depletion of internal Ca^{2+} stores controlled the extent of Ca^{2+} influx in nonexcitable cells [108]. This mechanism of Ca^{2+} entry served as a link between extracellular Ca^{2+} and intracellular Ca^{2+} stores. When the stores were full, no Ca^{2+} influx was detected, but when the stores were emptied, Ca^{2+} entry developed. This model, initially called capacitative calcium entry (CCE), was later supported by electrophysiological studies which established that depletion of Ca^{2+} stores activated a Ca^{2+} current in mast cells called the Ca^{2+} release-activated Ca^{2+} current, or ICRAC [109]. While the electrophysiologic properties of SOCE currents have been well documented, the molecular components of the underlying channels and the mechanism by which a cell senses store depletion and activates SOCE had remained elusive for many years. In 2005, independent groups used RNA interference (RNAi)-based screens to identify STIM1 as a key component of SOCE [110, 111]. STIM1 is a single-pass, transmembrane phosphoprotein that was initially cloned from stromal cells involved in pre-B cell differentiation and implicated as a tumor suppressor for rhabdoid tumors and rhabdomyosarcoma cell lines [112]. Two homologues of Drosophila STIM (dSTIM) have been identified in vertebrates, STIM1 and STIM2. The 3D structure of STIM1 has been predicted based on the amino acid sequence and

includes an EF-hand domain, a sterile-α-motif (SAM) domain, a transmembrane-spanning region, coiled-coil regions, and proline-rich N terminus [113]. The EF-hand domain of STIM1 has a high affinity for calcium (200–600μM range) and is located in the lumen of the ER where it senses changes in calcium store content [114]. The SAM domain of STIM1 is a protein–protein interaction domain that is also located in the lumen of the ER, a location not previously described for other SAM domain-containing proteins [115]. The cytosolic coiled coil domains are located at the C-terminus and are important for oligomerization and punctae formation that is required for activation of SOC channels [116]. Simultaneously with the identification of STIM1, Orai1 was identified in siRNA-based screens for mediators of SOCE and was found to be mutated in immunodeficient patients that lacked SOCE [117-119]. The Orai family of calcium entry channels includes three members and bares little resemblance to other ion channel families. Orai proteins are predicted to have four transmembrane spanning regions and share structural similarities with the gamma subunit of the L-type calcium channel (CaV gamma), transmembrane AMP receptor proteins and claudins [120]. Two studies analyzing mutations in the membrane spanning region of Orai1 demonstrated an altered ion selectivity of Icrac, indicating that Orai proteins represent the pore for ICRAC [121-123] (Fig. 9).

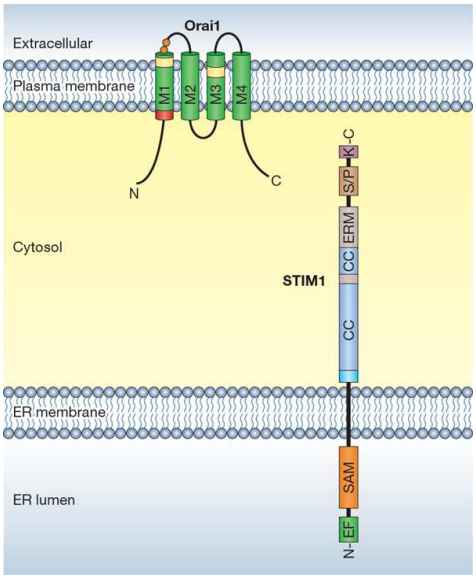

***Figure 9**: **Orai1 and STIM1.** Schematic representation of Orai1 and STIM1 domains and subcellular localization. (Adapted from [124]).*

When the [Ca^{2+}] of the ER ([Ca^{2+}]$_{ER}$) is at normal resting levels, STIM1 and Orai1 are sparsely distributed across the ER and plasma membrane, respectively. A depletion of [Ca^{2+}]$_{ER}$ causes STIM1 monomers to begin to aggregate until they form tetramers just below the plasma membrane. This may require translocation of part of the ER towards the plasma membrane so the ER comes within 10–25 nm of the plasma membrane [125]. At this location, Orai1 monomers aggregate to form a tetramer in response to the aggregation of STIM1 at this location [126]. STIM1–

Orai1 complexes form functional units that regulate and conduct the store-dependent Ca^{2+} influx, and a physical contact between the STIM1 tetramer and the Orai1 tetramer activates Ca^{2+} influx [127]. These events take seconds to tens of seconds to occur [124] (Fig. 10). These SOCE functional units can only form at a low density around the periphery of the cell, probably due to a relatively low abundance of these proteins in non–muscle cells and also due to infrequent plasma membrane–ER contacts.

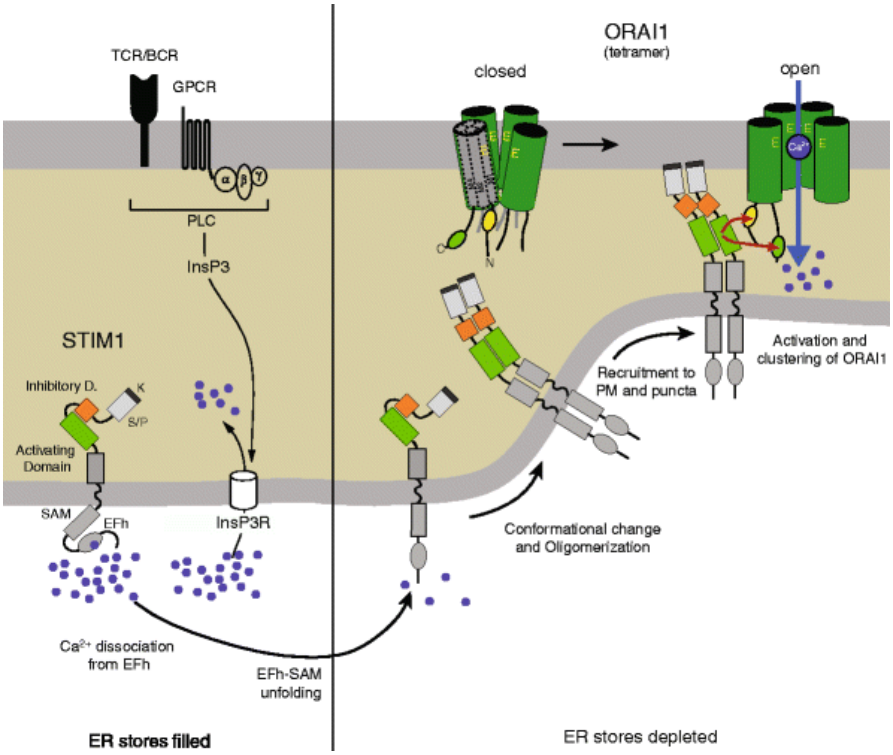

***Figure 10**: **Steps of SOCE.** In resting cells (left panel), STIM1 and Orai1 are dispersed throughout the ER and plasma membrane, respectively. Store depletion causes STIM1 to accumulate at locations where the ER is juxtaposed to the plasma membrane ('junctional ER'). At the same time, Orai1 accumulates in regions of the plasma membrane directly opposite the STIM1 clusters. The co-localization of STIM1 and Orai1 restricts channel activation and Ca^{2+} entry to these sites (right panel). (Adapted from [128]).*

Compared with skeletal muscle fibers, the non-excitable cells in which SOCE has been well described, represent cells that do not require a rapid and precise delivery of Ca^{2+}. This is reflected in a less-developed Ca^{2+} regulatory membrane system as compared with skeletal muscle fibers. Skeletal muscle fibers have become specialized in the rapid delivery and storage of Ca^{2+} for the purpose of supporting rapid and frequent contraction [129]. It also appears that SOCE has become specialized in skeletal muscle fibers. Calcium entry into a myofiber from the extracellular space has been largely overlooked as a mechanism of store refilling.

However, a recent challenge to the long held notion that muscle contraction can continue in the absence of external calcium was offered by studies demonstrating that repeated stimulation of isolated muscle fibers without external calcium results in the depletion of internal stores and loss of EC coupling [130]. As a consequence of store depletion, muscles fatigue and lose the ability to generate force. These effects are reversed by adding calcium to the perfusion bath [131, 132]. This mechanism, demonstrated in myogenic cell lines, primary embryonic myotubes, and isolated single myofibers, suggests an unrecognized but important role for SOCE in skeletal muscle function. Although the main actors of this trans-sarcolemmal Ca^{2+} flux have been identified [110, 111, 117, 119, 133]; there are still several important unresolved issues regarding SOCE in skeletal muscle, including the identification of mechanisms and molecules involved in the fine regulation of this pathway. The MS4A family includes proteins that share a predicted tetra-spanning membrane topology with N- and C-terminal cytoplasmic domains. CD20, the best studied member of this family, is conventionally expressed on the surface of B cells where it is involved in lymphocyte activation, proliferation, and differentiation [134]. The primary structure of CD20 indicates a multi-transmembrane domain configuration resembling that of ion channels or transporters [135]. Cell lines transfected with CD20 show an increased calcium conductance across the plasma membrane, strongly suggesting that CD20 functions as an important channel for regulating calcium homeostasis [136, 137]. Furthermore, reduced CD20 expression in B cell lines results in significantly decreased calcium entry across the plasma membrane [137, 138]. Beyond these findings, knowledge about the biology of CD20 is relatively scarce, and its precise functionality is still not understood. Remarkalby, some insight has been provided by studies showing that CD20 can associate with lipid raft domains of the plasma membrane, where it is probably involved in SOCE [139, 140]. Other critical details such as the kinetics of SOCE activation, the extent of store depletion required to activate SOCE, and even the functional role of SOCE in skeletal muscle remain to be defined [141]. However, it is possible to asses potential roles of SOCE in skeletal muscle by modeling. Ca^{2+} entering the fiber via SOCE could be to supplement $[Ca^{2+}]_{cyto}$ for contractile activation, refilling of the SR, simple balancing of Ca^{2+} fluxes across the surface membrane or perhaps even to regulate protein function within the junctional cleft. The role of SOCE in activating the contractile apparatus directly can be addressed by comparing the known Ca^{2+} flux rates to the cytoplasm from the SR and t–system. Even under conditions of maximum physiological DF_{Ca}, the flux rate of SOCE is some four orders of magnitude smaller compared to the SR Ca^{2+} release flux [142, 143]. As such, the store–dependent influx probably only introduces Ca^{2+} into the junctional membrane regions and thus there would not be a significant contribution from SOCE to the cell–wide Ca^{2+} transient during EC coupling (the role of SR Ca^{2+} release). Clearly, this rules out a role of SOCE directly providing any significant Ca^{2+} for contraction. The potential role of SOCE in refilling the SR to provide Ca^{2+} for continuing release from SR in fast–twitch muscle can be scrutinized also from known Ca^{2+} influx rates to the cytoplasm. The contribution is only significant under the assumption that Ca^{2+} release from SR is at its lowest (~25-μM per action potential) and stimulation frequency is ~5 Hz or lower. This indicates the contribution of SOCE to SR refilling in active fast–twitch muscle can only be minimal, if any. It should be noted that the amount of Ca^{2+} released during trains of action potentials in slow–twitch muscle is

much less than that in fast–twitch muscle [142]. Therefore, SOCE may contribute to the refilling of the SR of slow-twitch muscle under similar circumstances. A simpler role of SOCE, where SOCE may be providing a balancing influx of Ca^{2+} to maintain a consistent [Ca^{2+}] in the cell, remains possible. As $[Ca^{2+}]_{cyto}$ is high during prolonged EC coupling, extrusion mechanisms must eject some Ca^{2+} from the fiber. Replacing Ca^{2+} that is lost during such times may be the role of SOCE in muscle. All these possible roles need to be examined to allow for an in–depth understanding of SOCE in regulating muscle fatigue resistance, Ca^{2+}-related signaling, muscle development, and disease.

3. Myopathies

Diseases affecting skeletal muscle are defined as myopathies and are caused by a structural or functional alteration of the muscle. Myopathies can be hereditary or acquired. In particular, the muscular dystrophies (MDs) are inherited myogenic disorders characterized by progressive muscle wasting and weakness of variable distribution and severity [144, 145]. They share common histological features of ‘‘dystrophic’’ muscle biopsy changes that include variation in muscle fibre size, muscle fibre degeneration and regeneration, and replacement of muscle by connective tissue and fat [145-148]. The clinical and genetic heterogeneity of these conditions is well recognized, since differences arise comparing onset, disease progression and multisystem involvement [145]. The genes and their protein products that cause most of these disorders have now been identified. This information is essential to establish an accurate diagnosis and for reliable genetic counselling and prenatal diagnosis. Nevertheless there is, as yet, no way of greatly affecting the long-term course of any of these diseases. The major advances over the last two decades have in fact improved diagnostic precision and focused symptomatic management and are increasingly leading to development of cutting-edge therapies.
Based on distribution of predominant muscle weakness, six major forms can be delineated (Fig. 11): Duchenne and Becker type, Emery-Dreifuss, limb-girdle, Facioscapulohumeral, distal, oculopharyngeal, with the addition of congenital dystrophy, in which muscle weakness is more generalized.

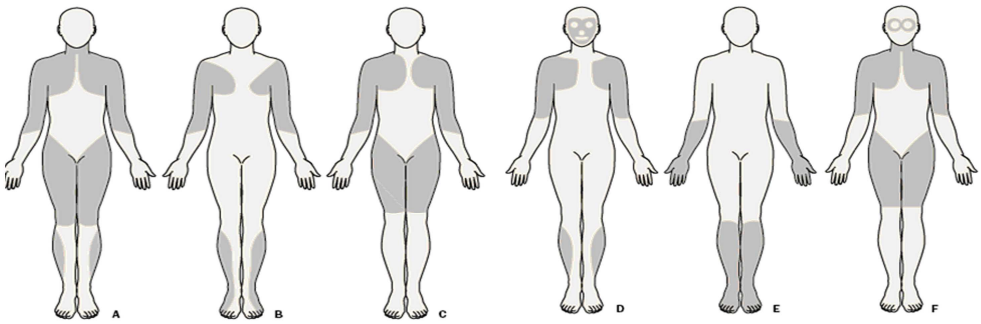

Figure 11: Distribution of predominant muscle weakness and wasting. *(A) Duchenne Muscular Dystrophy, (B) Emery-Dreifuss, (C) Limb-girdle, (D) Facioscapulohumeral, (E) Distal, and (F) Oculopharyngeal muscular dystrophy.*

3.1 Duchenne muscular dystrophy

Many of the dystrophies, but not all, are diseases of the dystrophin-glycoprotein complex and are today classified as dystrophinopathies. Duchenne Muscular Dystrophy (DMD) is the best known since it is one of the most frequent genetic human diseases (~1:3500 male births; [149]). The primary defect in DMD is the lack of dystrophin, a 427 kDa subsarcolemmal cytoskeletal protein, due to mutations in the dystrophin gene which is extraordinarily large (>2300 kB) and localized on the X chromosome at Xp21. Full-length dystrophin is a large rod-shaped protein that comprises four domains. The amino-terminal domain has homology with α-actinin and contains between 232 and 240 amino-acid residues depending on the isoform. The central - rod - domain is a succession of 25 triple-helical repeats similar to spectrin and contains about 3000 residues. There is a cysteinerich domain of 280 residues. The last - carboxy-terminal - domain comprises 420 residues [150-156]. The protein is associated with the plasma membrane of cardiac and skeletal muscle (sarcolemma) and its main role at the sarcolemma is to interact with integral membrane proteins (sarcoglycan, dystroglycans, syntrophin, and dystrobrevin complexes) that are assembled in the dystrophin–glycoprotein complex. This complex forms a bridge across the sarcolemma and flexibly connects the basal lamina of the extracellular matrix to the inner cytoskeleton [157, 158]. Furthermore, dystrophin interacts with the sarcomeric network by binding to F-actin [152, 157] (Fig. 12). One of the main roles of the dystrophin–glycoprotein complex is to stabilise the sarcolemma and to protect muscle fibres from long-term contraction-induced damage and necrosis [153, 157, 159-161]. In addition to its mechanical function, dystrophin–glycoprotein complex has recently been suggested to have a role in cellular communication by acting as a transmembrane signalling complex [157, 162]. This hypothesis is supported by the fact that the mechanisms of cell death due to mutations of the dystrophin–glycoprotein complex genes might be related to disruption of cell survival pathways and cellular defence mechanisms that are regulated by signalling cascades [157]. Dystrophin is also the target of a proline-directed, serine–threonine, and calmodulindependent kinase and is phosphorylated both *in vivo* and *in vitro* [157]. Although it has been shown that dystrophin phosphorylation affects its affinity for F-actin and syntrophin [163, 164], the phosporylation status might have a role in signal transduction.

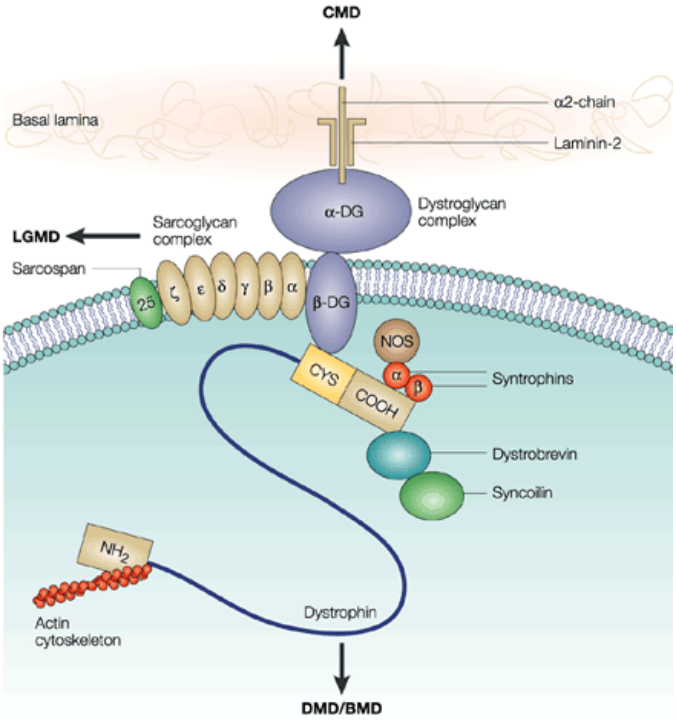

Figure 12: Dystrophin-glycoprotein complex

The dystrophin gene also has at least four internal promoters that give rise to shorter dystrophin proteins lacking the actin-binding terminus but retaining the cysteine rich and carboxy-terminus domains that contain the binding sites for dystroglycan, dystrobrevin, and syntrophin. Each of these internal promoters uses a unique first exon that splices into exons 30, 45, 56, and 63 to generate protein products of 260 kDa (Dp260), 140 kDa (Dp140), 116 kDa (Dp116), and 71 kDa (Dp71) (Fig. 13). Dp260 is expressed in high concentrations in the retina, where it coexists with the full-length brain and muscle isoforms [165, 166]. Dp140 is expressed in brain, retina, and kidney tissues [167]. Dp116 is only expressed in adult peripheral nerves [168]. Dp71 is detected in most non-muscle tissues including brain, retina, kidney, liver, and lung and it is present in cardiac but not skeletal muscle [169]. This isoform is commonly alternatively spliced such that the 13 carboxy-terminal dystrophin amino acids are replaced with a stretch of 31 new ones [170].

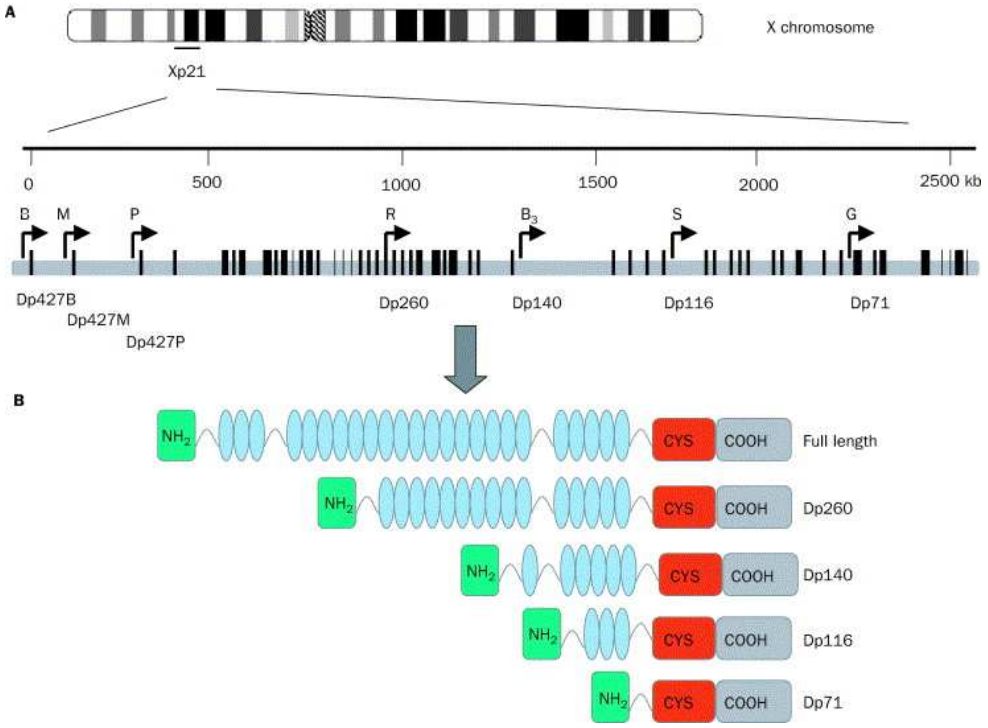

Figure 13: Organization of the dystrophin gene. (A) *Dys gene is located in Xp21. Arrows indicate the various promoters: in particular are brain (B), muscle (M), and Purkinje (P) promoters; R, B_3, S, and G represent the Dp260 (retinal), Dp140 (brain), Dp116 (Schwann cell), and Dp71 (general) promoters.* ***(B)*** *The domain composition of the various dystrophin proteins is indicated. (Adapted from [171]).*

More than 1500 deletion breakpoints have been detected in the human dystrophin gene only in European populations [172]. Today it seems clear that all DMD patients lack dystrophin independent of the underlying mutation, and it is believed that the absence of a functional protein accounts for the dystrophic phenotype. In DMD, the first clinical symptoms are usually observed before the age of three in affected boys who show a delay in reaching developmental milestones such as running and climbing. Before the age of 6, their gait becomes unsafe and waddling, and in the same period of time hypertrophy and pseudohypertrophy of calf, gluteal, quadriceps, and other muscles develops. Between 6 and 11 years of age muscle strength declines steadily, leaving boys wheelchair bound from about age 11. Death occurs before age 30 by respiratory failure (as a consequence of weakness of respiratory muscles) often in combination with respiratory infection or by cardiac failure [173]. The histological analysis of DMD muscle characteristically reveals eosinophilic hypercontracted muscle fibers, necrotic fibers, ongoing muscle regeneration, and the proliferation of fibroblasts within muscle tissue. The replacement of muscle tissue by connective tissue (fibrosis) is the major cause of muscle weakness. Several animal models of muscular dystrophy exist, including

the *mdx* mouse [149, 174]. Degeneration and regeneration of muscle fibers does also occur in *mdx* muscle, but fibrosis is seen to a much smaller extent and has a late onset [149].

3.2 Calcium as a pathogenic factor in DMD

Although the primary defect in DMD has been known for more than 20 years [175], neither the function of dystrophin nor the pathogenic mechanism of muscle dystrophy is sufficiently clarified. Two different, not necessarily exclusive, hypotheses have been put forward to explain the pathological changes caused by dystrophin deficiency, i.e., the “calcium hypothesis” and the “leaky membrane hypothesis” [149, 176-178]. The *calcium hypothesis* is based on early reports of Ca^{2+} accumulation in DMD muscle fibers. An alizarin red stain, a histochemical stain for Ca^{2+} deposits, showed increased numbers of positive fibers in DMD muscle compared with controls. Necrotic as well as non-necrotic fibers were alizarin red positive [179]. The total Ca^{2+} content of DMD muscle biopsies was found to be elevated compared with controls by a factor of 2.4 [180]. A similar Ca^{2+} increase was found in adult *mdx* muscles at all tested stages [181]. The mechanism of Ca^{2+} entry and its connection to dystrophin deficiency are still controversially discussed. An increased activity of plasma membrane Ca^{2+} channels in myotubes of DMD and *mdx* origin has been reported [182, 183]. Elevated resting levels of intracellular free Ca^{2+}, detected with fluorescent indicators, were observed in DMD myotubes [184] and *mdx* muscle fibers [185]. These data suggested a direct or indirect involvement of dystrophin in the muscular Ca^{2+} homeostasis and a close correlation between the lack of dystrophin and increased Ca^{2+} influx. In later studies, these findings could not be confirmed. Several groups showed unchanged free Ca^{2+} resting levels and Ca^{2+} transients in cultured myotubes of DMD and *mdx* origin [186, 187] and in *mdx* muscle fibers [186, 188, 189]. Interestingly, hyposmotic stress, a means to mimic mechanical stress, induced Ca^{2+} transients in myotubes [186], and they were more pronounced in *mdx* myotubes [190]. Contracting but not resting DMD myotubes, cocultured with spinal cord tissue, were more sensitive to hyposmotic shock than the controls [191]. Recently, the question of increased membrane Ca^{2+} permeability of dystrophin-deficient muscle was reinvestigated with the “manganese quench technique.” Bath application of Mn^{2+}, an ion known to quench fura 2 fluorescence, caused a faster progressive quench of intracellular fura 2 in *mdx* myotubes [183] and in adult *mdx* fibers [192] compared with controls. The effect could be inhibited by Gd31, other unspecific ion channel blockers, and amiloride. These observations indicate an increased Ca^{2+} flux through ion channels into *mdx* fibers. This influx is probably fairly well compensated by effective cellular Ca^{2+} transport systems, because resting Ca^{2+} levels were nearly unchanged. According to present knowledge, intact dystrophin-deficient muscle fibers can have normal free levels both at rest and after contractile activity. However, aggravated mechanical activity or mechanical stress can cause abnormally high and persistently increased Ca^{2+} levels in DMD and *mdx* muscle.

According to the *leaky membrane hypothesis*, the sarcolemma of dystrophin-deficient muscle fibers is more susceptible to lesions. This hypothesis was developed on the observation that increased concentrations of muscle-specific cytoplasmic proteins are present in the serum of DMD patients [173, 193, 194] and *mdx* mice [181, 195] even before the onset of muscle fiber degeneration. Creatine

kinase (CK) activity can be 100-fold higher in serum of DMD patients compared with controls [194]. In addition to CK, many other muscle-specific cytoplasmic proteins as pyruvate kinase, myoglobin [193], and PV [196] are found in the serum when skeletal muscle is dystrophin deficient. The release of cytoplasmic enzymes from dystrophin-deficient muscle has been reproduced with isolated muscle fibers [197] and cultured *mdx* and DMD muscle [198]. Not only efflux, but also influx of molecules into dystrophin-deficient muscle fibers has been shown *in vitro* and *in vivo*. Preparations of isolated *mdx* diaphragm exposed to eccentric contractions showed much higher intake of procion orange than control muscle [199]. This result was later confirmed with extensor digitorum longus muscle from 40-day-old but not from 2-wk-old *mdx* mice [195]. Matsuda et al. [200] demonstrated that uptake of molecules into *mdx* muscle fibers does occur *in vivo*. Intravenous injection of Evan's blue resulted in staining of *mdx* muscle fibers, indicating the uptake of the dye, which is in plasma bound to albumin, into dystrophin-deficient muscle fibers [153, 178, 200]. Evans blue does not cross into skeletal muscle fibers in normal mice [178]. Taken together, a bidirectional flow of molecules between the cytoplasmic and the extracellular space seems to be characteristic for dystrophin-deficient muscle *in vitro* and *in vivo*. This exchange of molecules occurs during normal mechanical muscle activity and is aggravated by mechanical stress.

If we return to the pathophysiology of dystrophin-deficient muscle, the above-mentioned calcium hypothesis and the leaky membrane hypothesis may be integrated to a "*mechanical hypothesis*." A higher fragility of the plasma membrane during mechanical activity seems to be the direct physiological consequence of the lack of dystrophin. This increased fragility results in short-lived membrane lesions of limited size, which allow the efflux of cytoplasmic molecules from the cell and also the influx of molecules into the sarcoplasm. The efflux of cytoplasmic components is probably an indicator of muscle membrane damage rather than of great pathophysiological importance. Among the molecules that enter the muscle fibers, Ca^{2+} are thought to be those with the greatest pathogenic consequences [176]. Increased influx of Ca^{2+} into the subsarcolemmal space can lead to the activation of degradative enzymes and overload and dysfunction of Ca^{2+} cycle and storage systems. This results in damage of the sarcolemma from interior, impairment of mitochondrial function, and modulation of intracellular signaling pathways. Because membrane lesions are of limited size in the beginning of the necrotic process and Ca^{2+} is quickly bound by target proteins, the early consequences of Ca^{2+} influx will probably be restricted to the subsarcolemmal space of the muscle fibers. A key factor may be an increased calpain activity. Possible substrates of calpains are the membrane cytoskeleton, the Ca^{2+}-ATPase of the plasma membrane, and ion channel proteins. The Ca^{2+} pump located in the plasma membrane is a preferred substrate of calpain in erythrocytes [201], and if attacked in dystrophin-deficient muscle, this calpain action would, in addition to provoking an excess of Ca^{2+} influx, disturb an important extrusion pathway. Using immunohistochemical staining, Kumamoto et al. [202] showed an increase in calpain especially in the myofibrillar area (Z disks) in atrophic DMD muscle fibers but not in morphologically intact fibers. This indicates that an increased calpain content of dystrophin-deficient muscle fibers is probably not an early event in the dystrophic process. An alternative pathway of cell damage involving mitochondrial dysfunction has been suggested for dystrophin-deficient muscle [203, 204]. Mitochondrial mRNAs have been found to be downregulated in *mdx* muscle [205],

and a lack of calmitine, a Ca^{2+}-binding protein present in mitochondria, was shown in DMD muscle. However, it is not clear whether mitochondrial dysfunction and energy depletion are critical and early steps in the dystrophic process. Another pathway of Ca^{2+} influx, in addition to that mediated by membrane lesions, was pointed out by Turner et al. [206]. They demonstrated that proteolytic cleavage of plasma membrane Ca^{2+} channels can lead to increased openings of these channels [206]. This could mean a loop of positive feedback of Ca^{2+} influx, Ca^{2+}-dependent proteolysis, and increased Ca^{2+} influx.

Among the Ca^{2+}-related pathways reported to be involved in skeletal myopathies, SOCE is probably the most recently discovered. The importance of SOCE in an excitable tissue such as skeletal muscle, although previously underappreciated, has recently been highlighted by data from mouse models and patients with immunodeficiency. Consistent with the proposed role of SOCE in store refilling and longterm Ca^{2+} homeostasis, skeletal muscle isolated from STIM1 deficient mice showed reduced tetanic force and fatigued rapidly upon repeated stimulation [207]. Moreover, loss of STIM1-dependent SOCE in mice results in a profound myopathy and perinatal mortality [207]. Morphologially, the myopathy in $Stim1^{-/-}$ mice is characterized by reduced muscle crosssectional area and mitochondriopathy. A similar if less pronounced myopathy in mice transgenic for the nonfunctional ORAI1-R93W mutant was also observed [208]. Myopathy in ORAI1- and STIM1-deficient patients becomes apparent soon after birth as global, nonprogressive muscular hypotonia with reduced muscle strength and endurance [209]. In ORAI1-deficient patients, it initially manifested through insufficient head control and general reduction in muscle tone [209, 210]. In the two patients surviving after HSCT, myopathy is characterized by delayed ambulation, reduced walking distance, and a positive Gowers' sign. In addition, both patients suffer from chronic pulmonary disease due to respiratory muscle insufficiency and retention of bronchial secretion resulting in a predisposition to recurrent chest infections and bronchiectasis [209]. A muscle biopsy from a patient with ORAI1-R91W mutation showed variations in muscle fiber size with a predominance of type I fibers and atrophic type II fibers suggesting a defect in fast twitch muscle fiber differentiation in the absence of functional ORAI1. Other structural abnormalities characteristic of congenital myopathies were not observed. A clinically similar nonprogressive global muscular hypotonia with partial iris hyoplasia was also observed in all three patients lacking STIM1 expression, although a muscle biopsy revealed no abnormalities [211]. Electromyograms in both ORAI1- and STIM1- deficient patients were normal. These findings suggest that SOCE mediated by ORAI1 and STIM1 is required for the differentiation and/or function of human skeletal muscle. The myopathy in human patients and gene-targeted mice is consistent with the robust expression of both ORAI1 and STIM1 in human and mouse skeletal muscle [209, 212-214] and colocalization of STIM1 with ryanodine receptor (RyR) 1 at the junction of plasma membrane T-tubules with the terminal cisternae of the sarcoplasmic reticulum (SR) [207]. Abnormalities in store operated Ca^{2+} influx are observed in pathologic states such as muscular dystrophy and malignant hyperthermia (Fig. 14). The mechanism by which abnormal SOCE contributes to the pathogenesis of these disorders is unclear but likely includes activation of maladaptive Ca^{2+} signaling pathways leading to disorders of metabolism, abnormal protein handling, and adverse remodeling.

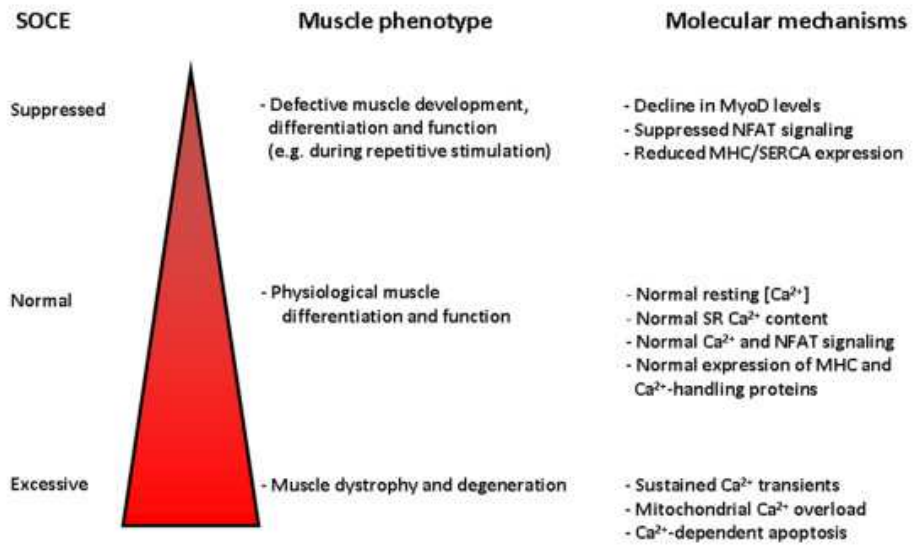

***Figure 14**: Schematic overview of the pathophysiological consequences of SOCE dysregulation based on mouse-model studies.*

MATERIALS AND METHODS

1. Isolation and characterization of blood-derived CD133$^+$ stem cells by flow cytometry

Circulating CD133$^+$ stem cells were collected from peripheral blood of normal subjects and DMD patients. The protocol of cell isolation was previously described [50]. After determination of the purity of the CD133$^+$ stem cells, we plated the cells in the presence of a proliferation medium (PM) composed of DMEM/F-12 (1:1); 20% FBS, including Hepes (N-(2-hydroxyethyl)piperazine-N'-(ethanesulfonic acid)) buffer (5 mM), glucose (0.6%), sodium bicarbonate (3 mM), and glutamine (2mM); SCF (100 ng/ml; TEBU, Frankfurt, Germany); VEGF (50 ng/ml; TEBU, Frankfurt, Germany); and LIF (20 ng/ml; R&DSystems, Minneapolis,MN, USA). Cell viability assay was performed using 7-Amino-actinomycin D (7-AAD) viability probe. For four-color flow cytometric analysis, at least 30 x 10^4 to 80 x 10^4 cells were incubated with the following monoclonal antibodies (mAbs): anti-CD133/2-phycoerythrin (PE) (Miltenyi Biotec, Germany), anti-CD34-Allophycocyanin (APC) (BD, Franklin Lakes, NJ, USA), anti-CDw90 (Thy-1)-fluorescein-isothiocyanate (FITC) (BD, Franklin Lakes, NJ, USA), anti-VEGF-R2 (KDR)-PE (R&D Systems, Minneapolis, MN, USA), anti-CD184 (CXCR4, fusin)-PE-Cy5 (BD, Franklin Lakes, NJ, USA), anti-CD45-FITC (BD, Franklin Lakes, NJ, USA), and anti-CD20-FITC (BD, Franklin Lakes, NJ, USA). For each mAb, an appropriate isotype-matched mouse immunoglobulin was used as a control. After staining performed at 4℃ for 20 min, cell suspensions were washed in PBS containing 1% heat inactivated FCS and 0.1% sodiumazide. Cells were analyzed using a FACSCalibur flow cytometer and PAINT-a Gate software (BD, Franklin Lakes, NJ, USA). The commercially available BDKit (BD, Franklin Lakes, NJ, USA) was used to quantify the number of CD20$^+$ cells among normal and dystrophic circulating CD133$^+$ stem cells. The commercially available Quantibrite™ Beads system (BD, Franklin Lakes,NJ,USA) was used to determine the number of CD20 molecules on membrane of normal and dystrophic circulating CD133$^+$ stem cells, according to manufacturer's instructions.

2. Evaluation of dystrophin isoforms expression in CD133$^+$ stem cells by RT-PCR and western blot

Total RNA was extracted from normal and dystrophic circulating CD133$^+$ stem cells by TrizolReagent (Invitrogen, Carlsbad, CA, USA). First-strand cDNA was prepared by using Super Script First Strand Synthesis System for RT-PCR (Invitrogen, Carlsbad, CA, USA), starting from 2 µg total RNA with oligo(dT)$_{12\text{-}18}$ primers. To investigate the expression of the most common dystrophin isoforms, we designed five different pairs of human-specific primers:

	forward primer	reverse primer
427kD	5'-CCTACAGGACTCAGATCTGG-3'	5'-GTCCTCTACTTCTTCCCACC-3'
260kD	5'-GCATCCAGTCTGCCCAGG-3'	5'-GAGACAGGACTCTTTGGGCAG-3'
140kD	5'-GGATGGCATTGGGCAGCG-3'	5'-GCTCTTTTCCAGGTTCAAGTGG-3'
116kD	5'-CCTCCAAGGTGAAATTGAAGC-3'	5'-CTGGCTTCCAAATGGGACC-3'
71kD	5'-CCACGAGACTCAAACAACTTGC-3'	5'-CTTGAGGTTGTGCTGGTCC-3'

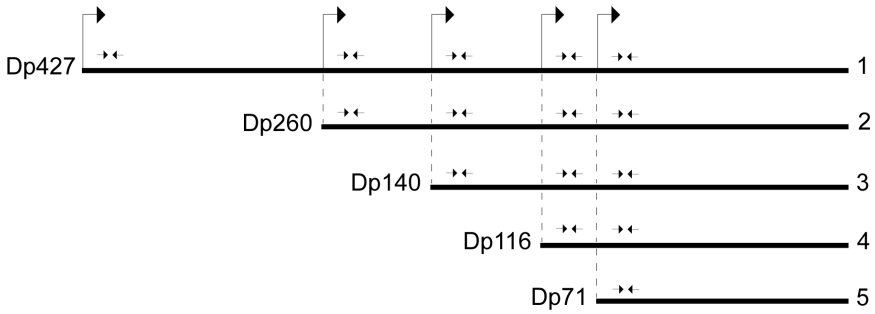

Map showing the five dystrophin isoforms and the primers used for amplification

The GAPDH gene was amplified as housekeeping using the following couple of primers: F(5'-GCACAAGAGGAAGAGAGAGAC-3') and R(5'-GATGGTACATGACAAGGTGCGG-3'). PCR was performed under the following conditions: 94℃ for 5 min, then 35 cycles at 94℃ for 40 s, 68℃ for 40 s, and 72℃ for 1 min. cDNA samples obtained from blood-derived $CD133^+$ stem cells cultured in proliferative conditions were used, and PCR products were analyzed on 2% agarose gels. For Western blot analysis of Dp71, normal and dystrophic circulating $CD133^+$ stem cells and $CD133^-$ cells were lysed directly in 1X sample buffer (1% SDS) containing 2 mg/ml aprotinin, 10 mg/ml leupeptin, 10 mM sodium fluoride (NaF), 1 mM sodium vanadate (Na_3VO_4) and 1 mM phenylmethylsulfonylfluoride (PMSF). Lysates were boiled 5 min and centrifuged at 10000 x g for 5 min to remove insoluble material. Total protein concentration was determined according to Lowry's method [215] and lysates were stored at -20℃. Samples were analyzed on 7.5%polyacrylamide gel, transferred to supported nitrocellulose membranes (Bio-Rad Laboratories, Hercules, CA, USA), and the filters were saturated in blocking solution (10 mM Tris, pH 7.4, 154 mM NaCl, 1%BSA, 10%horse serum, 0.075%Tween-20) overnight at 4℃. Primary antibodie s (NCL-Dys2 - Novocastra Laboratories, Newcastle, UK; anti-βactin - Sigma, Milan, Italy) were incubated for 90 min at room temperature and then followed by washing, detection with horseradish peroxidase (HRP) conjugated secondary antibodies (DakoCytomation, Carpinteria, CA, USA), and developed by enhanced chemiluminescence (ECL) (Amersham Biosciences, Piscataway, NJ, USA). Prestained molecular weight markers (Bio-Rad Laboratories, Hercules, CA, USA) were run on each gel. Bands were visualized by autoradiography using Amersham Hyperfilm™ (Amersham Biosciences, Piscataway, NJ, USA).

3. Immunoprecipitation and western blotting from blood-derived $CD133^+$ stem cells

For the precipitation of CD20 complexes, cells were pelletted at 3000 rpm for 7 min at 4℃ and then lysed in 1% Nonidet P-40 detergent buffer containing 20mM Tris, pH 8, 137 mM NaCl, 2 mM EDTA, 10% glycerol, 2 mg/ml aprotinin, 10 mg/ml leupeptin, 10mM NaF, 1mM Na_3VO_4 and 1mM PMSF. After 15 min on ice with occasional agitation, samples were centrifuged at 10000 x g for 10 min at 4℃ to remove insoluble material. Total protein concentration was determined according to

Lowry's method [215] and lysates were stored at -20℃. Lysates (200-300 mg of total proteins) were incubated with 10 mg of anti-CD20 antibody (M-20, Santa Cruz Biotechnology, Inc., Santa Cruz, CA, USA) and mixed overnight at 4℃ before adding 50 ml of Protein A/G PLUS-Agarose (Santa Cruz Biotechnology, Inc., Santa Cruz, CA, USA). Beads were incubated for 3h at 4℃ and then washed 3 times with PBS before addition of 30 ml of 1X sample buffer containing 1% SDS. Samples were boiled for 5 min, centrifuged at 10000 x g for 5 min at room temperature and supernatants (IP samples) were resolved on 10% polyacrylamide gels. After transfer to supported nitrocellulose membranes (Bio-Rad Laboratories, Hercules, CA, USA), the filters were processed with the proper antibodies as described above. CD20 phopshorylation was assayed using anti-phosphothreonine (H-2, Santa Cruz Biotechnology, Inc., Santa Cruz, CA, USA) and anti-phosphoserine (16B4, Santa Cruz Biotechnology, Inc., Santa Cruz, CA, USA) primary antibodies. To evaluate Lyn activation after interaction with CD20, filters were incubated with specific anti-Lyn antibody (#2732, Cell Signaling Technology, Inc., Danvers, MA, USA), then stripped and reprobed with anti-phosphotyrosine antibody (PY99, Santa Cruz Biotechnology, Inc., Santa Cruz, CA, USA). Obtained bands were acquired using the Epson Perfection 2400 PHOTO Scanner and the Epson Scan Software. Densitometric analysis were performed using ImageJ software (http://rsbweb.nih.-gov/ij/).

4. Measurement of cytoplasmic Ca^{2+} concentration in blood-derived $CD133^{+}$ stem cells

Measurement of cytoplasmic calcium concentration $[Ca^{2+}]_i$. Cells were suspended in a physiological solution (PS) containing NaCl 154 mM, KCl 5 mM, $MgCl_2$ 1 mM, $CaCl_2$ 1.8 mM, Glucose 10 mM, Hepes 10 mM (pH adjusted to 7.4 with NaOH) and centrifuged for 4 min at 1500 x g. Cells were loaded with Ca^{2+} indicators by incubation in the PS solution containing the acetoxy methyl ester (AM) of Fura-2 (9 µM in dimethyl sulfoxide [DMSO]) or Fluo3 (2 mM in DMSO) (Molecular Probes Europe, Leiden, The Netherlands), for 45 min at room temperature (20 – 22℃), in the dark, with gentle mixing. Cells were then centrifuged, resuspended in PS and allowed to complete hydrolysis of AM ester groups for 30 min at room temperature. Images were obtained with a fluorescence microscope (Nikon Eclipse 600), using a CFI Fluor 60X, 1.0 NA, water-immersion objective. Cells were settled, at low density, in a glass imaging chamber. Images were acquired by a CCD camera (Panasonic, WV-BP514E) and collected using Axon Imaging Workbench 2.2 software (Axon Instruments Inc., CA, USA), by averaging 16 frames (time of exposure 528 ms). To visualize changes of $[Ca^{2+}]_i$ Fluo3 loaded cells were imaged at 520 nm by exciting at 480 nm every 5 – 30 seconds to minimize dye photobleaching. The fluorescence signals, F_{base} and F, were computed as the mean pixel value in each region of interest covering a single cell, at the beginning and during the time course, respectively. The normalized change in fluorescence was reported as a pseudoratio, which is thought to approximately reflect $[Ca^{2+}]_i$ and was calculated using the equation: $\Delta F/F = (F-F_{base})/(F_{base}-B)$, where B is the background signal averaged over cell free areas. To measure the intracellular free Ca^{2+} levels, Fura-2 loaded cells were alternatively excited at 340 and 380 nm while they were imaged at 510 nm at room temperature. After background subtraction, ratio images were obtained by dividing pixel by pixel couples of digitized images at

340 and 380 nm. In each cell the fluorescence intensity was measured by the mean pixel value in a region of interest covering most of the cell area. Fluorescence values can be converted into ion concentrations according to the equation given by Grynkiewicz and colleagues [216]: $[Ca^{2+}] = K_d [(R-R_{min})/(R_{max}-R)] X (F_{f380}/F_{b380})$, where R is the ratio of the fluorescence intensities measured at 340 and 380 nm, R_{min} is the limiting value of R when all the indicator is in the Ca^{2+}-free form, R_{max} when it is saturated with calcium, K_d is the dissociation constant of the Fura-2-calcium complex, F_{f380} and F_{b380} are the fluorescence intensities of Ca^{2+}-free and Ca^{2+}-bound Fura-2 at 380 nm, respectively. For calibration, Ca^{2+}-saturated or Ca^{2+}-free dye can be set by 5 µM ionomycin in the presence of 2.5 mM Ca^{2+} or by 10 mM EGTA (ethyleneglycolbis(ß-aminoethyl ether)N,N-tetraacetic acid) in nominally Ca^{2+}-free solution, respectively. Ionomycin was purchased from Calbiochem (Inalco, Italy) whilst all other reagents were obtained from Sigma (Milan, Italy). We also performed measurements of intracellular calcium on normal and dystrophic circulating $CD133^+$ stem cells after stimulation with 100 ng/ml BDNF in RPMI 1640 medium (Gibco - Invitrogen, Carlsbad, CA, USA). The cells were analyzed 2h after BDNF stimulation.

5. ELISA assays on cell culture supernatants

After 24h of culture, media from normal and DMD blood-derived $CD133^+$ stem cells were collected and used for ELISA quantification of secreted cytokines. Quantikine® Immunoassay (R&D Systems, Minneapolis, MN, USA) specific for human IGF-1, VEGF, BDNF and TGFβ-1 were performed according to manufacturer's instructions. Media were added to a 96-well polystyrene microplate coated with specific monoclonal antibodies. Secreted cytokine was detected by treating the plates with the respective polyclonal or monoclonal HRP conjugated detection antibody. Enzyme substrate was added to generate a color product whose absorbance was read at 450 nm. A cytokine standard included in each assay was used to generate a standard curve that was used to calculate the amount of secreted cytokine per well. Samples were assayed in duplicate.

6. Animal models

All procedures involving living animals were performed in accordance with Italian law (D.L.vo 116/92 and subsequent additions), which conforms to the European Union guidelines. Experimental animals were obtained from Charles River Laboratories International, Inc. (Calco, Italy). Normal C57BL and immune-deficient SCID mice were used throughout this study. Severe combined immune-deficient (SCID) mice are generally devoid of functional B and T lymphocytes [217]; this deficit results from highly error-prone recombination of antigen receptor genes [218]. All mice were fed *ad libitum* and allowed continuous access to tap water. Animals were deeply anesthetized with 2% avertin (0.015 ml/kg) prior to sacrifice by cervical dislocation, and all efforts were made to minimize suffering.

7. Evaluation of CD20 expression in skeletal muscle by RT-PCR

Total RNA was extracted from cells, muscles, and single fibers using Trizol Reagent (Invitrogen, Carlsbad, CA, USA) according to manufacturer's instructions.

The C2C12 mouse myoblast cell line was commercially obtained from the ATCC (number CRL-1772). First-strand cDNA was prepared using the Super Script III First Strand Synthesis System for RT-PCR (Invitrogen, Carlsbad, CA, USA), starting from 1 µg of total RNA with oligo $(dT)_{12–18}$ primers. In mouse samples, CD20 expression was investigated using the following primer pairs:

	forward primer	reverse primer
F1-R1	5'-AGTTGAATGTAAGAAGCAAGC-3'	5'-AGCTTATACAGGCATATGGGC- 3'
F2-R2	5'-TCTCTAAGCCTCTTTGCTGC-3'	5'-AAGAAGGCAGAGATCAGCATCG-3'

The F1–R1 pair aligned in the 3'- UTR, while the F2–R2 pair was directed against the ORF (exons 5–6) of murine CD20 mRNA. RNA from C57BL spleen and from 3T3 fibro-blasts were used as positive and negative controls, respectively. PCR conditions were as follows: 92℃ for 1 min, 56℃ fo r 1 min, and 72℃ for 1 min (36 cycles). The obtained bands were sequenced to check the specificity of PCR amplification. The mouse GAPDH gene was amplified as a standard control, using the primer pair F (5'-GTGGCAAAGTGGAGATTGTTGCC-3') and R (5'-GATGAT GACCCGTTTGGCTCC-3') and the following PCR conditions: 92℃ for 1 min, 67℃ for 1 min, and 72℃ for 1 min (36 cycles). Human CD 20 mRNA was amplified with a primer pair aligning at the 3'-UTR:

	forward primer	reverse primer
Fh-Rh	5'-GCAACAGATGATTCCAACATGGGTG-3'	5'-ATGACCTGACACCTCACCGTTCAA-3'

PCR conditions were 94℃ for 1 min, 59℃ for 1 min, and 72℃ for 1 min (36 cycles). The human GAPDH gene was amplified using the primer pair F (5'-GCACAAGAGGAAGAGAGAGACC-3') and R (5'-GATGGTACATGACAAGGTGCGG-3') and the following PCR conditions: 94℃ for 1 min, 67℃ for 1 min, and 72℃ for 1 min (36 cycle s). All PCR products were analyzed on 2% agarose gels. Bands were visualized using the UVIsave Imaging System (UVItec Limited, Cambridge, UK).

8. Evaluation of CD20 expression in skeletal muscle by flow cytometry

About 6–8 x 10^4 C2C12 myoblasts were incubated with a goat polyclonal antibody directed against the extracellular loop of CD20 (anti-CD20 (I-20); Santa Cruz Biotechnology, Inc., Santa Cruz, CA, USA) (1:50), as well as with a rabbit monoclonal antibody directed against the C-terminal region of the protein (anti-CD20 (C-term); Merck Millipore, Darm-stadt, Germany) (1:20). A mild permeabilization (0.2% Tween-20 in PBS) was performed for 15 min at room temperature prior to staining cells with the anti-CD20 (C-term) monoclonal antibody. After overnight staining at 37℃ or 20 mi n of incubation at room temperature, cells were washed and exposed to the corresponding secondary antibody (Alexa Fluor 647-conjugated chicken anti-goat or Alexa Fluor 488-conjugated goat anti-rabbit; both from Molecular Probes, Invitrogen, Carlsbad, CA, USA) (1:100). Washing was performed to remove unbound secondary antibody, and cells were analyzed using a FC500 MCL System with CXP software (Beckman

Coulter, Miami, FL, USA). Cells exposed to the appropriate isotype control antibody were used as negative controls.

9. Evaluation of CD20 expression in skeletal muscle by western blot

C2C12 murine myoblasts/myotubes and CHQ human myoblasts were directly lysed in 1 x sample buffer (1% SDS) with a commercially available cocktail of protease and phosphatase inhibitors (Complete® and PhosSTOP®, respectively; both from Roche, Mannheim, Germany). TA, QA, and DIA were removed from three-month-old C57BL (n = 3) and SCID (n = 3) mice immediately after death by cervical dislocation. Samples dedicated to whole muscle analysis were snap-frozen in liquid nitrogen and stored at −80℃ until proces sed for total protein extraction. Samples dedicated to single fiber isolation were placed in 35-mm dishes containing DMEM HG (EuroClone, Pero, Italy) and exposed to a mild enzymatic digestion with 1.4% trypsin (Gibco-Invitrogen, Carlsbad, CA, USA) at 37℃. After 10 min, trypsin activity was blocked by transferring muscles into serum containing DMEM with 15% FBS (Invitrogen, Carlsbad, CA, USA), and fibers were mechanically dissected under an optical microscope (Zeiss) until vascular, connective, and adipose tissues were completely removed. For total protein extraction, muscles were homogenized using an electric homogenizer with a 1% Nonidet P-40 detergent buffer containing 20 mM Tris (pH 8), 137 mM NaCl, 2 mM EDTA, 10% glycerol, and the Complete® and PhosSTOP® cocktails. Similarly, single fibers were homogenized with an electric homogenizer directly in 1 x sample buffer (1% SDS) with Complete® and PhosSTOP® cocktails. Total protein concen-tration was determined according to Lowry's method [215]. Samples were resolved on 12% polyacrylamide gel, transferred to supported nitrocellulose membranes (Bio-Rad Laboratories, Hercules, CA, USA), and the filters were saturated in blocking solution (10 mM Tris (pH 7.4), 154 mM NaCl, 1% BSA, 10% horse serum, and 0.075% Tween-20). The anti-CD20 (M-20), a goat polyclonal directed against the C-terminal region of CD20 (1:200), and the anti-GAPDH (V-18) (1:1000) (Santa Cruz Biotechnology, Inc., Santa Cruz, CA, USA) antibodies were incubated for 90 min at room temperature, while the anti-CD20 (C-term) monoclonal antibody (1:500) was incubated overnight at 4℃. Detection was performed with horseradish pe roxidase (HRP)-conjugated secondary antibodies (DakoCytomation, Carpinteria, CA, USA), followed by enhanced chemiluminescence (ECL) development (Amersham Biosciences, Piscataway, NJ, USA). Prestained molecular weight markers (Bio- Rad Laboratories, Hercules, CA, USA) were run on each gel. Bands were visualized by autoradiography using Amersham HyperfilmTM. Images of bands were obtained using the CanoScan LiDE60 Scanner (Canon) and the Canon ScanGear Software. Densitometric analyses were performed using ImageJ software (http://rsbweb.nih.gov/ij/). To verify the ability of the anti-CD20 (M-20) antibody to recognize its specific target, positive sources of CD20 and C2C12 myoblasts were stained after antibody pre-incubation with a specific blocking peptide to compete the signal (antibody:peptide 1:1, overnight at 4 ◦C) (CD20 (M-20) blocking peptide) (0.2 µg/µl).

10. Analysis of CD20 localization in skeletal muscle by immunofluorescence

C2C12 myoblasts, C2C12-derived myotubes, and a series of 10 µm transverse cryosections from TA and QA of C57BL and SCID mice were examined by immunofluorescence staining. CD20 was detected with anti-CD20 (M-20) (1:20) and anti-CD20 (C-term) (1:100) antibodies. To verify the ability of the anti-CD20 (M-20) antibody to recognize its specific target, a positive source of CD20 (spleen cryosections from C57BL mice) was stained after anti-body pre-incubation with a specific blocking peptide to compete the signal (antibody:peptide 1:1, overnight at 4 ◦C) (CD20 (M-20) blocking peptide; Santa Cruz Biotechnology, Inc., Santa Cruz, CA, USA) (0.2 µg/µl). Laminin was stained using a rabbit polyclonal antibody from Sigma (Milan, Italy) (1:100). α-sarcoglycan was stained using a mouse monoclonal antibody from Novocastra Laboratories (Newcastle Upon Tyne, UK) (1:50). Nuclei were stained with DAPI. Alexa Fluor 488- and Alexa Fluor 594-conjugated secondary antibodies (1:100) were used. Images were captured using the Leica TCS SP2 confocal system equipped with a 63x/1.40–0.60 objective (Leica, Germany).

11. Preparation of skeletal muscle sarcolemma

Portions of skeletal muscle were thawed in 0.9% saline, then quickly trimmed of any adhering skin, nerves, fat, or connective tissue, and weighed. Individual sarcolemma fractions were prepared from 0.5 to 2 g portions of skeletal muscle. The isolation procedure was based on that of Severson et al. [219]. Each trimmed 0.5 to 2 g portion of skeletal muscle was transferred to a 50-ml glass beaker to which 10 ml of 50 mM $CaCl_2$ was added. The muscle was minced finely with stainless steel scissors and then homogenized on ice with an Ultraturrax homogenizer, applying three 15-s bursts with a 30-s rest between each. This homogenate was filtered, through two layers of cheesecloth to remove residual connective tissue, into a 50-ml plastic centrifuge tube and centrifuged at 3000 x g in a Sorvall centrifuge (model RC5C, rotor SS34) at 4℃ for 10 min. The supernatant was poured off, and 10 ml of 10 mM Tris–Cl (pH 8.0) was added to the pellet. The pellet was re-suspended using a Teflon pestle with 20 non-shearing strokes (up + down = 1). After wash, the pestle was rinsed with 5 ml of buffer to guard against loss of material. The suspension was then centrifuged again and the supernatant discarded. The pellet was washed and centrifuged twice more, in the same manner. The third and final supernatant was discarded. To the final pellet, 10 mM Tris–Cl (pH 8.0) was added at 4 ml/g of trimmed skeletal muscle. The pellet was then re-suspended using 20 strokes of the teflon pestle, as previously described, and the suspension was transferred to a 25-ml glass beaker containing a teflon-coated magnet. Each beaker was cov-ered with parafilm and stored at 4℃ overnight. The next day, the suspensions were stirred magnetically, while 50 mM lithium bromide (LiBr) was added, drop by drop, to a total concentration of 0.2 ml per 10 ml suspension. Stirring was continued for 3h to effect extraction of contractile elements. The LiBr-extracted suspension was then transferred to a 50-ml plastic centrifuge tube, 20 ml of 10 mM Tris–Cl (pH 8.0) was added, and the mixture was centrifuged at 10000 x g in a Sorvall centrifuge at 4℃ for 10 min. The supernatant was poured off and the pellet was re-suspended with 10 ml of 10 mM

Tris–Cl (pH 8.0) using 20 strokes of the teflon pestle, effectively washing the pellet. The re-suspended washed pellet was centrifuged at 6000 x g at 4℃ for 10 min and the supernatant was discarded. To the pellet, 25% potassium bromide (KBr) was added (4 ml/g of trimmed muscle) and the pellet was resuspended using 20 strokes of the teflon pestle, followed by centrifugation at 10000 x g in the Sorvall centrifuge at 4℃ for 30 min. The KBr-treated pellet was washed once with 10 mM Tris–Cl (pH 7.5) to remove residual KBr, using 20 strokes of the teflon pestle, and was centrifuged at 6000 x g at 4℃ for 10 min. The supernatant was discarded, and the final pellet was re-suspended in 200 µl of 1 x sample buffer containing 2% SDS, and boiled for 10 min. Isolated sarcolemma samples were stored at −20℃ until analysis.

12. Immunoprecipitation of CD20 from myoblasts and skeletal muscle tissue

Total protein extracts from C2C12 murine myoblasts, C57BL QA, SCID QA, and human muscular tissue were prepared in 1% Nonidet P-40 detergent buffer containing 20 mM Tris (pH 8), 137 mM NaCl, 2 mM EDTA, 10% glycerol, and Complete® and PhosSTOP® cock-tails. Total protein lysates (1000–1500 µg) were pre-cleared for 4h at 4℃ by adding 50 µl of Protein A/G PLUS-Agarose (Santa Cruz Biotechnology, Inc., Santa Cruz, CA, USA). Pre-cleared lysates were then incubated with 10–15 µg of anti-CD20 (M-20) antibody and mixed overnight at 4℃ before adding 50 µl of Protein A/G PLUS-Agarose. Beads were incubated for 4h at 4℃, then washed 5 times with PBS; 1 x sample buffer containing 1% SDS was added and the samples were boiled. Next, samples were centrifuged at 10000 x g for 5 min, and supernatants (IP samples) were collected. Proteins that were non-specifically adsorbed by beads were extracted with the same procedure at the end of the pre-clearing step and used as a control of IP specificity.

13. Mass spectrometry

MALDI-TOF analysis was carried out on CD20 IPs from C2C12 myoblasts and QA muscles (C57BL or SCID mice). Following monoD-electrophoresis, anti-CD20 stained bands that were also appreciable in silver-stained paired lanes from the same gel were recovered and processed for MS analysis. Each band was excised, cut in small pieces, and dried in a Speed Vac. The gels were soaked with ammonium bicarbonate 0.1 M and digested overnight with sequencing grade trypsin (Roche, Monza, Italy) at 37℃. The in-gel tryptic digest was extracted with 30 µl of 5% HCOOH:CH_3CN (1:1) and the peptide mixture was subjected to MALDI-TOF analysis using a Bruker Daltonics Reflex IV instrument (Bruker Daltonics, Milan, Italy) equipped with a nitrogen laser (337 nm) and operated in reflectron mode with a matrix of α-ciano-4-hydroxy-cinnamic acid in 0.1% TFA:CH_3CN (2:1). A 2 µl mixture (1:1) of matrix solution and sample was applied to the sample plate and air-dried at ambient temperature. External standards were used for calibration (Bruker peptide calibration standard). Each spectrum was accumulated for at least 200 laser shots. Measured peptide masses were used to search the Swiss-Prot, MSDB, TrEMBL, and NCBI sequence databases for protein identifications by the Mascot program (http://www.matrixscience.com).

14. MTT assay

To assess the effects of CD20 targeting on cell proliferation, C2C12 myoblasts were plated at 2 x 10^4 cells per 24-well tissue culture plate. The medium was replaced at 24h after seeding with fresh medium containing 4 or 20 µg/ml anti-CD20 (I-20) antibody. After 2h or overnight incubation, cell growth was measured using a standard MTT assay (Cell Proliferation Kit I; Roche, Monza, Italy) according to the instruction manual. Cells killed by exposure to distilled water were used as negative controls.

15. Apoptotic assay

For quantification of apoptotic death, C2C12 myoblasts were plated at 6–8 x 10^4 cells per 12-well tissue culture plate and treated for 2h or overnight with 4 µg/ml anti-CD20 (I-20) antibody. Next, cells were collected and stained with Annexin V and propidium iodide using the AnnexinV-FITC Apoptosis Detection Kit (Bender MedSystems, Wien, Austria) essentially following the instructions of the manufacturer. Samples were analyzed on a FC500 MCL Sys-tem with CXP software.

16. CD20 gene silencing

To obtain CD20-silenced C2C12 myoblasts, we used commercially available lentiviral particles containing three target-specific constructs that encode 19- to 25-nt (plus hairpin) shRNA designed to knock down CD20 mRNA (CD20 shRNA (m); Lentiviral Parti-cles, Santa Cruz Biotechnology, Inc., Santa Cruz, CA, USA). Briefly, cells were plated at 10^4 cells per 48-well tissue culture plate, and 10^5 infectious units of virus were added to the culture medium (MOI = 10). The medium was replaced 24 h after infection, and infected cells were selected with puromycin (1–2 µg/ml) (Sigma, Milan, Italy) for 3 weeks. Using the same procedure, we also pre-pared C2C12 myoblasts infected with an shRNA construct encoding a scrambled sequence that will not lead to the specific degradation of any known cellular mRNA (Control shRNA; Lentiviral Particles, Santa Cruz Biotechnology, Inc., Santa Cruz, CA, USA), for use as controls. As described above, semi-quantitative RT-PCR and WB were performed on puromycin-selected cells to monitor CD20 expression knock down.

17. Quantitative evaluation of intracellular Ca^{2+} dynamics in skeletal myoblasts

Normal or silenced C2C12 myoblasts were cultured for 24–36h before measuring store-operated Ca^{2+} entry. Cells receiving antibody treatment were incubated overnight with 4 µg/ml anti-CD20 (I-20) or anti-FLAG (used as control) (Sigma-Aldrich; Italy). Cultures were loaded for 45 min at 37℃ with 1 µM Fura-2-AM (Life Technologies, Italy) in Krebs–Ringer solution buffered with HEPES, 125 mM NaCl, 5 mM KCl, 1.2 mM $MgSO_4$, 2 mM $CaCl_2$, 10 mM glucose, and 25 mM HEPES (pH 7.4), and were washed twice with pre-warmed calcium free Krebs–Ringer solution before recordings were made. Cells were recorded in calcium free Krebs–Ringer solution added with 500 µM EGTA (Sigma–Aldrich; Italy), then exposed to 10 µM thapsigargin (Sigma–Aldrich; Italy). Following cell response, 2 mM $CaCl_2$ was

added to the solution and SOCE response was recorded. The recording setting comprised an inverted microscope (Leica, DMI600B) equipped with a Ca^{2+} imaging unit. Polychrome IV (TILL Photonics; Germany) was used as a light source. Fura-2 fluorescence images were collected with a Andor CCD Camera (Axon Instruments, CA, USA) and analyzed with Imaging WorkBench 6 (INDEC BioSystem, Santa Clara USA). Single-cell 340/380 nm fluorescence ratios were analyzed with Origin 6.0 (Microcal Software Inc., MA, USA).

18. Statistics

Values are expressed as mean ± SEM. Statistical comparison among three or more groups was conducted using one-way ANOVA, followed by Bonferroni's multiple comparison test to determine significance (*P < 0.05, **P < 0.01, ***P < 0.001). Otherwise, Student's t-test was applied.

RESULTS

1. CD20-related pathway affecting intracellular Ca^{2+} is differently activated in dystrophic circulating progenitors retaining myogenic potential

The myogenic capacity of human blood-derived progenitors expressing the CD133 surface marker was previously described [50, 220]. However, the conditions of calcium-release and the role of SOCCs in these cells are not known. The extensively reported impairment of Ca^{2+} homeostasis affecting dystrophic muscular cells, together with its central role in all living cells physiology, prompted us to focus our efforts on the evaluation of calcium handling in normal and dystrophic blood-derived $CD133^+$ stem cells and, eventually, on the molecular characterization of highlighted differences.

1.1 Immunophenotyping of blood-derived $CD133^+$ stem cells

Surface antigens expressed by normal and dystrophic circulating CD133+ stem cells were characterized by means of flow cytometry analysis. Hoechst 33342 staining did not reveal the presence of Side Population (SP) fraction among isolated $CD133^+$ cells (99% ± 1% [mean ± SD])(data not shown), moreover up to 98% of blood-derived $CD133^+$ stem cells showed a lin^- phenotype ($CD4^-$ $CD8^-$ $CD3^-$ $CD19^-$ $CD33^-$ $CD38^-$) (data not shown). Normal and dystrophic circulating $CD133^+$ stem cells represented less than 0.2% (range 0.04 ± 0.1%, n = 12 normal blood; range 0.06 – 0.2%, n = 33 DMD blood) of total blood mononucleated cells as previously described [50]. Interestingly, normal and dystrophic circulating $CD133^+$ stem cells co-expressed the B-cell marker CD20 (Fig. 1A). More than 92% of normal and dystrophic circulating $CD133^+CD20^+$ cells also co-expressed CXCR4 and CD34 antigens (Fig. 1A). By FACS analysis, the percentage of $CD133^+$ stem cells expressing the CD20 antigen was not statistically significantly higher in the DMD subpopulation than the normal counterpart (27.9% ± 11% vs. 30.1% ± 13.1%; $p>0.5$) (Fig. 1A). Moreover, two subpopulations within the circulating $CD133^+CD20^+$ cells were observed distinguishing the $CD133^+CD20^{bright}$ (1.7 ± 2.1 and 2.1 ± 1.5 cells/ml from normal and dystrophic blood samples, respectively; $p>0.5$) and the $CD133^+CD20^{dim}$ (0.8 ± 0.3 vs. 1.1 ± 0.5 cells/ml; from normal and dystrophic blood samples, respectively; $p>0.5$) (Fig. 1B). In order to quantify the number of CD20 molecules on the circulating $CD133^+CD20^+$ cells we used the Quantibrite™ Beads system. By this method we found no significant differences between the number of CD20 antigens expressed in normal and dystrophic $CD133^+CD20^{bright}$ (27780 ± 12681 vs. 31419 ± 18112 antibody bound per cell, ABC; $p>0.5$) and $CD133^+CD20^{dim}$ (1307 ± 491 vs. 1469 ± 1023 antibody bound per cell, ABC; $p>0.5$) (Fig. 1C). These results demonstrate that the percentage of circulating $CD133^+CD20^+$ cells and the number of CD20 molecules expressed on the cell membrane is similar in normal and dystrophic specimens.

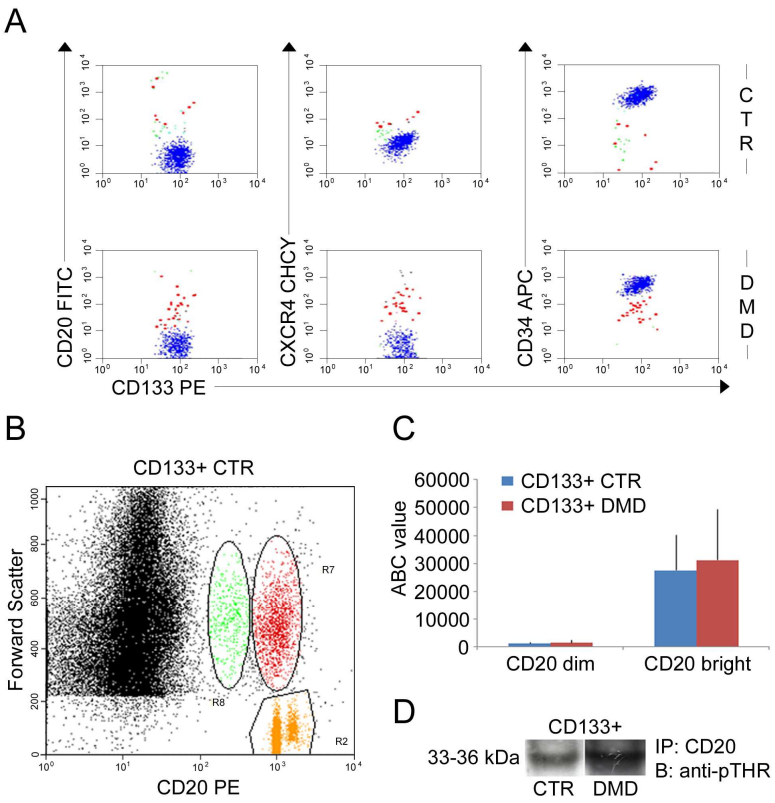

Figure 1: Characterization of blood-derived CD133+ stem cells immunophenotype. (A) *FACS immunophenotyping of the fractionated normal (lane CTR) and dystrophic (lane DMD) circulating CD133$^+$ stem cells. Normal and dystrophic circulating CD133$^+$ stem cells coexpressed the B-cell marker CD20, and more than 92% of normal and dystrophic circulating CD133$^+$CD20$^+$ cells also co-expressed CXCR4 and CD34 antigens.* ***(B)*** *The BDKit analysis allowed us to identify two subpopulations within the circulating CD133$^+$ stem cells distinguishing the CD133$^+$CD20^{bright} and the CD133$^+$CD20^{dim}.* ***(C)*** *The BD Quantibrite™ Beads system was used to quantify the number of CD20 molecules on the circulating CD133$^+$CD20$^+$ cells. No significant differences were found in the number of CD20 antigens expressed by normal and dystrophic CD133$^+$CD20^{bright} and CD133$^+$CD20^{dim}.* ***(D)*** *Immunoblotting results showed an increased phosphorylation of CD20 on threonine residues in dystrophic circulating CD133$^+$ stem cells (lane DMD)in comparison to the normal counterpart (lane CTR).*

1.2 CD20 phosphorylation is enhanced in dystrophic blood-derived CD133$^+$ stem cells

To test whether the unexpected expression of CD20 antigen in the circulating normal and dystrophic CD133$^+$ stem cells could be related to a possible functional pathway, we decided to look at its phosphorylation state by performing immunoprecipitation experiments followed by Western blotting. No tyrosine residues or recognized signaling motifs occur in any of the cytoplasmic regions of

CD20, although there are a number of consensus sites for serine or threonine phosphorylation [138]. CD20 was immunoprecipitated from normal and dystrophic circulating CD133$^+$ stem cells, separated by SDS-PAGE, transferred to membranes and probed with anti-phosphoserine or anti-phosphothreonine antibody. No difference was observed concerning serine phosphorylation between normal and dystrophic circulating CD133$^+$ stem cells (data not shown), while CD20 showed a higher threonine phosphorylation in dystrophic circulating CD133$^+$ stem cells (Fig. 1D). Taken together these observations supported the state of activation of the CD20 antigen, particularly in dystrophic circulating CD133$^+$ stem cells.

1.3 Impairment of calcium homeostasis in dystrophic blood-derived CD133$^+$ stem cells

Since CD20 expression and its phosphorylation state in circulating CD133$^+$ stem cells could be involved in the regulation of the calcium homeostasis [135-138], we first performed measurements of $[Ca^{2+}]_i$ on normal and dystrophic blood-derived CD133$^+$ stem cells. In these experiments, we evaluated the number of cells displaying a concentration of cytosolic free calcium to be higher than a reference value of 100 nM. In order to quantify the intracellular calcium, we used the dual wavelength ratiometric dye Fura-2. In this experiment, we found a significantly higher percentage of cells exceeding this reference value in dystrophic circulating CD133$^+$ stem cells compared to the normal counterpart ($p<0.001$) (Fig. 2A). We also noted that dystrophic circulating CD133$^+$CD20$^+$ cells displayed a higher susceptibility than their normal counterparts to increase $[Ca^{2+}]_i$ in response to both high $[K]_o$ (100 mM) and ionomycin (1 mM) (Fig. 2B). This feature was not further studied. However, these data suggest an impairment of Ca^{2+} homeostasis in the circulating dystrophic CD133$^+$CD20$^+$ cells.

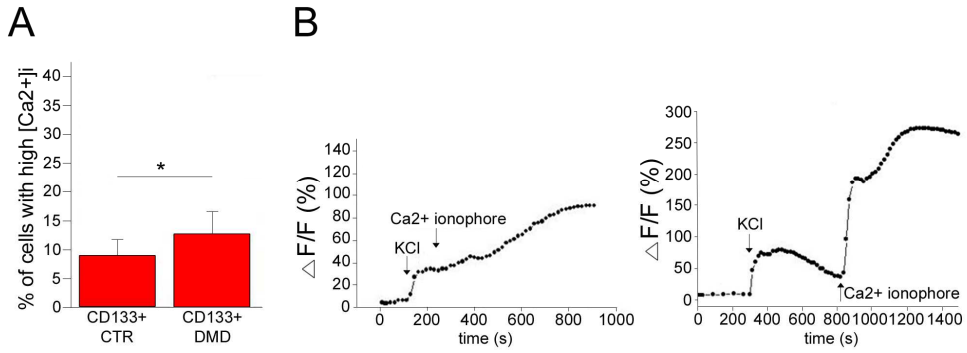

Figure 2: Evaluation of intracellular free Ca2+ in normal and DMD blood-derived CD133+ stem cells. (A) *The number of normal and dystrophic blood-derived CD133$^+$ stem cells displaying an $[Ca^{2+}]_i$ exceeding the reference value of 100 nM was quantified and expressed as percentage (%) of the total cells analyzed. The number of cells with high $[Ca^{2+}]_i$ was significantly higher in DMD blood-derived CD133$^+$ stem cells than in normal counterpart ($p<0.001$).* ***(B)*** *Illustrates the time course of the change in the Fluo3 emission in normal (left side) and dystrophic (right side) circulating CD133$^+$CD20$^+$ cells, induced by raising the extracellular KCl concentration from 5 to 100mM and then applying calcium ionophore during the early response steady state. $[Ca^{2+}]_i$ increase, measured as*

pseudoratio (ΔF/F%), was abnormally high in dystrophic circulating CD133$^+$CD20$^+$ cells.

1.4 Abnormal BDNF release from dystrophic blood-derived CD133$^+$ stem cells

Since no natural agonist for CD20 has been identified until now, we considered the possibility that CD20 channel and/or signal transduction activity can be indirectly activated by cytokines or growth factors after interaction with their own receptors and consequent activation of intracellular signaling cascades. Following this hypothesis, we decided to perform an ELISA screening, looking for released factors over-expressed by dystrophic circulating CD133$^+$ stem cells. Supernatants were collected after 24 h of culture and the concentrations of IGF-1, VEGF, BDNF and TGFβ-1 were measured. Results are expressed as a ratio concentration/cell number in culture. While IGF-1 and VEGF were detected in similar amounts in normal and dystrophic circulating CD133$^+$ stem cell supernatants (IGF-1: 1.1 x 10^{-7} normal vs. 1.8 x 10^{-7} dystrophic) (Fig. 3A); (VEGF: 2.0 x 10^{-3} normal vs. -8.5 x 10^{-4} dystrophic) (Fig. 3B), BDNF and TGFβ-1 displayed a different release profile comparing healthy and dystrophic circulating CD133$^+$ stem cells. BDNF measurement in dystrophic blood derived CD133$^+$ stem cell supernatant returned a ratio that was six-fold increased in comparison to that obtained from normal cells (1.5 x 10^{-4} normal vs. 6.1 x 10^{-4} dystrophic; $p<0.05$) (Fig.3C). A similar trend was observed considering TGF-β1, with a ratio of 5.8 x 10^{-3} in normal circulating CD133$^+$ stem cells that increased to a value of 2.6 x 10^{-2} in dystrophic circulating CD133$^+$ stem cells ($p<0.05$, Fig. 3D). In order to verify whether the increased ratio obtained after BDNF and TGFβ-1 dosage in DMD supernatants was a CD133$^+$ stem cells specific feature, we performed the same measurements on normal and dystrophic CD133$^-$ cells. Even with no significant difference, TGFβ-1 ratio showed the same increasing trend observed in dystrophic circulating CD133$^+$ stem cells (Fig. 3F). On the contrary, the ratio obtained after BDNF dosage was similar comparing normal and dystrophic CD133$^-$ cells (Fig. 3E). Reported data clearly describe two different phenomena: 1) a generalized TGFβ-1 over-expression affecting dystrophic circulating cells, with no difference between CD133 positive and negative fractions; 2) a BDNF over-expression that specifically affects dystrophic circulating CD133$^+$ stem cells, thus promoting this cytokine as a possible candidate for the indirect modulation of CD20 phosphorylation and signaling activity.

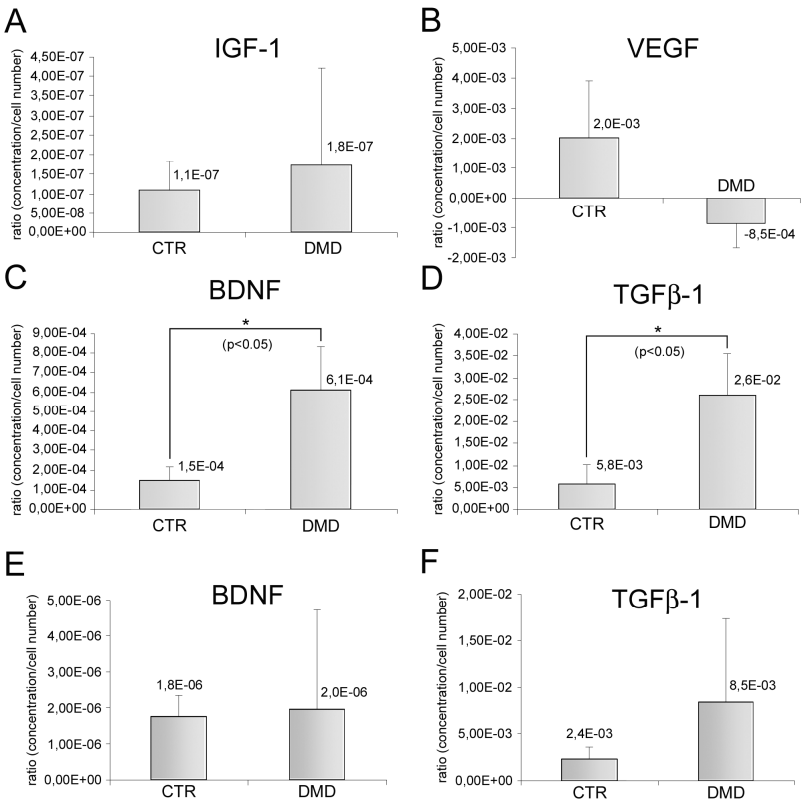

Figure 3: ELISA quantification of cytokines release by normal and DMD blood-derived CD133+ stem cells. (A and B) *IGF-1 and VEGF were detected in similar amounts in normal and dystrophic circulating CD133$^+$ stem cell supernatants.* ***(C)*** *BDNF measurement in dystrophic blood-derived CD133$^+$ stem cell supernatant returned a ratio that was six-fold increased in comparison to that obtained from normal cells.* ***(D)*** *A similar trend was observed considering TGF-ß1.* ***(E and F)*** *Measurements performed on normal and dystrophic CD133$^-$ cell supernatants allowed to identify BDNF over-expression as an exclusive property of dystrophic circulating CD133$^+$ stem cells. On the contrary, TGF-ß1 over-expression affects dystrophic cells with no difference between CD133 positive and negative fractions.*

1.5 BDNF induces CD20-related intracellular signaling activation in dystrophic blood-derived CD133$^+$ stem cells

Since all the functions of BDNF are mediated by the TrkB pathway, including the protein kinase C (PKC), an enzyme involved in CD20 phosphorylation [134, 221-223], we investigated the role of BDNF in CD20 phosphorylation and signaling modulation. We first decided to evaluate the effect of BDNF on CD20 phosphorylation performing immunoprecipitation and Western blotting experiments. Normal and dystrophic circulating CD133$^+$ stem cells were stimulated with BDNF (100 ng/ml for 2h) and CD20 immunoprecipitation was performed on cell lysates followed by phosphothreonine immunoblotting. After BDNF treatment, a strong

induction of CD20 phosphorylation was observed both in normal and dystrophic blood-derived $CD133^+$ stem cells (Fig. 4A). Moreover, in dystrophic circulating $CD133^+$ stem cells CD20 was heavily threonine-phosphorylated also in basal condition, probably as a consequence of the higher BDNF release described above (Fig. 4A). Tyrosine kinases can associate with the cytoplasmic regions of cell-surface molecules by different mechanisms, promoting intracellular signaling transduction. Previous studies reported CD20-specific association with src-family members Lyn, Fyn and Lck, along with a tyrosine phosphorylated protein (p75/80) later identified as PAG, a ubiquitous adaptor protein [138, 224, 225]. Importantly, it is possible that changes in either the conformation of CD20 or its phosphorylation state, or both, could regulate its association with such kinases. To determine whether or not BDNF induced phosphorylation is followed by the activation of CD20-related downstream signaling pathway, we performed experiments in order to analyze CD20-recruited src kinases and their activation state. Considering that Lyn accounted for most of the protein tyrosine kinase (PTK) activity in the CD20 complex [224], we focused our attention on this src-family member. Immune complexes were prepared from lysates of normal and dystrophic circulating $CD133^+$ stem cells using anti-CD20 antibody. After SDS-PAGE separation, membranes were blotted with anti-Lyn antibody, then stripped and re-probed for the evaluation of tyrosine phopshorylation. Densitometric analysis performed on obtained bands showed that, although Lyn was co-immunoprecipitated with CD20 in all the conditions tested, after BDNF stimulation CD20 immune complexes contained a higher Lyn content both in normal and dystrophic circulating $CD133^+$ stem cells, suggesting an induction of Lyn-CD20 interaction after BDNF exposure (Fig. 4B). Particularly, even if CD20-recruited Lyn was higher in dystrophic unstimulated blood-derived $CD133^+$ stem cells in comparison to normal unstimulated bloodderived $CD133^+$ stem cells (threefold increase), the effects promoted by BDNF on Lyn association to CD20 were more consistent in dystrophic circulating $CD133^+$ stem cells (+43%) than in normal circulating $CD133^+$ stem cells (+30%) (Fig. 4C). Membrane reprobing with anti-phosphotyrosine antibody allowed us to analyze the activation state of CD20-recruited Lyn. After BDNF treatment, only dystrophic circulating $CD133^+$ stem cells showed phosphorylation increase in the Lyn fraction co-immunoprecipitated with CD20 (Fig. 4D). As a consequence, the ratio phopsho/total protein decreased differently in normal (–29%) and dystrophic circulating $CD133^+$ stem cells (–9%) (Fig. 4E). Together, these results demonstrate that CD20-related signaling can be indirectly modulated by BDNF. Interestingly, effects on CD20 threonine phosphorylation and Lyn recruitment were observed, even if with different intensity, both in normal and dystrophic circulating $CD133^+$ stem cells. On the contrary, only in dystrophic blood-derived $CD133^+$ stem cells does recruited Lyn undergo phosphorylation after BDNF treatment, possibly promoting the activation of additional intracellular pathways that can act synergically with TrkB.

1.6 BDNF induces a different increase of intracellular Ca^{2+} levels in normal and dystrophic blood-derived $CD133^+$ stem cells

Differences concerning the activation of CD20-recruited Lyn after BDNF stimulation, observed while comparing normal and dystrophic circulating $CD133^+$ stem cells, invited us to consider the effects on cytosolic Ca^{2+} promoted by a potential simultaneous activation of TrkB and CD20-Lyn pathways in dystrophic circulating $CD133^+$ stem cells. As previously described, once activated, TrkB can drive intracellular Ca^{2+} release by means of PLCγ activation and consequent production of the second messenger IP3. Lyn activation triggers a cascade of signaling events mediated by Lyn phosphorylation of tyrosine residues within the immunoreceptor tyrosine-based activation motifs of receptor proteins, and subsequent recruitment and activation of other kinases, PLCγ2 and phosphoinositide 3-kinase (PI3-K) [226]. These kinases provide activation signals that play critical roles in proliferation, cell differentiation and Ca^{2+} mobilization. Since in normal cells Lyn is recruited by CD20 but fails to become phosphorylated, the synergic action between the two pathways after BDNF exposure could take place only in dystrophic circulating $CD133^+$ stem cells, where a more intense increase of $[Ca^{2+}]_i$ is thus expected. To assess this hypothesis, we performed experiments for the quantification of intracellular free Ca^{2+} in normal and dystrophic circulating $CD133^+$ stem cells in the unstimulated condition (basal) and after BDNF treatment. In normal circulating $CD133^+$ stem cells we found that BDNF was able to induce an increase in $[Ca^{2+}]_i$ that, even if appreciable, was not significant when compared to cells analyzed in basal condition ($p=0.122$) (Fig. 4F). In contrast, calcium measurements performed on dystrophic circulating $CD133^+$ stem cells showed a significant increase between basal and BDNF treated cells ($p<0.001$) (Fig. 4F). Moreover, the observed intracellular Ca^{2+} increase was much higher in comparison to that obtained in normal circulating $CD133^+$ stem cells subjected to identical treatment (Fig. 4F). Data reported here describe a different response to BDNF in normal and dystrophic circulating $CD133^+$ stem cells in terms of intracellular calcium release, reflecting the fact that only in dystrophic circulating $CD133^+$ stem cells does the CD20-Lyn pathway undergo activation after BDNF exposure, leading to the supplementary calcium release observed.

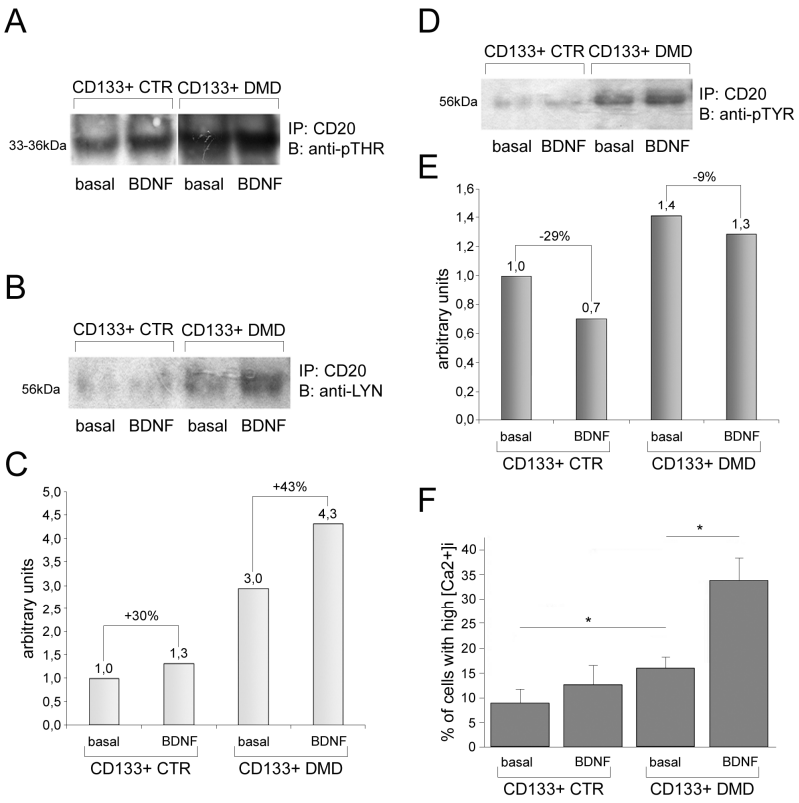

Figure 4: BDNF modulation of CD20-related signaling pathway. (A) *Induction of CD20 phosphorylation by BDNF in normal and dystrophic blood-derived CD133$^+$ stem cell. In dystrophic circulating CD133$^+$ stem cells CD20 was heavily threonine-phosphorylated also in basal condition.* ***(B)*** *After BDNF stimulation CD20 immune complexes contained a higher Lyn content both in normal and dystrophic circulating CD133$^+$ stem cells, suggesting an induction of Lyn-CD20 interaction.* ***(C)*** *The effects promoted by BDNF on Lyn association to CD20 were more consistent in dystrophic (+43%) than in normal circulating CD133$^+$ (+30%).* ***(D and E)*** *Only dystrophic circulating CD133$^+$ stem cells showed a phosphorylation increase in the Lyn fraction co-immunoprecipitated with CD20 after exposure to BDNF. As a consequence, the ratio phopsho/total protein decreased differently in normal (–29%) and dystrophic circulating CD133$^+$ stem cells (–9%).* ***(F)*** *Calcium measurements performed on dystrophic circulating CD133$^+$ stem cells showed a significant increase between basal and BDNF treated cells ($p<0.001$). Such increase was much higher in comparison to that obtained in normal circulating CD133$^+$ stem cells subjected to identical treatment. Data were collected from 2070 basal CTR, 2080 basal DMD, 2668 BDNF CTR and 2118 BDNF DMD cells. The differences marked by an asterisk are statistically significant ($p<0.001$ ANOVA).*

1.7 Blood-derived CD133$^+$ stem cells express the Dp71 dystrophin isoform

Total mRNA was collected and analyzed by RT-PCR. Normal blood-derived CD133$^+$ stem cells expressed the mRNA of the ubiquitous 71 kDa dystrophin isoform (Fig. 5A). No expression of the 116-kD, 140-kD, 260-kD and 427 kDa dystrophin isoforms mRNA was observed in these cells (Fig. 5A). On the contrary, although the DMD genotypes analyzed (Δ11–13; Δ26– 30; Δ45– 52; Δ4-6-8-12-13; Δ17–44; Δ42– 51; Δ43– 45; Δ49– 52; exon 2 duplication) were formally compatible with the expression of Dp71, all the dystrophin isoforms mRNA were absent in dystrophic circulating CD133+ stem cells, including the Dp71 (Fig. 5A). As expected, the Western blot analysis confirmed the expression of the Dp71 dystrophin isoform only in the normal blood-derived CD133$^+$ stem cells (Fig. 5B). Importantly, neither normal nor dystrophic circulating CD133$^-$ cells expressed the Dp71 dystrophin isoform (Fig. 5B), demonstrating that the expression of Dp71 is a CD133$^+$ stem cells specific feature.

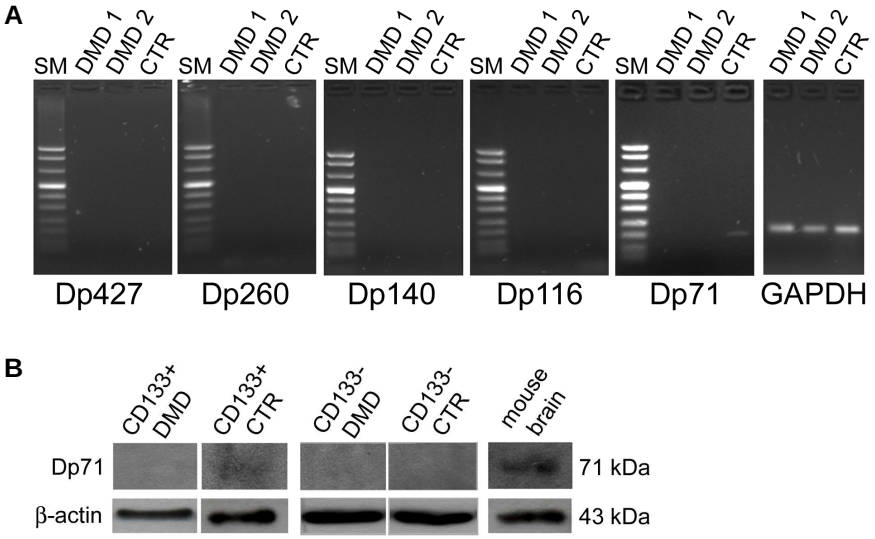

Figure 5: Dp71 expression by circulating CD133+ stem cells. (A) *PCR results from normal and dystrophic blood-derived CD133$^+$ stem cells after seven days of culture in proliferation (stem-cell-conditioned) media. The first five gels correspond to the expression of the different dystrophin isoforms indicated in (A). Last gel corresponds to the amplification of the GAPDH gene as standard (PCR fragment 150 bp). Only the Dp71 mRNA is expressed by normal circulating CD133$^+$ stem cells in these conditions (PCR fragment 193 bp). (Size Marker, SM).* ***(B)*** *Immunoblotting analysis confirmed that only normal blood derived CD133$^+$ stem cells are able to express the Dp71 dystrophin isoform also at protein level (lane CD133$^+$ CTR). Neither normal nor dystrophic CD133$^-$ cells expressed the Dp71 at protein level (lanes CD133$^-$ DMD and CD133$^-$ CTR). Mouse brain homogenate was used as control. β-actin immunoblotting indicated that the same protein concentration was present in all specimens.*

2. CD20 is expressed in skeletal myoblasts and contributes to calcium handling by modulating SOCE

Different studies showed that CD20 can associate with lipid raft domains of the plasma membrane, where it is probably involved in store-operated Ca^{2+} entry (SOCE) [139, 140]. The main actors of this process have been identified [110, 111, 117, 119, 133]; however, there are still several important unresolved issues regarding SOCE in skeletal muscle, including the identification of mechanisms and molecules involved in the fine regulation of this crucial pathway. The possible contribution of CD20 to the regulation of Ca^{2+} handling in skeletal muscle is an important point to address, especially considering that circulating $CD133^{+}$ progenitors and committed muscular cells share common mesodermic origins. Human muscle biopsies for research purposes are not easy to obtain, particularly from DMD patients. Accordingly, we started to evaluate the expression and the role of CD20 as a mediator/modulator of SOCE in C2C12 murine skeletal myoblasts cell line.

2.1 CD20 mRNA is detected in myoblasts and mature muscle fibers

To investigate CD20 expression in C2C12 myoblasts, we first assayed for the presence of CD20 mRNA by RT-PCR analysis. Total RNA was collected and analyzed using two pairs of specific primers, one directed against the 3'-UTR (F1–R1) and one targeting the ORF (F2–R2). CD20 transcript was clearly detectable in growing C2C12 myoblasts, and its expression was maintained after 10 days of differentiation (myotubes) (Fig. 6A). To evaluate CD20 expression in mature fibers, we analyzed three muscle types that differ in myosin heavy chain isoform content, anatomical localization, and function-ality. CD20 mRNA was present in tibialis anterior (TA), quadriceps (QA), and diaphragm (DIA) from 3-month-old C57BL mice (Fig. 6B). Since data on CD20 expression from whole muscle may be biased by the presence of non-muscular CD20-expressing cells (e.g., cir-culating B-cells), we confirmed these results by performing RT-PCR on single muscle fibers. We detected CD20 mRNA in single fibers isolated from TA, QA, and DIA of C57BL mice (Fig. 6C), thus verifying the expression of CD20 at the mRNA level from myoblasts to mature muscle fibers. Sequencing of RT-PCR products from spleen, whole muscle, and isolated muscle fibers confirmed the amplified cDNA as CD20 (Fig. 6D).

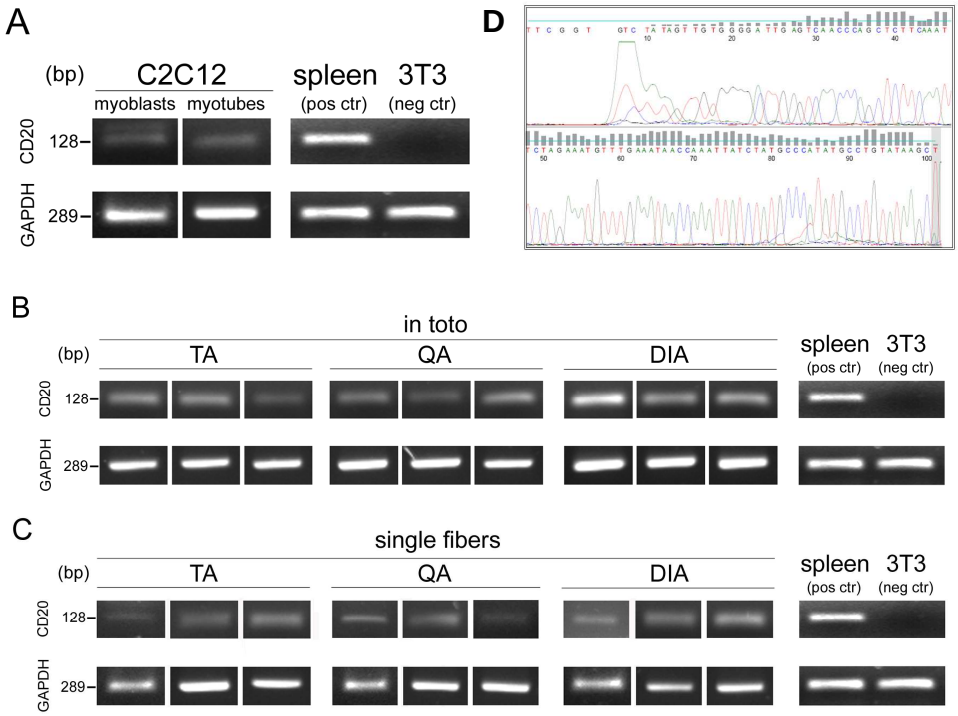

Figure 6: RT-PCR analysis of CD20 expression. (A) *The presented bands were obtained using F1–R1 primers targeting the 3'-UTR of CD20 mRNA. Amplification with F2–R2 primers targeting the ORF of CD20 mRNA produced identical results.* ***(A)*** *CD20 mRNA was successfully amplified from growing C2C12 myoblasts and C2C12-derived myotubes.* ***(B)*** *Analysis of whole muscles returned a CD20-specific band in TA, QA, and DIA from C57BL mice.* ***(C)*** *CD20 mRNA was also detected in isolated muscle fibers from the same muscles, providing evidence of a muscle-specific expression.* ***(D)*** *Bands obtained after F1–R1 amplification from spleen, whole muscle, and isolated fibers were sequenced to confirm the identity of amplified product as CD20. RNA from C57BL spleen and 3T3 fibroblasts were used as positive and negative controls, respectively. GAPDH was used as a loading control.*

2.2 Localization of CD20 in muscle cells and fibers

Using western blot analysis with a polyclonal anti-CD20 antibody, proteins with molecular weights corresponding to that of CD20 (33–37 kD) were identified in both growing C2C12 myoblasts and C2C12-derived myotubes (Fig. 7A). The same signal was obtained in TA, QA, and DIA whole muscles and single fibers (Fig. 7B and C), revealing the presence of CD20 protein in all assayed samples. We considered that our findings of CD20 in mature muscle fibers could be due to a fusion process involving circulating $CD20^+$ cells *in vivo*. To address this crucial point, we performed WB analysis on muscles isolated from SCID mice, which completely lack any potentially contaminating $CD20^+$ B-lymphocytes due to genetic depletion [217, 218]. Importantly, the polyclonal anti-CD20 antibody still stained a

33- to 37-kD band in TA, QA, and DIA muscles from SCID mice (Fig. 7D). WB analysis using a monoclonal anti-CD20 anti-body confirmed these results in all tested muscle samples (Fig. 7E). CD20 protein expression was comparable in C57BL whole muscles and single fibers, as well as in TA, QA and DIA from SCID mice (data not shown). Notably, we failed to detect CD20 by WB in brain, kidney, and lung (Fig. 7F), indicating that this protein is not broadly expressed. Flow cytometry analysis revealed up to 80% $CD20^+$ C2C12 myoblasts with both polyclonal (Fig. 8A) and monoclonal (Fig. 8B) anti-CD20 antibodies, confirming the expression of CD20 protein and suggesting its membrane localization. To investigate the spatial localization of CD20, immunofluorescence analyses were performed on C2C12 myoblasts/myotubes and cryosections from C57BL and SCID muscles. In cultured C2C12 myoblasts/myotubes, CD20 staining showed a spotted pattern surrounding the entire cell body, typical of surface antigens when detected in culture. Additionally, CD20 nearly co-localized with laminin, suggesting its membrane localization on cultured muscle cells [227] (Fig. 8C and D). The membrane localization of CD20 was also observed in adult muscle fibers from C57BL mice, where the signal returned by the monoclonal anti-CD20 antibody co-localized with the transmembrane protein α-sarcoglycan (Fig. 8E). Moreover, IF experiments confirmed the expression and the membrane localization of CD20 in TA and QA muscles isolated from immune-deficient SCID mice (Fig. 8F). IF observations were supported by WB analyses on isolated sarcolemma from C57BL TA, QA, and DIA, which confirmed CD20 expression at the membrane level in adult muscle fibers (Fig. 7G). Pre-exposure of anti-CD20 antibody to a specific blocking peptide resulted in a significant reduction of signal on a positive source of CD20 (C57BL spleen), as well as on C2C12 myoblasts, verifying the antibody's ability to bind its specific target (data not shown). Together, these data demonstrated the expression of CD20 protein in muscle, and excluded the possibility that this result was an artifact due to contaminating circulating $CD20^+$ cells.

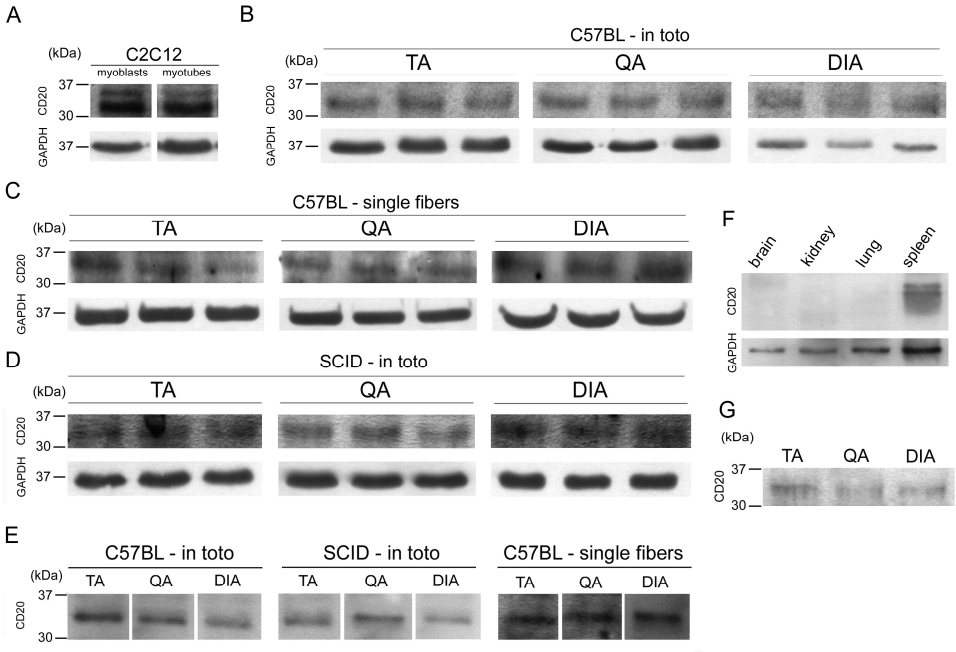

Figure 7: Western blot analysis of CD20 expression. (A–C) *Immunoblotting experiments using the anti-CD20 (M-20) antibody confirmed the presence of CD20 at the protein level in C2C12 myoblasts/myotubes, as well as in C57BL TA, QA, and DIA whole muscles and single fibers.* ***(D)*** *A CD20 band was also obtained with the same antibody in whole muscles isolated from B cell-depleted SCID mice, confirming that the CD20 expression was truly from muscle cells.* ***(E)*** *WB data were confirmed using a monoclonal antibody directed against the C-terminal region of CD20 in C57BL (in toto and as single fibers) and SCID (in toto) muscles.* ***(F)*** *WB analyses were performed on brain, kidney, and lung from C57BL mice using the anti-CD20 (M-20) antibody, revealing that CD20 was not broadly expressed in all tissues.* ***(G)*** *Membrane localization of CD20 was assessed by performing WB with anti-CD20 (M-20) antibody on isolated sarcolemma from C57BL TA, QA, and DIA muscles.*

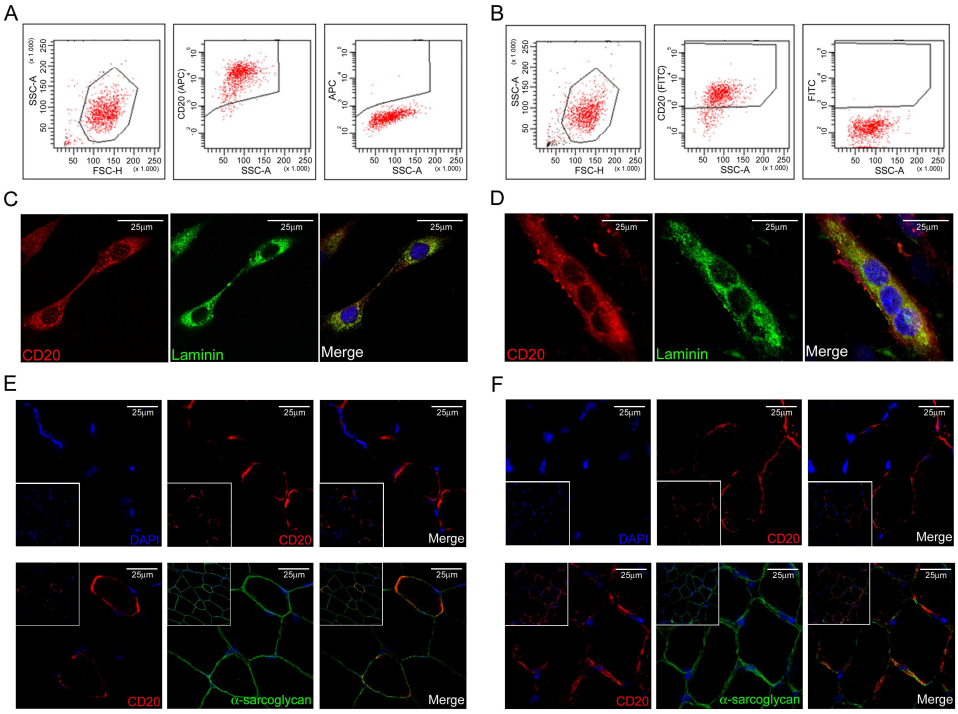

Figure 8: Analysis of CD20 localization. *Flow cytometry analysis returned about 80% CD20^{+} C2C12 myoblasts, using both a polyclonal* ***(A)*** *and a monoclonal* ***(B)*** *anti-CD20 antibody; cells stained with the appropriate isotype control (goat and rabbit IgG, respectively), were assayed as controls. Immunofluorescence staining was performed to evaluate the spatial localization of CD20 in C2C12 myoblasts/myotubes and adult muscle fibers. The anti-CD20 (M-20) antibody showed a spotted pattern surrounding the entire cell body and nearly co-localizing with laminin, suggesting the membrane localization of CD20 in myoblasts* ***(C)*** *and myotubes* ***(D)****. Muscle fibers expressing CD20 at the sarcolemma were detected using the anti-CD20 (C-term) monoclonal antibody in TA and QA muscles from C57BL* ***(E)*** *and SCID mice* ***(F)****. The signal referring to CD20 co-localized with the transmembrane protein α-sarcoglycan. Images labeled as merge show the combination of all stained elements (CD20, laminin/ α-sarcoglycan, and nuclei).*

2.3 Identification of CD20 by mass spectrometry

To substantiate these findings, mass spectrometry (MS) was used to identify CD20 in skeletal muscle cells and tissue. CD20 immunoprecipitates were prepared from C2C12 myoblasts and QA muscles from C57BL or SCID mice, resolved by SDS-PAGE, and blotted with an anti-CD20 antibody. Stained bands that were also appreciable in silver-stained paired lanes from the same gel were recovered and processed for MS analysis, following in situ diges-tion and peptide extraction. CD20-derived peptides were detected in two bands from C2C12 myoblasts and three bands from C57BL and SCID QA (Fig. 9A), suggesting the presence of multiple CD20 isoforms in all analyzed samples. Approximately 50% amino acid sequence coverage was obtained (Fig. 9B) and the identified pep-tides returned a 100% alignment match, exclusively with CD20 (data not shown), confirming its expression in C2C12 myoblasts and adult muscle.

A

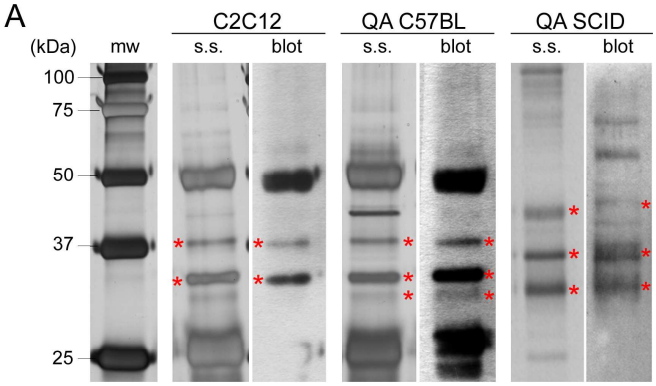

B

PEPTIDE	SEQUENCE	MW calculated[a]	MW observed[a]
1-11	MSGPFPAEPTK	1161.56	1161.81
1-21	MSGPFPAEPTKGPLAMQPAPK	2152.09	2152.63
12-40	GPLAMQPAPKVNLKRTSSLVGPTQSFFMR	3158.70	3159.18
22-26	VNLKR	629.40	629.05
27-40	TSSLVGPTQSFFMR	1577.77	1577.73
101-110	TSRKSLVKAK	1117.70	1117.81
104-110	KSLVKAK	773.53	773.65
105-110	SLVKAK	645.43	646.30
109-144	AKVIMSSLSLFAAISGIILSIMDILNMTLSHFLKMR	3965.19	3965.99
200-211	LVTAGIVENEWK	1358.73	1357.78
200-216	LVTAGIVENEWKRMCTR	2063.05	2064.01
213-216	MCTR	567.24	566.65
213-229	MCTRSKSNVVLLSAGEK	1879.97	1880.37
217-235	SNVVLLSAGEKNEQTIKMK	2045.12	2045.81
236-251	MKEEIIELSGVSSQPK	1774.92	1775.43

[a] The MWs are reported as monoisotopic mass

Figure 9: Mass spectrometry. (A) *Using the anti-CD20 (M-20) antibody, CD20 complexes were immunoprecipitated from C2C12 myoblasts, C57BL QA, and SCID QA, and resolved by SDS-PAGE. IP samples were split on multiple lanes of the same gel, some dedicated to WB and the others to silver staining. Bands stained with the anti-CD20 (M-20) antibody were identified and recovered from the*

silver-stained lanes for MS analysis. Two bands from myoblasts and three bands from C57BL and SCID QA were analyzed. ***(B)*** *The in-gel tryptic digest was extracted with 30 µl of 0.1% TFA:CH3CN (1:1), and the peptide mixture was subjected to MALDI-TOF analysis, operating in positive reflector mode with a matrix of α-ciano-4-hydroxy-cinnamic acid. Identified peptides were representative of 46.7% of the CD20 primary sequence.*

2.4 C2C12 proliferation and viability are not affected by anti-CD20 antibody

We next investigated the functional aspect of CD20 expression in skeletal muscle. In the context of B-lymphocytes, CD20 is usually related to cell-cycle progression and proliferation [228, 229]. Importantly, CD20 is tar-geted by clinical monoclonal antibodies that can deplete B cells *in vivo* via a Ca^{2+}-related apoptotic pathway [230-234]. To assess whether CD20 exerted similar functions in skeletal muscle, we assayed cell proliferation and apoptotic death on C2C12 myoblasts after exposure to anti-CD20 antibody. The MTT assay revealed no differences in proliferation behavior between untreated C2C12 myoblasts (OD ± SEM, 0.984 ± 0.063) and those treated for 2h with anti-CD20 antibody (4 µg/ml: 1.005 ± 0.024; 20 µg/ml: 0.952 ± 0.015) (Fig. 10A). Overnight treatment returned similar results (untreated 1.517 ± 0.061; 4 µg/ml: 1.342 ± 0.133; 20 µg/ml: 1.283 ± 0.060) (Fig. 10A). Similarly, flow cytometry analysis of Annexin V/propidium iodide (PI)-stained cells did not show any induction of apoptosis in C2C12 myoblasts after treatment with anti-CD20 antibody, either after 2h (% $AnnexinV^{+}PI^{+}$ ± SEM, 0.27 ± 0.09% vs. untreated 2h: 0.36 ± 0.09%) or overnight antibody exposure (0.4 ± 0.1% vs. untreated ON: 0.47 ± 0.09%) (Fig. 10B). These data describe a lack of coupling between anti-CD20 treatment and proliferative/apoptotic pathways, indicating that the function of CD20 in C2C12 myoblasts differs from that previously reported for CD20 in B-cells.

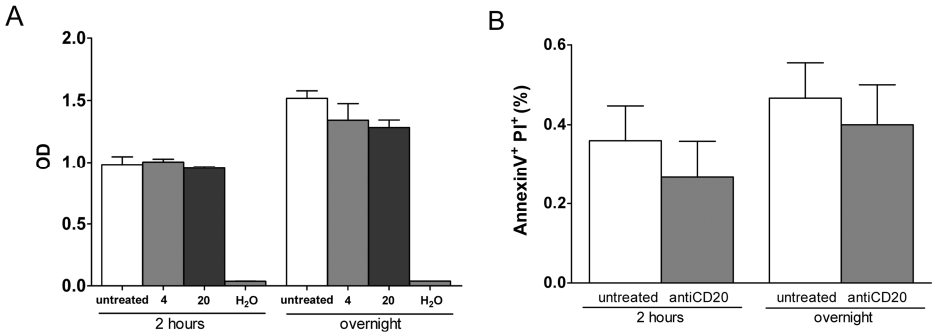

Figure 10: Evaluation of cell proliferation and viability after CD20 antibody targeting. (A) *The MTT assay revealed no differences in proliferation rates among C2C12 myoblasts that were exposed or not to the anti-CD20 (I-20) antibody, regardless of antibody concentration (4 or 20 µg/ml) or treatment duration (2h or overnight) (n = 3 for each condition).* ***(B)*** *Analysis of Annexin V-PI-stained C2C12 myoblasts showed that exposure to the anti-CD20 (I-20) antibody (4 µg/ml) had no effects on apoptotic cell death, either after 2h or overnight treatment (n = 6 for each condition).*

2.5 Stable CD20 silencing in C2C12 myoblasts

To expand the approaches aimed to investigate CD20 functionality in skeletal muscle, we stably knock down CD20 expression in C2C12 myoblasts. Cells were exposed to lentiviral particles delivering constructs that encode shRNA designed to target CD20 mRNA. Knock-down efficiency was assayed after selection of infected cells by RT-PCR and WB, revealing 70% knock down of CD20 gene expression (Fig. 11A) and 60% silencing at the protein level (Fig. 11B).

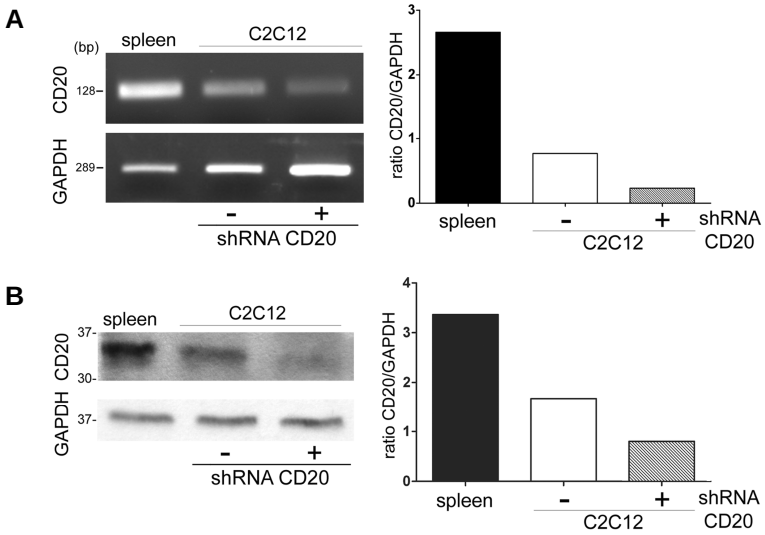

Figure 11: Evaluation of CD20 silencing. (A and B) *CD20 expression knock down was monitored by semi-quantitative RT-PCR and WB, after puromycin selection of infected cells. The F1–R1 primers (aligning in the 3'-UTR of CD20 mRNA) and the anti-CD20 (M20) antibody were used. C57BL spleen was assayed as a positive control, and GAPDH was used as a loading control.*

2.6 CD20 targeting affects store-operated Ca^{2+} entry in C2C12 myoblasts

To further investigate the function of CD20 expression in skeletal muscle, we explored its involvement in the control of intracellular Ca^{2+} dynamics. Several previous reports have suggested that CD20 may regulate Ca^{2+} influx by modulating or acting directly as a SOC channel [136, 137, 225, 235, 236]. Accordingly, we assessed whether CD20 targeting modulates the magnitude of SOCE in C2C12 myoblasts. After loading with Fura-2, cells displayed a homogeneous staining without dye accumulation into intracellular compartments (Fig. 12A). Real-time fluorescence recording was performed at resting conditions, then during the store-depletion step and throughout the increase of external Ca^{2+} concentration, such that both the preparative (store depletion) and effective (Ca^{2+} re-entry) phases of SOCE were monitored. After addition of extra-cellular Ca^{2+}, the 340/380 nm ratio showed a significantly lower increase in anti-CD20 treated myoblasts (n = 42) (Fig. 12C), indicating that Ca^{2+} re-entry induced by store-depletion was impaired in this condition (Δ340/380 ± SEM, untreated: 0.053 ± 0.003; anti-CD20: 0.025 ± 0.003; P

< 0.001) (Fig. 12G). Cells receiving control antibody (anti-FLAG; n = 32) (Fig. 12D) behaved identically to untreated cells (n = 41) (Fig. 12B), supporting the specificity of our observations (Δ340/380 ± SEM, untreated: 0.053 ± 0.003; anti-FLAG: 0.058 ± 0.003; P > 0.05) (Fig. 12G). Measurements of SOCE were also performed on CD20-silenced C2C12 myoblasts. Consistently to what observed after anti-CD20 treatment, SOCE was markedly reduced in CD20-silenced C2C12 myoblasts (n = 43) (Fig. 12E), as indicated by the lower increase in the 340/380 nm ratio measured after extracellular Ca^{2+} raising (Δ340/380 ± SEM, untreated: 0.053 ± 0.003; RNAi CD20: 0.020 ± 0.001; P < 0.001) (Fig. 12G). On the contrary, in cells infected with an shRNA encoding a scrambled sequence (n = 20) (Fig. 12F) the 340/380 nm ratio showed an increase comparable to that of untreated cells (Δ340/380 ± SEM, untreated: 0.053 ± 0.003; RNAi scrambled: 0.066 ± 0.005; P > 0.05) (Fig. 12G). Importantly, similar Δ340/380 nm ratios were observed in response to thapsigargin in all the conditions tested, ruling out the possibility that the impairment of SOCE observed after CD20-targeting was related to a lower depletion efficacy (Δ340/380 ± SEM, untreated: 0.053 ± 0.002; anti-CD20: 0.049 ± 0.002; anti-FLAG: 0.052 ± 0.004; RNAi CD20: 0.061 ± 0.006; RNAi scrambled: 0.047 ± 0.004; P > 0.05) (Fig. 12H). Similarly, the levels of intracellular Ca^{2+} recorded at rest were homogeneous among all the experimental conditions analyzed, with the exception of anti-CD20 treated cells showing a significantly higher concentration (data not shown). To assess whether CD20 targeting specifically modulated SOCE, cells were assayed in the presence of the SOC influx inhibitor BTP2. No differences were observed in Δ340/380 nm ratio when comparing anti-CD20- treated (n = 21) or CD20-silenced C2C12 myoblasts (n = 22) to cells receiving the SOCE blocker alone (n = 20), suggesting that CD20 targeting was ineffective if SOCE could not occur (Δ340/380 ± SEM, BTP2: 0.012 ± 0.001; BTP2 + anti-CD20: 0.012 ± 0.001; BTP2 + RNAi CD20: 0.013 ± 0.001; P > 0.05) (Fig. 12I).

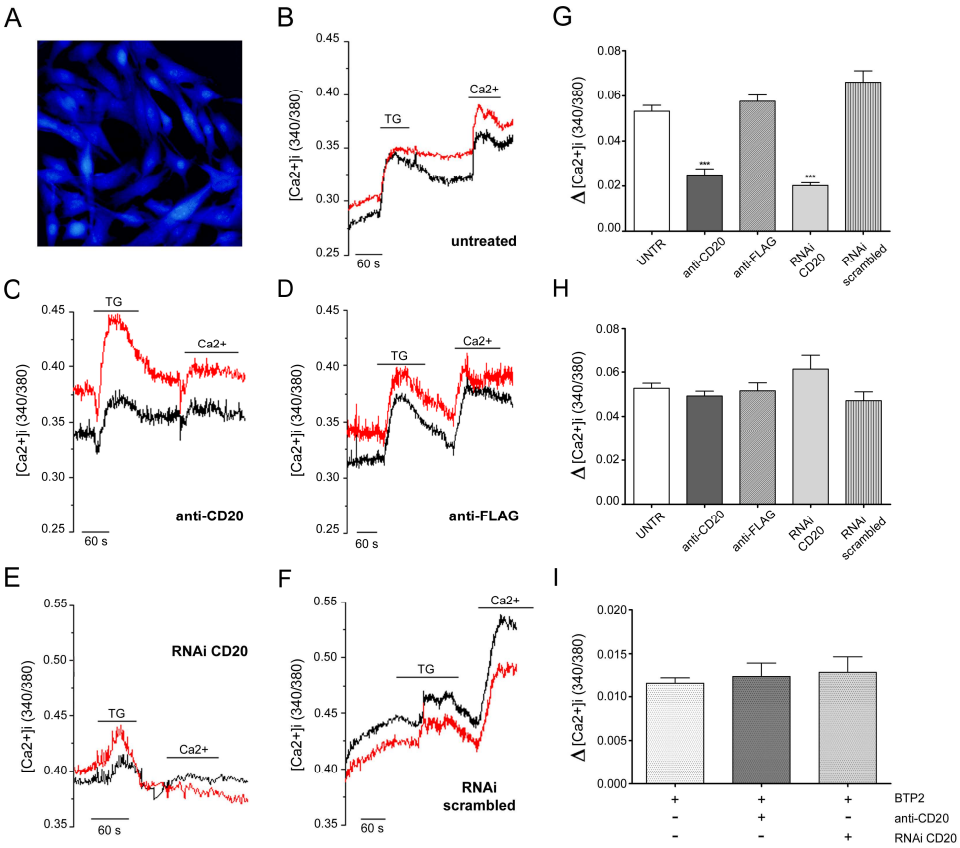

Figure 12: SOCE measurements on CD20-targeted C2C12 myoblasts. (A) *Ca^{2+} measurements were performed on cells displaying an homogeneous staining after loading with Fura-2-AM, thus avoiding biases due to dye accumulation into intracellular compartments.* ***(B–F)*** *Representative traces of the 340/380 nm excitation ratio are shown for each experimental condition assayed. Fluorescence was real-time recorded starting at rest, then during the store-depletion step with thapsigargin and throughout the addition of extracellular Ca^{2+}.* ***(G)*** *SOCE changes were quantified as _340/380 nm excitation ratio after addition of 2 mM extracellular Ca^{2+}. SOCE was significantly impaired after exposure to the anti-CD20 (I-20) antibody or CD20-gene silencing. Cells receiving control antibody (anti-FLAG) or scrambled shRNA did not showed significant differences in SOCE magnitude in comparison to untreated cells. ***P < 0.001, referring to Bonferroni's multiple comparison post-test outcome vs. untreated group.* ***(H)*** *C2C12 myoblasts showed a comparable response to thapsigargin in all the conditions tested, indicating that store-depletion occurred with analogous efficiency.* ***(I)*** *CD20 antibody (I-20) targeting or gene silencing was ineffective when the specific SOC influx inhibitor BTP2 was used, giving evidence that SOCE was specifically affected by CD20-targeting.*

2.7 Expression of CD20 in human myoblasts and skeletal muscle tissue

Finally, we assessed CD20 expression in human muscle cells and tissue. Human CD20 mRNA was amplified from CHQ cells, a line of human skeletal myoblasts, as well as from adult muscular tissue (Fig. 13A). A band in the molecular range of 33–37 kD was stained by the anti-CD20 (M-20) antibody, revealing CD20 expression at the protein level (Fig. 13B). This observation was supported by MS analysis, with 10 CD20-derived peptides identified in IP from adult human muscle (Fig. 13C).

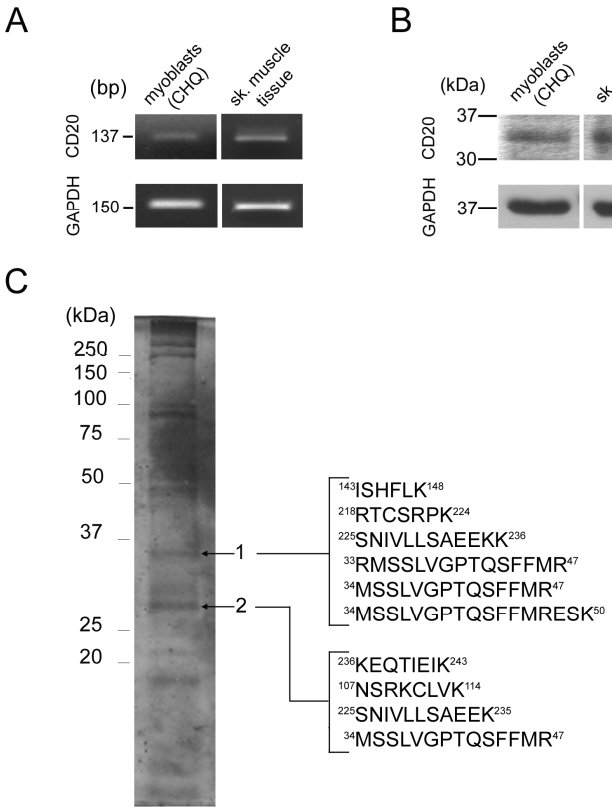

Figure 13: Expression of CD20 in human skeletal muscle. (A) *CD20 mRNA was successfully amplified from human myoblasts and muscular tissue.* ***(B)*** *The anti-CD20 (M-20) antibody stained a band in the molecular range of 33–37 kD, suggesting CD20 expression at the protein level in human muscular cells and tissue.* ***(C)*** *The presence of CD20 protein was confirmed by MS analysis, allowing identification of 10 CD20- derived peptides in IP from adult muscular tissue. The anti-CD20 (M-20) antibody was used to perform IP.*

DISCUSSION

Being involved in the control of cell growth, differentiation, metabolism, and gene expression, the calcium ion plays an essential role in the physiology of all living cells. Accordingly, multiple mechanisms contribute to the precise control of its intracellular concentration ($[Ca^{2+}]_i$) [70, 71, 237]. Particularly in skeletal muscle, the efficient regulation of cytosolic Ca^{2+} is crucial for tissue functionality [95]. Indeed, impairment of Ca^{2+} homeostasis has been shown to contribute to the etiology of muscle fiber injury, especially in some muscular disorders such as Duchenne muscular dystrophy (DMD) [179, 180, 238-240]. DMD is a progressive neuromuscular disease characterized by lack of dystrophin, a 427kD protein expressed at the inner face of the sarcolemma [175, 241]. The absence of dystrophin has two main consequences: (a) the cell membrane is more fragile and can be damaged during eccentric muscle contraction; (b) membrane proteins, especially ion channels, are deregulated. Strong perturbations of calcium handling were observed in DMD muscle fibers [179, 180, 239]. Moreover, studies performed on dystrophic muscle cells from *mdx* mice, the animal model of DMD [174], have suggested that a persistent intake of Ca^{2+} activates Ca-sensitive proteolytic and phospholipolytic activities [238, 240] resulting in the degradation of dystrophic muscle tissue. Alterations of the sodium permeability were not observed in DMD or *mdx* myoblasts, ruling out a general (nonspecific) increase of ionic permeability through membrane wounds and supporting the involvement of specific transmembrane channels and intracellular pathways. In particular, the store operated calcium channels (SOCCs) seem to be involved in the entries of Ca^{2+} in the dystrophic muscle fibers [86]. Although the impairment of Ca^{2+} homeostasis affecting dystrophic muscular cells has been extensively reported, the conditions of calcium-release and the role of SOCCs in dystrophic myogenic progenitors were not investigated before. To start addressing this issue, we firstly characterized the immunophenotype of normal and dystrophic blood-derived $CD133^+$ progenitors, whose myogenic potential was previously demonstrated [50, 220]. Unexpectedly, expression of the membrane antigen CD20 was detected. Knowledge about the biology of CD20 is relatively scarce, and its precise functionality is still not understood. However, evidences of its involvement in calcium homeostasis are growing. Cell lines transfected with CD20 show an increased calcium conductance across the plasma membrane, strongly suggesting that CD20 functions as an important channel for regulating calcium homeostasis [136, 137]. Furthermore, reduced CD20 expression in B cell lines result in significantly decreased calcium entry across the plasma membrane [137, 138]. Finally, some insight has been provided by studies showing that CD20 can associate with lipid raft domains of the plasma membrane, where it is probably involved in store-operated Ca^{2+} entry (SOCE) (Deans et al., 1998; Li et al., 2004). Together with these findings, supporting a direct role of CD20 in the regulation of transmembrane conductive Ca^{2+} flux, a CD20-related pathway able to modulate intracellular Ca^{2+} was also described. Indeed, CD20 was shown to be a component of a multimolecular complex including the src-family tyrosine kinases Lyn, Fyn and Lck, together with a 75/80 kD protein phosphorylated on tyrosine residues *in vivo* [224]. CD20-associated p75/80 has been identified as PAG, an ubiquitous, highly tyrosine-phosphorylated adaptor protein localized exclusively to lipid rafts [242, 243]. Also

known as Csk-binding protein (Cbp), PAG recruits Csk to lipid rafts to maintain resident src-family tyrosine kinases in the inactive state. Changes in either the conformation of CD20 or its phosphorylation state, or both, could regulate its association with Lyn, Fyn and Lck, resulting in an activation of such kinases and initiating of downstream signaling [138, 224, 225]. The activation of Lyn, the src-kinase accounted for most of the PTK activity in the CD20 complex [224], triggers a cascade of events leading to Ca^{2+} mobilization from intracellular stores after activation of PLCγ2 and PI3-K [226]. Quantitative measurements of $[Ca^{2+}]_i$ revealed an higher percentage of dystrophic cells exceeding the reference value of 100 nM ($p<0.001$), giving evidence, for the first time, of an altered regulation of intracellular Ca^{2+} affecting dystrophic blood-derived $CD133^+$ stem cells. Additionally, an higher percentage of $CD133^+CD20^+$ cells was detected in DMD than normal blood. To investigate the possible involvement of CD20 in the intracellular Ca^{2+} overload observed in dystrophic cells, experiments were performed to quantify its expression as well as to evaluate its phosphorylation. While the number of CD20 molecules on the membrane of normal and DMD blood-derived $CD133^+$ stem cells was not significantly different, the greater threonine phosphorylation observed in dystrophic cells possibly reflected a more consistent activation of CD20-related signaling. These results sustained an involvement of CD20 in the Ca^{2+} impairment affecting dystrophic $CD133^+$ stem cells, reasonably related to its signaling activity rather than to a different number of molecules expressed. Given the absence of physiological agonists, we started to look for a soluble, released factor potentially able to indirectly activate CD20. ELISA assays demonstrated an abnormal release of BDNF from dystrophic circulating $CD133^+$ stem cells. We thus focused our attention on the molecular pathways undergoing activation after BDNF interaction with its receptor, TrkB. Presented results demonstrated a connection between BDNF/TrkB signaling and CD20 activation, since a strong induction of CD20 phosphorylation was observed after cell exposure to BDNF. Reasonably, the heavy threonine-phosphorylation detected in un-stimulated DMD cells depended on the higher BDNF release described above. Moreover, we showed that BDNF-induced CD20 phosphorylation was not followed by the same events in normal and dystrophic cells. Although CD20-Lyn interaction was observed in both normal and dystrophic circulating $CD133^+$ stem cells after BDNF treatment, only in DMD cells does the recruited src-kinase undergo phosphorylation. This was likely to promote the activation of additional intracellular pathways that, by acting in synergy with TrkB-related signaling, contribute to the modulation of intracellular Ca^{2+} levels. Our data described a situation where the same stimulus (BDNF) resulted in a different response in normal and dystrophic blood-derived $CD133^+$ stem cells in term of intracellular Ca^{2+} rise, according to the activation of different signaling pathways. Indeed, while the exposure to BDNF of $CD133^+$ stem cells isolated from normal blood will only result in the activation of TrkB signaling, in dystrophic cells the synergic activation of TrkB and CD20-Lyn pathways will take place, leading to a supplemental intracellular free calcium increase. These considerations were strongly supported by measurements of intracellular free Ca^{2+} in BDNF-stimulated normal and dystrophic circulating $CD133^+$ stem cells, revealing a more consistent increase of $[Ca^{2+}]_i$ in dystrophic cells, as expected. Together, these data demonstrated that the intracellular Ca^{2+} overload observed in DMD blood-derived $CD133^+$ stem cells involved, at least, two mechanisms acting in synergy: 1) an increased BDNF release, leading to an autocrine/paracrine activation of TrkB

pathway; 2) the activation of CD20-Lyn signaling, resulting in a supplementary intracellular calcium increase. We speculated that the absence of dystrophin in DMD circulating $CD133^+$ stem cells may affect membrane integrity, leading to an abnormal activation of CD20-related signaling. Interestingly, we described the absence of Dp71 protein in dystrophic circulating $CD133^+$ stem cells. Several works reported a reduced and/or compromised expression of Dp71, the ubiquitous dystrophin isoform, in dystrophic tissues that, at least formally, cannot be explained considering the site of mutation on the DMD gene. Altered Dp71 transcripts were found in astrocytes of patients with severe cerebral dysfunction [244] and an impaired oligomerization of Dp71 has been demonstrated in Dp427-deficient *mdx* brain [245]. Furthermore, a reduced expression of Dp71 was observed in endothelial and glial cells derived from *mdx* fetuses, newborn and adult mice, associated with impaired blood-brain barrier (BBB) development [246]. Finally, association of Dp71 with the cell membrane was demonstrated [247], identified in the platelet membrane cytoskeleton [248], and a critical role for the clustered localization of potassium channels in retinal glial cells was described [249]. These data suggested that the absence of Dp71 in the DMD circulating $CD133^+$ stem cells may account for the impairment of CD20-related signaling pathway, resulting in intracellular Ca^{2+} overload. However, further studies are needed to demonstrate the existence of a functional relationship between Dp71 and CD20, whether mediated by a CD20-Dp71 direct interaction or by an indirect link involving other dystrophin associated proteins. The rescue of dystrophin expression in engineered dystrophic circulating $CD133^+$ stem cells provided the recovery of muscle force and endurance after engraftment into dystrophic animal models [220]. So far, we do not know whether the expression of Dp71 dystrophin isoform on the engineered dystrophic circulating $CD133^+$ stem cells may also account for intracellular Ca^{2+} normalization. However, in dystrophin deficient cells where expression of full-length dystrophin was forced by plasmid microinjection, the development of calcium-handling abnormalities was prevented by maintaining the resting $[Ca^{2+}]_i$ at low levels and decreasing global calcium-release amplitudes [250]. Furthermore, mini-dystrophin (which lacks 17 repeats of the central rod domain) retains the ability to negatively regulate store-dependent calcium influx and to restore a normal calcium homeostasis. The domains involved in the negative control of SOCCs may be situated in the C-terminal domain, a protein region present in all dystrophin isoforms, included Dp71, and where binding sites for dystrophin associated proteins can be found. Additional research focused on CD20-related signaling in blood-derived $CD133^+$ stem cells may enhance the understanding of their differentiative behavior and, in so doing, may contribute to the development of experimental strategies for the treatment of DMD. In this context, toward which the main efforts of our lab are focused, the possible contribution of CD20 to the regulation of Ca^{2+} handling in skeletal muscle is an important point to address. Moreover, it should be taken into account that circulating $CD133^+$ progenitors and committed muscular cells share common mesodermic origins, so that similar altered pathways could be found. Human muscle biopsies for research purposes are not easy to obtain, particularly from DMD patients. Accordingly, we started to evaluate whether CD20 is expressed and contributes to calcium handling in C2C12 murine skeletal myoblasts cell line. Our findings unequivocally described CD20 expression in C2C12 myoblasts/myotubes and mature muscle fibers, both at the mRNA and protein levels. RT-PCR, flow cytometry, WB, and IF data were

supported by MS analysis that identified 15 CD20-related peptides after immunoprecipitation from C2C12 myoblasts, C57BL QA, and SCID QA whole lysates. Data obtained from C57BL-isolated muscle fibers, together with observations in C2C12 myoblast pure populations, provided strong evidence supporting muscle-specific CD20 expression. Furthermore, CD20 detection in muscles isolated from B cell-depleted SCID mice confirmed the muscular origin of our findings, by excluding potential contamination and/or fusion with circulating $CD20^+$ cells. Being detected at the membrane level in both myoblasts and mature fibers from different muscles, the observed muscular CD20 expression pattern differed from that in B cells, where CD20 is expressed in early B-cell precursors and mature B-cells but is lost with differentiation into plasma cells [251, 252]. Interestingly, IF analysis of C2C12 myoblasts/myotubes and of C57BL and SCID muscles revealed that CD20 was not widely expressed on all muscle cells and fibers. Functional experiments showed that proliferation and viability of C2C12 myoblasts were not affected by anti-CD20 treatment, highlighting differences in comparison to previous descriptions of CD20 function in B cells. Discrepancies in term of expression time-course and/or functionality are quite common when comparing the behavior of a protein in two distinct environments. Differences may arise from protein expression level, presence/absence of tissue-specific binding partners, or from tissue-specific features. Although recent studies have made significant advancements in the field [117, 207, 213, 253], there are relatively few reports of SOCE activity in skeletal muscle, and the function/regulation of SOC channels in this tissue is not fully understood [130, 254, 255]. Previous studies have suggested CD20 involvement in regulating calcium homeostasis, possibly through a SOCE mechanism. The present data strongly implicate CD20 as a novel modulator of this pathway in C2C12 myoblasts. By using different targeting approaches, we showed that CD20 inhibition specifically impaired Ca^{2+} re-entry after store-depletion in C2C12 myoblasts. The observed reduction in Ca^{2+} re-entry magnitude after antibody binding or gene silencing, suggested a role for CD20 as a component of the SOCE machinery in these cells. Previous studies have demonstrated increased transmembrane Ca^{2+} conductance after transfection of CD20 cDNA [136, 137, 235, 256]. Since the exposure to thapsigargin displayed similar effects in untreated and CD20-targeted C2C12 myoblasts, the observed impairment of SOCE can reasonably be addressed to a specific impairment of Ca^{2+} re-entry, ruling out biases due to different starting points at the end of store-depletion. Although in different cell types, the elevation of intracellular Ca^{2+} upon anti-CD20 antibody binding has been extensively reported before [234, 257-259]. Interestingly, also in C2C12 myoblasts a significantly higher intracellular Ca^{2+} concentration at rest was measured when CD20 inhibition was achieved through antibody binding. Since CD20-silenced C2C12 myoblasts displayed normal levels of resting Ca^{2+}, we speculate that in these cells intracellular Ca^{2+} raising after CD20 inhibition can be bypassed through an adaptive response, possibly leading to the expression or up-regulation of other proteins involved in Ca^{2+} homeostasis. Data presented provide novel insights into the expression pattern of CD20, confirming its membrane localization in skeletal muscle myoblasts and adult fibers. Analysis of SOCE in C2C12 myoblasts after CD20 targeting with specific antibody or gene silencing revealed a specific impairment of the observed phenomenon. It is not yet known whether CD20 modulates SOCE by acting alone or, more likely, through interaction with other proteins. Further work is needed to study the functional

impact of SOCE modulation through CD20 targeting in muscle cells and tissue, as well as to extend the present findings to human skeletal muscle.

CONCLUSIONS

The calcium ion plays an essential role in the physiology of all living cells. Particularly in skeletal muscle, the efficient regulation of cytosolic Ca^{2+} is crucial for tissue functionality and impairment of Ca^{2+} homeostasis has been involved in the etiology of Duchenne muscular dystrophy (DMD). Although the impairment of Ca^{2+} homeostasis affecting dystrophic muscular cells has been extensively reported, the pathways involved in calcium-release and the role of store-operated Ca^{2+} channels in dystrophic myogenic progenitors were not investigated before.

The main findings reported in the *first section* of the thesis are summarized below:

- Quantitative calcium measurements revealed an higher $[Ca^{2+}]_i$ in dystrophic blood-derived $CD133^+$ stem cells giving evidence, for the first time, of an altered Ca^{2+} regulation in dystrophic progenitors retaining myogenic potential.
- CD20-related signaling is involved in the Ca^{2+} impairment observed in dystrophic $CD133^+$ stem cells.
- Connection between BDNF/TrkB signaling and CD20 activation was demonstrated, although this was not followed by the same molecular events in normal and dystrophic cells.
- CD20-Lyn interaction was observed in both normal and dystrophic circulating $CD133^+$ stem cells after BDNF treatment, but only in DMD cells does the recruited src-kinase undergo phosphorylation.
- Measurements of intracellular free Ca^{2+} in BDNF-stimulated normal and dystrophic circulating $CD133^+$ stem cells revealed more consistent increase of $[Ca^{2+}]_i$ in dystrophic cells.

Together, these data demonstrated that the intracellular Ca^{2+} overload observed in DMD blood-derived $CD133^+$ stem cells involved, at least, two mechanisms acting in synergy: 1) an increased BDNF release, leading to an autocrine/paracrine activation of TrkB pathway; 2) the activation of CD20-Lyn signaling, resulting in a supplementary intracellular calcium increase. We speculated that the absence of dystrophin in DMD circulating $CD133^+$ stem cells may affect membrane integrity, leading to an abnormal activation of CD20-related signaling.

The main efforts of our lab are focused on the development of experimental strategies to ameliorate the phenotype of dystrophic patients. In this context, the possible contribution of CD20 to the regulation of Ca^{2+} handling in skeletal muscle is an important point to address, especially considering that circulating $CD133^+$ progenitors and committed muscular cells share common mesodermic origins. Human muscle biopsies for research purposes are not easy to obtain, particularly from DMD patients. Accordingly, we started to evaluate whether CD20 is expressed and contributes to calcium handling in C2C12 murine skeletal myoblasts cell line. Interestingly, several studies demonstrated the association of CD20 with lipid raft domains of the plasma membrane, where it probably functions as a store-operated Ca^{2+} channel. Recent works indicated that store-operated Ca^{2+} entry (SOCE) plays a central role in skeletal muscle physiology and development, but there remain a number of unresolved issues relating to SOCE modulation in this tissue.

The main findings reported in the *second section* of the thesis are summarized below:

- CD20 is expressed at the membrane of C2C12 myoblasts/myotubes and mature muscle fibers, both at the mRNA and protein levels.
- Functional experiments showed that proliferation and viability of C2C12 myoblasts were not affected by anti-CD20 treatment.
- CD20 inhibition specifically impaired Ca^{2+} re-entry after store-depletion in C2C12 myoblasts, suggesting a role for CD20 as a component of the SOCE machinery in these cells.

FUTURE PERSPECTIVES

- To investigate the existence of a *functional relation between Dp71 and CD20*, possibly mediated by a direct interaction or by an indirect link involving other dystrophin associated proteins.

- To understand whether *CD20-related signaling affects the differentiative potential of normal and dystrophic blood-derived CD133$^+$ stem cells*, both *in vitro* and *in vivo*.

- To *improve the characterization of CD20 expression in skeletal muscle*. Given that CD20 was not widely expressed on all muscle fibres, the correlation with different myosin isoforms is an intringuingly point to address in order to highlight the contribute of CD20 to muscular specific features.

- To study the *functional impact of SOCE modulation through CD20* in muscle cells and tissue, starting from myoblasts differentiation after CD20 targeting.

- To understand whether *CD20 modulates SOCE by acting alone or, more likely, through interaction with other proteins*. Accordingly, a functional interaction with the main actors of SOCE (ORAI1 and STIM1) should be investigated.

- To extend the findings concerning CD20 to *dystrophic* and *human* skeletal muscle

REFERENCES

[1] Buckingham M. Skeletal muscle formation in vertebrates. Curr Opin Genet Dev. 2001;11:440-448.

[2] Aoyama H,Asamoto K. Determination of somite cells: independence of cell differentiation and morphogenesis. Development. 1988;104:15-28.

[3] Tajbakhsh S,Buckingham M. The birth of muscle progenitor cells in the mouse: spatiotemporal considerations. Curr Top Dev Biol. 2000;48:225-268.

[4] Cossu G,Borello U. Wnt signaling and the activation of myogenesis in mammals. Embo J. 1999;18:6867-6872.

[5] Dietrich S, Abou-Rebyeh F, Brohmann H, Bladt F, Sonnenberg-Riethmacher E, Yamaai T, Lumsden A, Brand-Saberi B,Birchmeier C. The role of SF/HGF and c-Met in the development of skeletal muscle. Development. 1999;126:1621-1629.

[6] Borycki AG, Li J, Jin F, Emerson CP,Epstein JA. Pax3 functions in cell survival and in pax7 regulation. Development. 1999;126:1665-1674.

[7] Epstein JA, Shapiro DN, Cheng J, Lam PY,Maas RL. Pax3 modulates expression of the c-Met receptor during limb muscle development. Proc Natl Acad Sci U S A. 1996;93:4213-4218.

[8] Williams BA,Ordahl CP. Pax-3 expression in segmental mesoderm marks early stages in myogenic cell specification. Development. 1994;120:785-796.

[9] Bober E, Franz T, Arnold HH, Gruss P,Tremblay P. Pax-3 is required for the development of limb muscles: a possible role for the migration of dermomyotomal muscle progenitor cells. Development. 1994;120:603-612.

[10] Kassar-Duchossoy L, Giacone E, Gayraud-Morel B, Jory A, Gomes D,Tajbakhsh S. Pax3/Pax7 mark a novel population of primitive myogenic cells during development. Genes Dev. 2005;19:1426-1431.

[11] Relaix F, Rocancourt D, Mansouri A,Buckingham M. Divergent functions of murine Pax3 and Pax7 in limb muscle development. Genes Dev. 2004;18:1088-1105.

[12] Relaix F, Rocancourt D, Mansouri A,Buckingham M. A Pax3/Pax7-dependent population of skeletal muscle progenitor cells. Nature. 2005;435:948-953.

[13] Punch VG, Jones AE,Rudnicki MA. Transcriptional networks that regulate muscle stem cell function. Wiley Interdiscip Rev Syst Biol Med. 2009;1:128-140.

[14] Bajard L, Relaix F, Lagha M, Rocancourt D, Daubas P,Buckingham ME. A novel genetic hierarchy functions during hypaxial myogenesis: Pax3 directly activates Myf5 in muscle progenitor cells in the limb. Genes Dev. 2006;20:2450-2464.

[15] Hu P, Geles KG, Paik JH, DePinho RA,Tjian R. Codependent activators direct myoblast-specific MyoD transcription. Dev Cell. 2008;15:534-546.

[16] McKinnell IW, Ishibashi J, Le Grand F, Punch VG, Addicks GC, Greenblatt JF, Dilworth FJ,Rudnicki MA. Pax7 activates myogenic genes by recruitment of a histone methyltransferase complex. Nat Cell Biol. 2008;10:77-84.

[17] Tajbakhsh S, Rocancourt D, Cossu G,Buckingham M. Redefining the genetic hierarchies controlling skeletal myogenesis: Pax-3 and Myf-5 act upstream of MyoD. Cell. 1997;89:127-138.

[18] Rawls A, Valdez MR, Zhang W, Richardson J, Klein WH,Olson EN. Overlapping functions of the myogenic bHLH genes MRF4 and MyoD revealed in double mutant mice. Development. 1998;125:2349-2358.

[19] Rudnicki MA, Schnegelsberg PN, Stead RH, Braun T, Arnold HH,Jaenisch R. MyoD or Myf-5 is required for the formation of skeletal muscle. Cell. 1993;75:1351-1359.

[20] Mauro A. Satellite cell of skeletal muscle fibers. J Biophys Biochem Cytol. 1961;9:493-495.

[21] Bentzinger CF, Wang YX,Rudnicki MA. Building muscle: molecular regulation of myogenesis. Cold Spring Harb Perspect Biol. 2012;4:

[22] Le Grand F, Jones AE, Seale V, Scime A,Rudnicki MA. Wnt7a activates the planar cell polarity pathway to drive the symmetric expansion of satellite stem cells. Cell Stem Cell. 2009;4:535-547.

[23] Ciciliot S,Schiaffino S. Regeneration of mammalian skeletal muscle. Basic mechanisms and clinical implications. Curr Pharm Des. 2010;16:906-914.

[24] Mann CJ, Perdiguero E, Kharraz Y, Aguilar S, Pessina P, Serrano AL,Munoz-Canoves P. Aberrant repair and fibrosis development in skeletal muscle. Skelet Muscle. 2011;1:21.

[25] Serrano AL, Mann CJ, Vidal B, Ardite E, Perdiguero E,Munoz-Canoves P. Cellular and molecular mechanisms regulating fibrosis in skeletal muscle repair and disease. Curr Top Dev Biol. 2011;96:167-201.

[26] Ryall JG, Schertzer JD,Lynch GS. Cellular and molecular mechanisms underlying age-related skeletal muscle wasting and weakness. Biogerontology. 2008;9:213-228.

[27] Wynn TA. Cellular and molecular mechanisms of fibrosis. J Pathol. 2008;214:199-210.

[28] Bonniaud P, Margetts PJ, Ask K, Flanders K, Gauldie J,Kolb M. TGF-beta and Smad3 signaling link inflammation to chronic fibrogenesis. J Immunol. 2005;175:5390-5395.

[29] Spencer MJ, Montecino-Rodriguez E, Dorshkind K,Tidball JG. Helper (CD4(+)) and cytotoxic (CD8(+)) T cells promote the pathology of dystrophin-deficient muscle. Clin Immunol. 2001;98:235-243.

[30] Perdiguero E, Sousa-Victor P, Ruiz-Bonilla V, Jardi M, Caelles C, Serrano AL,Munoz-Canoves P. p38/MKP-1-regulated AKT coordinates macrophage transitions and resolution of inflammation during tissue repair. J Cell Biol. 2011;195:307-322.

[31] Qu-Petersen Z, Deasy B, Jankowski R, Ikezawa M, Cummins J, Pruchnic R, Mytinger J, Cao B, Gates C, Wernig A,Huard J. Identification of a novel population of muscle stem cells in mice: potential for muscle regeneration. J Cell Biol. 2002;157:851-864.

[32] Miller JB, Schaefer L,Dominov JA. Seeking muscle stem cells. Curr Top Dev Biol. 1999;43:191-219.

[33] Baroffio A, Hamann M, Bernheim L, Bochaton-Piallat ML, Gabbiani G,Bader CR. Identification of self-renewing myoblasts in the progeny of single human muscle satellite cells. Differentiation. 1996;60:47-57.

[34] Bischoff R,Heintz C. Enhancement of skeletal muscle regeneration. Dev Dyn. 1994;201:41-54.

[35] Lee JH,Kemp DM. Human adipose-derived stem cells display myogenic potential and perturbed function in hypoxic conditions. Biochem Biophys Res Commun. 2006;341:882-888.

[36] Jaffredo T, Gautier R, Eichmann A,Dieterlen-Lievre F. Intraaortic hemopoietic cells are derived from endothelial cells during ontogeny. Development. 1998;125:4575-4583.

[37] Kumaravelu P, Hook L, Morrison AM, Ure J, Zhao S, Zuyev S, Ansell J,Medvinsky A. Quantitative developmental anatomy of definitive haematopoietic stem cells/long-term repopulating units (HSC/RUs): role of the aorta-gonad-mesonephros (AGM) region and the yolk sac in colonisation of the mouse embryonic liver. Development. 2002;129:4891-4899.

[38] North TE, de Bruijn MF, Stacy T, Talebian L, Lind E, Robin C, Binder M, Dzierzak E,Speck NA. Runx1 expression marks long-term repopulating hematopoietic stem cells in the midgestation mouse embryo. Immunity. 2002;16:661-672.

[39] Oshima H, Payne TR, Urish KL, Sakai T, Ling Y, Gharaibeh B, Tobita K, Keller BB, Cummins JH,Huard J. Differential myocardial infarct repair with muscle stem cells compared to myoblasts. Mol Ther. 2005;12:1130-1141.

[40] Payne TR, Oshima H, Sakai T, Ling Y, Gharaibeh B, Cummins J,Huard J. Regeneration of dystrophin-expressing myocytes in the mdx heart by skeletal muscle stem cells. Gene Ther. 2005;12:1264-1274.

[41] Zheng B, Cao B, Crisan M, Sun B, Li G, Logar A, Yap S, Pollett JB, Drowley L, Cassino T, Gharaibeh B, Deasy BM, Huard J,Peault B. Prospective identification of myogenic endothelial cells in human skeletal muscle. Nat Biotechnol. 2007;25:1025-1034.

[42] Cossu G,Bianco P. Mesoangioblasts--vascular progenitors for extravascular mesodermal tissues. Curr Opin Genet Dev. 2003;13:537-542.

[43] Tagliafico E, Brunelli S, Bergamaschi A, De Angelis L, Scardigli R, Galli D, Battini R, Bianco P, Ferrari S, Cossu G,Ferrari S. TGFbeta/BMP activate the smooth muscle/bone differentiation programs in mesoangioblasts. J Cell Sci. 2004;117:4377-4388.

[44] Brunelli S, Tagliafico E, De Angelis FG, Tonlorenzi R, Baesso S, Ferrari S, Niinobe M, Yoshikawa K, Schwartz RJ, Bozzoni I, Ferrari S,Cossu G. Msx2 and necdin combined activities are required for smooth muscle differentiation in mesoangioblast stem cells. Circ Res. 2004;94:1571-1578.

[45] Lamagna C,Bergers G. The bone marrow constitutes a reservoir of pericyte progenitors. J Leukoc Biol. 2006;80:677-681.

[46] Dellavalle A, Sampaolesi M, Tonlorenzi R, Tagliafico E, Sacchetti B, Perani L, Innocenzi A, Galvez BG, Messina G, Morosetti R, Li S, Belicchi M, Peretti G, Chamberlain JS, Wright WE, Torrente Y, Ferrari S, Bianco P,Cossu G. Pericytes of human skeletal muscle are myogenic precursors distinct from satellite cells. Nat Cell Biol. 2007;9:255-267.

[47] Meregalli M, Farini A, Parolini D, Maciotta S,Torrente Y. Stem cell therapies to treat muscular dystrophy: progress to date. BioDrugs. 2007;24:237-247.

[48] Caplan AI. Why are MSCs therapeutic? New data: new insight. J Pathol. 2009;217:318-324.

[49] Stamm C, Friehs I, Choi YH, Zurakowski D, McGowan FX,del Nido PJ. Cytosolic calcium in the ischemic rabbit heart: assessment by pH- and temperature-adjusted rhod-2 spectrofluorometry. Cardiovasc Res. 2003;59:695-704.

[50] Torrente Y, Belicchi M, Sampaolesi M, Pisati F, Meregalli M, D'Antona G, Tonlorenzi R, Porretti L, Gavina M, Mamchaoui K, Pellegrino MA, Furling D, Mouly V, Butler-Browne GS, Bottinelli R, Cossu G,Bresolin N. Human circulating AC133(+) stem cells restore dystrophin expression and ameliorate function in dystrophic skeletal muscle. J Clin Invest. 2004;114:182-195.

[51] Torrente Y, Belicchi M, Marchesi C, Dantona G, Cogiamanian F, Pisati F, Gavina M, Giordano R, Tonlorenzi R, Fagiolari G, Lamperti C, Porretti L, Lopa R, Sampaolesi M, Vicentini L, Grimoldi N, Tiberio F, Songa V, Baratta P, Prelle A, Forzenigo L, Guglieri M, Pansarasa O, Rinaldi C, Mouly V, Butler-Browne GS, Comi GP, Biondetti P, Moggio M, Gaini SM, Stocchetti N, Priori A, D'Angelo MG, Turconi A, Bottinelli R, Cossu G, Rebulla P,Bresolin N. Autologous transplantation of muscle-derived CD133+ stem cells in Duchenne muscle patients. Cell Transplant. 2007;16:563-577.

[52] Asakura A, Seale P, Girgis-Gabardo A,Rudnicki MA. Myogenic specification of side population cells in skeletal muscle. J Cell Biol. 2002;159:123-134.

[53] Lepper C, Conway SJ,Fan CM. Adult satellite cells and embryonic muscle progenitors have distinct genetic requirements. Nature. 2009;460:627-631.

[54] De Angelis L, Berghella L, Coletta M, Lattanzi L, Zanchi M, Cusella-De Angelis MG, Ponzetto C,Cossu G. Skeletal myogenic progenitors originating from embryonic dorsal aorta coexpress endothelial and myogenic markers and contribute to postnatal muscle growth and regeneration. J Cell Biol. 1999;147:869-878.

[55] Lee JY, Qu-Petersen Z, Cao B, Kimura S, Jankowski R, Cummins J, Usas A, Gates C, Robbins P, Wernig A,Huard J. Clonal isolation of muscle-derived cells capable of enhancing muscle regeneration and bone healing. J Cell Biol. 2000;150:1085-1100.

[56] Torrente Y, Tremblay JP, Pisati F, Belicchi M, Rossi B, Sironi M, Fortunato F, El Fahime M, D'Angelo MG, Caron NJ, Constantin G, Paulin D, Scarlato G,Bresolin N. Intraarterial injection of muscle-derived CD34(+)Sca-1(+) stem cells restores dystrophin in mdx mice. J Cell Biol. 2001;152:335-348.

[57] Mitchell KJ, Pannerec A, Cadot B, Parlakian A, Besson V, Gomes ER, Marazzi G,Sassoon DA. Identification and characterization of a non-satellite cell muscle resident progenitor during postnatal development. Nat Cell Biol. 2010;12:257-266.

[58] Pittenger MF, Mackay AM, Beck SC, Jaiswal RK, Douglas R, Mosca JD, Moorman MA, Simonetti DW, Craig S,Marshak DR. Multilineage potential of adult human mesenchymal stem cells. Science. 1999;284:143-147.

[59] Nesti LJ, Jackson WM, Shanti RM, Koehler SM, Aragon AB, Bailey JR, Sracic MK, Freedman BA, Giuliani JR,Tuan RS. Differentiation potential of multipotent progenitor cells derived from war-traumatized muscle tissue. J Bone Joint Surg Am. 2008;90:2390-2398.

[60] Meng J, Adkin CF, Arechavala-Gomeza V, Boldrin L, Muntoni F,Morgan JE. The contribution of human synovial stem cells to skeletal muscle regeneration. Neuromuscul Disord. 2010;20:6-15.

[61] Ichim TE, Alexandrescu DT, Solano F, Lara F, Campion Rde N, Paris E, Woods EJ, Murphy MP, Dasanu CA, Patel AN, Marleau AM, Leal A,Riordan NH. Mesenchymal stem cells as anti-inflammatories: implications for treatment of Duchenne muscular dystrophy. Cell Immunol. 2010;260:75-82.

[62] Song HY, Lee MJ, Kim MY, Kim KH, Lee IH, Shin SH, Lee JS,Kim JH. Lysophosphatidic acid mediates migration of human mesenchymal stem cells stimulated by synovial fluid of patients with rheumatoid arthritis. Biochim Biophys Acta. 2010;1801:23-30.

[63] Rafei M, Birman E, Forner K,Galipeau J. Allogeneic mesenchymal stem cells for treatment of experimental autoimmune encephalomyelitis. Mol Ther. 2009;17:1799-1803.

[64] De Bari C, Dell'Accio F, Vandenabeele F, Vermeesch JR, Raymackers JM,Luyten FP. Skeletal muscle repair by adult human mesenchymal stem cells from synovial membrane. J Cell Biol. 2003;160:909-918.

[65] Miranville A, Heeschen C, Sengenes C, Curat CA, Busse R,Bouloumie A. Improvement of postnatal neovascularization by human adipose tissue-derived stem cells. Circulation. 2004;110:349-355.

[66] Moon MH, Kim SY, Kim YJ, Kim SJ, Lee JB, Bae YC, Sung SM,Jung JS. Human adipose tissue-derived mesenchymal stem cells improve postnatal neovascularization in a mouse model of hindlimb ischemia. Cell Physiol Biochem. 2006;17:279-290.

[67] Cai L, Johnstone BH, Cook TG, Tan J, Fishbein MC, Chen PS,March KL. IFATS collection: Human adipose tissue-derived stem cells induce angiogenesis and nerve sprouting following myocardial infarction, in conjunction with potent preservation of cardiac function. Stem Cells. 2009;27:230-237.

[68] Valina C, Pinkernell K, Song YH, Bai X, Sadat S, Campeau RJ, Le Jemtel TH,Alt E. Intracoronary administration of autologous adipose tissue-derived stem cells improves left ventricular function, perfusion, and remodelling after acute myocardial infarction. Eur Heart J. 2007;28:2667-2677.

[69] Berridge MJ, Bootman MD,Lipp P. Calcium--a life and death signal. Nature. 1998;395:645-648.

[70] Berridge MJ, Lipp P,Bootman MD. The versatility and universality of calcium signalling. Nat Rev Mol Cell Biol. 2000;1:11-21.

[71] Clapham DE. Calcium signaling. Cell. 1995;80:259-268.

[72] Chin ER, Olson EN, Richardson JA, Yang Q, Humphries C, Shelton JM, Wu H, Zhu W, Bassel-Duby R,Williams RS. A calcineurin-dependent transcriptional pathway controls skeletal muscle fiber type. Genes Dev. 1998;12:2499-2509.

[73] Wu H, Kanatous SB, Thurmond FA, Gallardo T, Isotani E, Bassel-Duby R,Williams RS. Regulation of mitochondrial biogenesis in skeletal muscle by CaMK. Science. 2002;296:349-352.

[74] Jansen KM,Pavlath GK. Molecular control of mammalian myoblast fusion. Methods Mol Biol. 2008;475:115-133.

[75] Horsley V, Jansen KM, Mills ST,Pavlath GK. IL-4 acts as a myoblast recruitment factor during mammalian muscle growth. Cell. 2003;113:483-494.

[76] Barnoy S, Glaser T,Kosower NS. Calpain and calpastatin in myoblast differentiation and fusion: effects of inhibitors. Biochim Biophys Acta. 1997;1358:181-188.

[77] Friday BB, Horsley V,Pavlath GK. Calcineurin activity is required for the initiation of skeletal muscle differentiation. J Cell Biol. 2000;149:657-666.

[78] Friday BB, Mitchell PO, Kegley KM,Pavlath GK. Calcineurin initiates skeletal muscle differentiation by activating MEF2 and MyoD. Differentiation. 2003;71:217-227.

[79] O'Connor RS, Mills ST, Jones KA, Ho SN,Pavlath GK. A combinatorial role for NFAT5 in both myoblast migration and differentiation during skeletal muscle myogenesis. J Cell Sci. 2007;120:149-159.

[80] Pavlath GK,Horsley V. Cell fusion in skeletal muscle--central role of NFATC2 in regulating muscle cell size. Cell Cycle. 2003;2:420-423.

[81] Passier R, Zeng H, Frey N, Naya FJ, Nicol RL, McKinsey TA, Overbeek P, Richardson JA, Grant SR,Olson EN. CaM kinase signaling induces cardiac hypertrophy and activates the MEF2 transcription factor in vivo. J Clin Invest. 2000;105:1395-1406.

[82] Shen T, Liu Y, Randall WR,Schneider MF. Parallel mechanisms for resting nucleo-cytoplasmic shuttling and activity dependent translocation provide dual control of transcriptional regulators HDAC and NFAT in skeletal muscle fiber type plasticity. J Muscle Res Cell Motil. 2006;27:405-411.

[83] Song K, Backs J, McAnally J, Qi X, Gerard RD, Richardson JA, Hill JA, Bassel-Duby R,Olson EN. The transcriptional coactivator CAMTA2 stimulates cardiac growth by opposing class II histone deacetylases. Cell. 2006;125:453-466.

[84] Han J, Gong P, Reddig K, Mitra M, Guo P,Li HS. The fly CAMTA transcription factor potentiates deactivation of rhodopsin, a G protein-coupled light receptor. Cell. 2006;127:847-858.

[85] Rosenberg P, Hawkins A, Stiber J, Shelton JM, Hutcheson K, Bassel-Duby R, Shin DM, Yan Z,Williams RS. TRPC3 channels confer cellular memory of recent neuromuscular activity. Proc Natl Acad Sci U S A. 2004;101:9387-9392.

[86] Vandebrouck C, Martin D, Colson-Van Schoor M, Debaix H,Gailly P. Involvement of TRPC in the abnormal calcium influx observed in dystrophic (mdx) mouse skeletal muscle fibers. J Cell Biol. 2002;158:1089-1096.

[87] Zanou N, Shapovalov G, Louis M, Tajeddine N, Gallo C, Van Schoor M, Anguish I, Cao ML, Schakman O, Dietrich A, Lebacq J, Ruegg U, Roulet E, Birnbaumer L,Gailly P. Role of TRPC1 channel in skeletal muscle function. Am J Physiol Cell Physiol. 2009;298:C149-162.

[88] Li Y, Jia YC, Cui K, Li N, Zheng ZY, Wang YZ,Yuan XB. Essential role of TRPC channels in the guidance of nerve growth cones by brain-derived neurotrophic factor. Nature. 2005;434:894-898.

[89] Bezzerides VJ, Ramsey IS, Kotecha S, Greka A,Clapham DE. Rapid vesicular translocation and insertion of TRP channels. Nat Cell Biol. 2004;6:709-720.

[90] Yuan JP, Kiselyov K, Shin DM, Chen J, Shcheynikov N, Kang SH, Dehoff MH, Schwarz MK, Seeburg PH, Muallem S,Worley PF. Homer binds TRPC family channels and is required for gating of TRPC1 by IP3 receptors. Cell. 2003;114:777-789.

[91] Stiber JA, Tabatabaei N, Hawkins AF, Hawke T, Worley PF, Williams RS,Rosenberg P. Homer modulates NFAT-dependent signaling during muscle differentiation. Dev Biol. 2005;287:213-224.

[92] Louis M, Zanou N, Van Schoor M,Gailly P. TRPC1 regulates skeletal myoblast migration and differentiation. J Cell Sci. 2008;121:3951-3959.

[93] Formigli L, Sassoli C, Squecco R, Bini F, Martinesi M, Chellini F, Luciani G, Sbrana F, Zecchi-Orlandini S, Francini F,Meacci E. Regulation of transient receptor potential canonical channel 1 (TRPC1) by sphingosine 1-phosphate in C2C12 myoblasts and its relevance for a role of mechanotransduction in skeletal muscle differentiation. J Cell Sci. 2009;122:1322-1333.

[94] Franzini-Armstrong C. Architecture and regulation of the Ca2+ delivery system in muscle cells. Appl Physiol Nutr Metab. 2009;34:323-327.

[95] Melzer W, Herrmann-Frank A,Luttgau HC. The role of Ca2+ ions in excitation-contraction coupling of skeletal muscle fibres. Biochim Biophys Acta. 1995;1241:59-116.

[96] MacLennan DH. Ca2+ signalling and muscle disease. Eur J Biochem. 2000;267:5291-5297.

[97] Periasamy M,Kalyanasundaram A. SERCA pump isoforms: their role in calcium transport and disease. Muscle Nerve. 2007;35:430-442.

[98] Levitsky DO. Three types of muscles express three sodium-calcium exchanger isoforms. Ann N Y Acad Sci. 2007;1099:221-225.

[99] Nicoll DA, Quednau BD, Qui Z, Xia YR, Lusis AJ,Philipson KD. Cloning of a third mammalian Na+-Ca2+ exchanger, NCX3. J Biol Chem. 1996;271:24914-24921.

[100] Sacchetto R, Margreth A, Pelosi M,Carafoli E. Colocalization of the dihydropyridine receptor, the plasma-membrane calcium ATPase isoform 1 and the sodium/calcium exchanger to the junctional-membrane domain of transverse tubules of rabbit skeletal muscle. Eur J Biochem. 1996;237:483-488.

[101] Allen DG, Lamb GD,Westerblad H. Skeletal muscle fatigue: cellular mechanisms. Physiol Rev. 2008;88:287-332.

[102] Beard NA, Wei L,Dulhunty AF. Ca(2+) signaling in striated muscle: the elusive roles of triadin, junctin, and calsequestrin. Eur Biophys J. 2009;39:27-36.

[103] Murphy RM, Larkins NT, Mollica JP, Beard NA,Lamb GD. Calsequestrin content and SERCA determine normal and maximal Ca2+ storage levels in sarcoplasmic reticulum of fast- and slow-twitch fibres of rat. J Physiol. 2009;587:443-460.

[104] Ikemoto N, Antoniu B, Kang JJ, Meszaros LG,Ronjat M. Intravesicular calcium transient during calcium release from sarcoplasmic reticulum. Biochemistry. 1991;30:5230-5237.

[105] Launikonis BS, Zhou J, Royer L, Shannon TR, Brum G,Rios E. Depletion "skraps" and dynamic buffering inside the cellular calcium store. Proc Natl Acad Sci U S A. 2006;103:2982-2987.

[106] Park H, Park IY, Kim E, Youn B, Fields K, Dunker AK,Kang C. Comparing skeletal and cardiac calsequestrin structures and their calcium binding: a proposed mechanism for coupled calcium binding and protein polymerization. J Biol Chem. 2004;279:18026-18033.

[107] Royer L,Rios E. Deconstructing calsequestrin. Complex buffering in the calcium store of skeletal muscle. J Physiol. 2009;587:3101-3111.

[108] Putney JW, Jr. A model for receptor-regulated calcium entry. Cell Calcium. 1986;7:1-12.

[109] Hoth M,Penner R. Depletion of intracellular calcium stores activates a calcium current in mast cells. Nature. 1992;355:353-356.

[110] Liou J, Kim ML, Heo WD, Jones JT, Myers JW, Ferrell JE, Jr.,Meyer T. STIM is a Ca2+ sensor essential for Ca2+-store-depletion-triggered Ca2+ influx. Curr Biol. 2005;15:1235-1241.

[111] Roos J, DiGregorio PJ, Yeromin AV, Ohlsen K, Lioudyno M, Zhang S, Safrina O, Kozak JA, Wagner SL, Cahalan MD, Velicelebi G,Stauderman KA. STIM1, an essential and conserved component of store-operated Ca2+ channel function. J Cell Biol. 2005;169:435-445.

[112] Manji SS, Parker NJ, Williams RT, van Stekelenburg L, Pearson RB, Dziadek M,Smith PJ. STIM1: a novel phosphoprotein located at the cell surface. Biochim Biophys Acta. 2000;1481:147-155.

[113] Putney JW, Jr. New molecular players in capacitative Ca2+ entry. J Cell Sci. 2007;120:1959-1965.

[114] Stathopulos PB, Li GY, Plevin MJ, Ames JB,Ikura M. Stored Ca2+ depletion-induced oligomerization of stromal interaction molecule 1 (STIM1) via the EF-SAM region: An initiation mechanism for capacitive Ca2+ entry. J Biol Chem. 2006;281:35855-35862.

[115] Williams RT, Senior PV, Van Stekelenburg L, Layton JE, Smith PJ,Dziadek MA. Stromal interaction molecule 1 (STIM1), a transmembrane protein with growth suppressor activity, contains an extracellular SAM domain modified by N-linked glycosylation. Biochim Biophys Acta. 2002;1596:131-137.

[116] Huang GN, Zeng W, Kim JY, Yuan JP, Han L, Muallem S,Worley PF. STIM1 carboxyl-terminus activates native SOC, I(crac) and TRPC1 channels. Nat Cell Biol. 2006;8:1003-1010.

[117] Feske S, Gwack Y, Prakriya M, Srikanth S, Puppel SH, Tanasa B, Hogan PG, Lewis RS, Daly M,Rao A. A mutation in Orai1 causes immune deficiency by abrogating CRAC channel function. Nature. 2006;441:179-185.

[118] Peinelt C, Vig M, Koomoa DL, Beck A, Nadler MJ, Koblan-Huberson M, Lis A, Fleig A, Penner R,Kinet JP. Amplification of CRAC current by STIM1 and CRACM1 (Orai1). Nat Cell Biol. 2006;8:771-773.

[119] Vig M, Peinelt C, Beck A, Koomoa DL, Rabah D, Koblan-Huberson M, Kraft S, Turner H, Fleig A, Penner R,Kinet JP. CRACM1 is a plasma membrane protein essential for store-operated Ca2+ entry. Science. 2006;312:1220-1223.

[120] Wissenbach U, Philipp SE, Gross SA, Cavalie A,Flockerzi V. Primary structure, chromosomal localization and expression in immune cells of the murine ORAI and STIM genes. Cell Calcium. 2007;42:439-446.

[121] Prakriya M, Feske S, Gwack Y, Srikanth S, Rao A,Hogan PG. Orai1 is an essential pore subunit of the CRAC channel. Nature. 2006;443:230-233.

[122] Vig M, Beck A, Billingsley JM, Lis A, Parvez S, Peinelt C, Koomoa DL, Soboloff J, Gill DL, Fleig A, Kinet JP,Penner R. CRACM1 multimers form the ion-selective pore of the CRAC channel. Curr Biol. 2006;16:2073-2079.

[123] Yeromin AV, Zhang SL, Jiang W, Yu Y, Safrina O,Cahalan MD. Molecular identification of the CRAC channel by altered ion selectivity in a mutant of Orai. Nature. 2006;443:226-229.

[124] Lewis RS. The molecular choreography of a store-operated calcium channel. Nature. 2007;446:284-287.

[125] Luik RM, Wu MM, Buchanan J,Lewis RS. The elementary unit of store-operated Ca2+ entry: local activation of CRAC channels by STIM1 at ER-plasma membrane junctions. J Cell Biol. 2006;174:815-825.

[126] Penna A, Demuro A, Yeromin AV, Zhang SL, Safrina O, Parker I,Cahalan MD. The CRAC channel consists of a tetramer formed by Stim-induced dimerization of Orai dimers. Nature. 2008;456:116-120.

[127] Luik RM, Wang B, Prakriya M, Wu MM,Lewis RS. Oligomerization of STIM1 couples ER calcium depletion to CRAC channel activation. Nature. 2008;454:538-542.

[128] Feske S. CRAC channelopathies. Pflugers Arch. 2010;460:417-435.

[129] Rome LC. Design and function of superfast muscles: new insights into the physiology of skeletal muscle. Annu Rev Physiol. 2006;68:193-221.

[130] Kurebayashi N,Ogawa Y. Depletion of Ca2+ in the sarcoplasmic reticulum stimulates Ca2+ entry into mouse skeletal muscle fibres. J Physiol. 2001;533:185-199.

[131] Ma J,Pan Z. Junctional membrane structure and store operated calcium entry in muscle cells. Front Biosci. 2003;8:d242-255.

[132] Pan Z, Yang D, Nagaraj RY, Nosek TA, Nishi M, Takeshima H, Cheng H,Ma J. Dysfunction of store-operated calcium channel in muscle cells lacking mg29. Nat Cell Biol. 2002;4:379-383.

[133] Zhang SL, Yeromin AV, Zhang XH, Yu Y, Safrina O, Penna A, Roos J, Stauderman KA,Cahalan MD. Genome-wide RNAi screen of Ca(2+) influx identifies genes that regulate Ca(2+) release-activated Ca(2+) channel activity. Proc Natl Acad Sci U S A. 2006;103:9357-9362.

[134] Tedder TF,Schlossman SF. Phosphorylation of the B1 (CD20) molecule by normal and malignant human B lymphocytes. J Biol Chem. 1988;263:10009-10015.

[135] Einfeld DA, Brown JP, Valentine MA, Clark EA,Ledbetter JA. Molecular cloning of the human B cell CD20 receptor predicts a hydrophobic protein with multiple transmembrane domains. Embo J. 1988;7:711-717.

[136] Bubien JK, Zhou LJ, Bell PD, Frizzell RA,Tedder TF. Transfection of the CD20 cell surface molecule into ectopic cell types generates a Ca2+ conductance found constitutively in B lymphocytes. J Cell Biol. 1993;121:1121-1132.

[137] Li H, Ayer LM, Lytton J,Deans JP. Store-operated cation entry mediated by CD20 in membrane rafts. J Biol Chem. 2003;278:42427-42434.

[138] Deans JP, Li H,Polyak MJ. CD20-mediated apoptosis: signalling through lipid rafts. Immunology. 2002;107:176-182.

[139] Deans JP, Robbins SM, Polyak MJ,Savage JA. Rapid redistribution of CD20 to a low density detergent-insoluble membrane compartment. J Biol Chem. 1998;273:344-348.

[140] Li H, Ayer LM, Polyak MJ, Mutch CM, Petrie RJ, Gauthier L, Shariat N, Hendzel MJ, Shaw AR, Patel KD,Deans JP. The CD20 calcium channel is localized to microvilli and constitutively associated with membrane rafts: antibody binding increases the affinity of the association through an epitope-dependent cross-linking-independent mechanism. J Biol Chem. 2004;279:19893-19901.

[141] Launikonis BS, Barnes M,Stephenson DG. Identification of the coupling between skeletal muscle store-operated Ca2+ entry and the inositol trisphosphate receptor. Proc Natl Acad Sci U S A. 2003;100:2941-2944.

[142] Baylor SM,Hollingworth S. Sarcoplasmic reticulum calcium release compared in slow-twitch and fast-twitch fibres of mouse muscle. J Physiol. 2003;551:125-138.

[143] Launikonis BS,Rios E. Store-operated Ca2+ entry during intracellular Ca2+ release in mammalian skeletal muscle. J Physiol. 2007;583:81-97.

[144] Emery A. Muscular dystrophy--the facts. Neuromuscul Disord. 1995;5:521.

[145] Emery AE. The muscular dystrophies. Lancet. 2002;359:687-695.

[146] Briguet A, Courdier-Fruh I, Foster M, Meier T,Magyar JP. Histological parameters for the quantitative assessment of muscular dystrophy in the mdx-mouse. Neuromuscul Disord. 2004;14:675-682.

[147] Chen YW, Zhao P, Borup R,Hoffman EP. Expression profiling in the muscular dystrophies: identification of novel aspects of molecular pathophysiology. J Cell Biol. 2000;151:1321-1336.

[148] Davies KE,Nowak KJ. Molecular mechanisms of muscular dystrophies: old and new players. Nat Rev Mol Cell Biol. 2006;7:762-773.

[149] Hoffman EP,Gorospe JRM. The animal models of Duchenne muscular dystrophy: windows on the pathophysiological consequences of dystrophin deficiency. Curr Top Membr. 1991;38:113-154.

[150] Sadoulet-Puccio HM,Kunkel LM. Dystrophin and its isoforms. Brain Pathol. 1996;6:25-35.

[151] Roberts RG. Dystrophins and dystrobrevins. Genome Biol. 2001;2:REVIEWS3006.

[152] Cohn RD,Campbell KP. Molecular basis of muscular dystrophies. Muscle Nerve. 2000;23:1456-1471.

[153] Straub V,Campbell KP. Muscular dystrophies and the dystrophin-glycoprotein complex. Curr Opin Neurol. 1997;10:168-175.

[154] Davies KE, Tinsley JM,Blake DJ. Molecular analysis of Duchenne muscular dystrophy: past, present, and future. Ann N Y Acad Sci. 1995;758:287-296.

[155] Tinsley JM, Blake DJ, Pearce M, Knight AE, Kendrick-Jones J,Davies KE. Dystrophin and related proteins. Curr Opin Genet Dev. 1993;3:484-490.

[156] Love DR, Byth BC, Tinsley JM, Blake DJ,Davies KE. Dystrophin and dystrophin-related proteins: a review of protein and RNA studies. Neuromuscul Disord. 1993;3:5-21.

[157] Rando TA. The dystrophin-glycoprotein complex, cellular signaling, and the regulation of cell survival in the muscular dystrophies. Muscle Nerve. 2001;24:1575-1594.

[158] Campbell KP,Kahl SD. Association of dystrophin and an integral membrane glycoprotein. Nature. 1989;338:259-262.

[159] Culligan KG, Mackey AJ, Finn DM, Maguire PB,Ohlendieck K. Role of dystrophin isoforms and associated proteins in muscular dystrophy (review). Int J Mol Med. 1998;2:639-648.

[160] Hoffman EP,Dressman D. Molecular pathophysiology and targeted therapeutics for muscular dystrophy. Trends Pharmacol Sci. 2001;22:465-470.

[161] Michalak M,Opas M. Functions of dystrophin and dystrophin associated proteins. Curr Opin Neurol. 1997;10:436-442.

[162] Petrof BJ. Molecular pathophysiology of myofiber injury in deficiencies of the dystrophin-glycoprotein complex. Am J Phys Med Rehabil. 2002;81:S162-174.

[163] Ilsley JL, Sudol M,Winder SJ. The interaction of dystrophin with beta-dystroglycan is regulated by tyrosine phosphorylation. Cell Signal. 2001;13:625-632.

[164] Madhavan R,Jarrett HW. Calmodulin-activated phosphorylation of dystrophin. Biochemistry. 1994;33:5797-5804.

[165] Pillers DA, Bulman DE, Weleber RG, Sigesmund DA, Musarella MA, Powell BR, Murphey WH, Westall C, Panton C, Becker LE,et al. Dystrophin expression in the human retina is required for normal function as defined by electroretinography. Nat Genet. 1993;4:82-86.

[166] D'Souza VN, Nguyen TM, Morris GE, Karges W, Pillers DA,Ray PN. A novel dystrophin isoform is required for normal retinal electrophysiology. Hum Mol Genet. 1995;4:837-842.

[167] Lidov HG, Selig S,Kunkel LM. Dp140: a novel 140 kDa CNS transcript from the dystrophin locus. Hum Mol Genet. 1995;4:329-335.

[168] Byers TJ, Lidov HG,Kunkel LM. An alternative dystrophin transcript specific to peripheral nerve. Nat Genet. 1993;4:77-81.

[169] Bar S, Barnea E, Levy Z, Neuman S, Yaffe D,Nudel U. A novel product of the Duchenne muscular dystrophy gene which greatly differs from the known isoforms in its structure and tissue distribution. Biochem J. 1990;272:557-560.

[170] Austin RC, Howard PL, D'Souza VN, Klamut HJ,Ray PN. Cloning and characterization of alternatively spliced isoforms of Dp71. Hum Mol Genet. 1995;4:1475-1483.

[171] Muntoni F, Torelli S,Ferlini A. Dystrophin and mutations: one gene, several proteins, multiple phenotypes. Lancet Neurol. 2003;2:731-740.

[172] Danieli GA, Mioni F, Muller CR, Vitiello L, Mostacciuolo ML,Grimm T. Patterns of deletions of the dystrophin gene in different European populations. Hum Genet. 1993;91:342-346.

[173]

[174] Bulfield G, Siller WG, Wight PA,Moore KJ. X chromosome-linked muscular dystrophy (mdx) in the mouse. Proc Natl Acad Sci U S A. 1984;81:1189-1192.

[175] Hoffman EP, Brown RH, Jr.,Kunkel LM. Dystrophin: the protein product of the Duchenne muscular dystrophy locus. Cell. 1987;51:919-928.

[176] Gillis JM. Membrane abnormalities and Ca homeostasis in muscles of the mdx mouse, an animal model of the Duchenne muscular dystrophy: a review. Acta Physiol Scand. 1996;156:397-406.

[177] McArdle A, Edwards RH,Jackson MJ. How does dystrophin deficiency lead to muscle degeneration?--evidence from the mdx mouse. Neuromuscul Disord. 1995;5:445-456.

[178] Straub V, Rafael JA, Chamberlain JS,Campbell KP. Animal models for muscular dystrophy show different patterns of sarcolemmal disruption. J Cell Biol. 1997;139:375-385.

[179] Bodensteiner JB,Engel AG. Intracellular calcium accumulation in Duchenne dystrophy and other myopathies: a study of 567,000 muscle fibers in 114 biopsies. Neurology. 1978;28:439-446.

[180] Jackson MJ, Jones DA,Edwards RH. Measurements of calcium and other elements in muscle biopsy samples from patients with Duchenne muscular dystrophy. Clin Chim Acta. 1985;147:215-221.

[181] Glesby MJ, Rosenmann E, Nylen EG,Wrogemann K. Serum CK, calcium, magnesium, and oxidative phosphorylation in mdx mouse muscular dystrophy. Muscle Nerve. 1988;11:852-856.

[182] Fong PY, Turner PR, Denetclaw WF,Steinhardt RA. Increased activity of calcium leak channels in myotubes of Duchenne human and mdx mouse origin. Science. 1990;250:673-676.

[183] Hopf FW, Turner PR, Denetclaw WF, Jr., Reddy P,Steinhardt RA. A critical evaluation of resting intracellular free calcium regulation in dystrophic mdx muscle. Am J Physiol. 1996;271:C1325-1339.

[184] Mongini T, Ghigo D, Doriguzzi C, Bussolino F, Pescarmona G, Pollo B, Schiffer D,Bosia A. Free cytoplasmic Ca++ at rest and after cholinergic stimulus is increased in cultured muscle cells from Duchenne muscular dystrophy patients. Neurology. 1988;38:476-480.

[185] Turner PR, Westwood T, Regen CM,Steinhardt RA. Increased protein degradation results from elevated free calcium levels found in muscle from mdx mice. Nature. 1988;335:735-738.

[186] Pressmar J, Brinkmeier H, Seewald MJ, Naumann T,Rudel R. Intracellular Ca2+ concentrations are not elevated in resting cultured muscle from Duchenne (DMD) patients and in MDX mouse muscle fibres. Pflugers Arch. 1994;426:499-505.

[187] Rivet-Bastide M, Imbert N, Cognard C, Duport G, Rideau Y,Raymond G. Changes in cytosolic resting ionized calcium level and in calcium transients during in vitro development of normal and Duchenne muscular dystrophy cultured skeletal muscle measured by laser cytofluorimetry using indo-1. Cell Calcium. 1993;14:563-571.

[188] Gailly P, Boland B, Himpens B, Casteels R,Gillis JM. Critical evaluation of cytosolic calcium determination in resting muscle fibres from normal and dystrophic (mdx) mice. Cell Calcium. 1993;14:473-483.

[189] Head SI. Membrane potential, resting calcium and calcium transients in isolated muscle fibres from normal and dystrophic mice. J Physiol. 1993;469:11-19.

[190] Leijendekker WJ, Passaquin AC, Metzinger L,Ruegg UT. Regulation of cytosolic calcium in skeletal muscle cells of the mdx mouse under conditions of stress. Br J Pharmacol. 1996;118:611-616.

[191] Imbert N, Vandebrouck C, Constantin B, Duport G, Guillou C, Cognard C,Raymond G. Hypoosmotic shocks induce elevation of resting calcium level in Duchenne muscular dystrophy myotubes contracting in vitro. Neuromuscul Disord. 1996;6:351-360.

[192] Tutdibi O, Brinkmeier H, Rudel R,Fohr KJ. Increased calcium entry into dystrophin-deficient muscle fibres of MDX and ADR-MDX mice is reduced by ion channel blockers. J Physiol. 1999;515 (Pt 3):859-868.

[193] Florence JM, Fox PT, Planer GJ,Brooke MH. Activity, creatine kinase, and myoglobin in Duchenne muscular dystrophy: a clue to etiology? Neurology. 1985;35:758-761.

[194] Zellweger H, Durnin R,Simpson J. The diagnostic significance of serum enzymes and electrocardiogram in various muscular dystrophies. Acta Neurol Scand. 1972;48:87-101.

[195] McArdle A, Edwards RH,Jackson MJ. Time course of changes in plasma membrane permeability in the dystrophin-deficient mdx mouse. Muscle Nerve. 1994;17:1378-1384.

[196] Jockusch H, Reininghaus J, Stuhlfauth I,Zippel M. Reduction of myosin-light-chain phosphorylation and of parvalbumin content in myotonic mouse muscle and its reversal by tocainide. Eur J Biochem. 1988;171:101-105.

[197] Menke A,Jockusch H. Decreased osmotic stability of dystrophin-less muscle cells from the mdx mouse. Nature. 1991;349:69-71.

[198] Menke A,Jockusch H. Extent of shock-induced membrane leakage in human and mouse myotubes depends on dystrophin. J Cell Sci. 1995;108 (Pt 2):727-733.

[199] Petrof BJ, Shrager JB, Stedman HH, Kelly AM,Sweeney HL. Dystrophin protects the sarcolemma from stresses developed during muscle contraction. Proc Natl Acad Sci U S A. 1993;90:3710-3714.

[200] Matsuda R, Nishikawa A,Tanaka H. Visualization of dystrophic muscle fibers in mdx mouse by vital staining with Evans blue: evidence of apoptosis in dystrophin-deficient muscle. J Biochem. 1995;118:959-964.

[201] Salamino F, Sparatore B, Melloni E, Michetti M, Viotti PL, Pontremoli S,Carafoli E. The plasma membrane calcium pump is the preferred calpain substrate within the erythrocyte. Cell Calcium. 1994;15:28-35.

[202] Kumamoto T, Ueyama H, Watanabe S, Yoshioka K, Miike T, Goll DE, Ando M,Tsuda T. Immunohistochemical study of calpain and its endogenous inhibitor in the skeletal muscle of muscular dystrophy. Acta Neuropathol. 1995;89:399-403.

[203] Lucas-Heron B, Le Ray B,Schmitt N. Does calmitine, a protein specific for the mitochondrial matrix of skeletal muscle, play a key role in mitochondrial function? FEBS Lett. 1995;374:309-311.

[204] Wrogemann K,Pena SD. Mitochondrial calcium overload: A general mechanism for cell-necrosis in muscle diseases. Lancet. 1976;1:672-674.

[205] Gannoun-Zaki L, Fournier-Bidoz S, Le Cam G, Chambon C, Millasseau P, Leger JJ,Dechesne CA. Down-regulation of mitochondrial mRNAs in the mdx mouse model for Duchenne muscular dystrophy. FEBS Lett. 1995;375:268-272.

[206] Turner PR, Schultz R, Ganguly B,Steinhardt RA. Proteolysis results in altered leak channel kinetics and elevated free calcium in mdx muscle. J Membr Biol. 1993;133:243-251.

[207] Stiber J, Hawkins A, Zhang ZS, Wang S, Burch J, Graham V, Ward CC, Seth M, Finch E, Malouf N, Williams RS, Eu JP,Rosenberg P. STIM1 signalling controls store-operated calcium entry required for development and contractile function in skeletal muscle. Nat Cell Biol. 2008;10:688-697.

[208] Bergmeier W, Oh-Hora M, McCarl CA, Roden RC, Bray PF,Feske S. R93W mutation in Orai1 causes impaired calcium influx in platelets. Blood. 2009;113:675-678.

[209] McCarl CA, Picard C, Khalil S, Kawasaki T, Rother J, Papolos A, Kutok J, Hivroz C, Ledeist F, Plogmann K, Ehl S, Notheis G, Albert MH, Belohradsky BH, Kirschner J, Rao A, Fischer A,Feske S. ORAI1 deficiency and lack of store-operated Ca2+ entry cause immunodeficiency, myopathy, and ectodermal dysplasia. J Allergy Clin Immunol. 2009;124:1311-1318 e1317.

[210] Partiseti M, Le Deist F, Hivroz C, Fischer A, Korn H,Choquet D. The calcium current activated by T cell receptor and store depletion in human lymphocytes is absent in a primary immunodeficiency. J Biol Chem. 1994;269:32327-32335.

[211] Picard C, McCarl CA, Papolos A, Khalil S, Luthy K, Hivroz C, LeDeist F, Rieux-Laucat F, Rechavi G, Rao A, Fischer A,Feske S. STIM1 mutation associated with a syndrome of immunodeficiency and autoimmunity. N Engl J Med. 2009;360:1971-1980.

[212] Gwack Y, Srikanth S, Oh-Hora M, Hogan PG, Lamperti ED, Yamashita M, Gelinas C, Neems DS, Sasaki Y, Feske S, Prakriya M, Rajewsky K,Rao A. Hair loss and defective T- and B-cell function in mice lacking ORAI1. Mol Cell Biol. 2008;28:5209-5222.

[213] Vig M, DeHaven WI, Bird GS, Billingsley JM, Wang H, Rao PE, Hutchings AB, Jouvin MH, Putney JW,Kinet JP. Defective mast cell effector functions in mice lacking the CRACM1 pore subunit of store-operated calcium release-activated calcium channels. Nat Immunol. 2008;9:89-96.

[214] Williams RT, Manji SS, Parker NJ, Hancock MS, Van Stekelenburg L, Eid JP, Senior PV, Kazenwadel JS, Shandala T, Saint R, Smith PJ,Dziadek MA. Identification and characterization of the STIM (stromal interaction molecule) gene family: coding for a novel class of transmembrane proteins. Biochem J. 2001;357:673-685.

[215] Lowry OH, Rosebrough NJ, Farr AL,Randall RJ. Protein measurement with the Folin phenol reagent. J Biol Chem. 1951;193:265-275.

[216] Grynkiewicz G, Poenie M,Tsien RY. A new generation of Ca2+ indicators with greatly improved fluorescence properties. J Biol Chem. 1985;260:3440-3450.

[217] Perryman LE,Torbeck RL. Combined immunodeficiency of Arabian horses: confirmation of autosomal recessive mode of inheritance. J Am Vet Med Assoc. 1980;176:1250-1251.

[218] Schuler W, Weiler IJ, Schuler A, Phillips RA, Rosenberg N, Mak TW, Kearney JF, Perry RP,Bosma MJ. Rearrangement of antigen receptor genes is defective in mice with severe combined immune deficiency. Cell. 1986;46:963-972.

[219] Severson DL, Drummond GI,Sulakhe PV. Adenylate cyclase in skeletal muscle. Kinetic properties and hormonal stimulation. J Biol Chem. 1972;247:2949-2958.

[220] Benchaouir R, Meregalli M, Farini A, D'Antona G, Belicchi M, Goyenvalle A, Battistelli M, Bresolin N, Bottinelli R, Garcia L,Torrente Y. Restoration of human dystrophin following transplantation of exon-skipping-engineered DMD patient stem cells into dystrophic mice. Cell Stem Cell. 2007;1:646-657.

[221] Genot EM, Meier KE, Licciardi KA, Ahn NG, Uittenbogaart CH, Wietzerbin J, Clark EA,Valentine MA. Phosphorylation of CD20 in cells from a hairy cell leukemia cell line. Evidence for involvement of calcium/calmodulin-dependent protein kinase II. J Immunol. 1993;151:71-82.

[222] Valentine MA, Licciardi KA, Clark EA, Krebs EG,Meier KE. Insulin regulates serine/threonine phosphorylation in activated human B lymphocytes. J Immunol. 1993;150:96-105.

[223] Valentine MA, Meier KE, Rossie S,Clark EA. Phosphorylation of the CD20 phosphoprotein in resting B lymphocytes. Regulation by protein kinase C. J Biol Chem. 1989;264:11282-11287.

[224] Deans JP, Kalt L, Ledbetter JA, Schieven GL, Bolen JB,Johnson P. Association of 75/80-kDa phosphoproteins and the tyrosine kinases Lyn, Fyn, and Lck with the B cell molecule CD20. Evidence against involvement of the cytoplasmic regions of CD20. J Biol Chem. 1995;270:22632-22638.

[225] Deans JP, Schieven GL, Shu GL, Valentine MA, Gilliland LA, Aruffo A, Clark EA,Ledbetter JA. Association of tyrosine and serine kinases with the B cell surface antigen CD20. Induction via CD20 of tyrosine phosphorylation and activation of phospholipase C-gamma 1 and PLC phospholipase C-gamma 2. J Immunol. 1993;151:4494-4504.

[226] Yamanashi Y, Fukui Y, Wongsasant B, Kinoshita Y, Ichimori Y, Toyoshima K,Yamamoto T. Activation of Src-like protein-tyrosine kinase Lyn and its association with phosphatidylinositol 3-kinase upon B-cell antigen receptor-mediated signaling. Proc Natl Acad Sci U S A. 1992;89:1118-1122.

[227] Schuler F,Sorokin LM. Expression of laminin isoforms in mouse myogenic cells in vitro and in vivo. J Cell Sci. 1995;108 (Pt 12):3795-3805.

[228] Clark EA,Shu G. Activation of human B cell proliferation through surface Bp35 (CD20) polypeptides or immunoglobulin receptors. J Immunol. 1987;138:720-725.

[229] Tedder TF,Engel P. CD20: a regulator of cell-cycle progression of B lymphocytes. Immunol Today. 1994;15:450-454.

[230] Maloney DG, Grillo-Lopez AJ, White CA, Bodkin D, Schilder RJ, Neidhart JA, Janakiraman N, Foon KA, Liles TM, Dallaire BK, Wey K, Royston I, Davis T,Levy R. IDEC-C2B8 (Rituximab) anti-CD20 monoclonal antibody therapy in patients with relapsed low-grade non-Hodgkin's lymphoma. Blood. 1997;90:2188-2195.

[231] McLaughlin P, White CA, Grillo-Lopez AJ,Maloney DG. Clinical status and optimal use of rituximab for B-cell lymphomas. Oncology (Williston Park). 1998;12:1763-1769; discussion 1769-1770, 1775-1767.

[232] Onrust SV, Lamb HM,Balfour JA. Rituximab. Drugs. 1999;58:79-88; discussion 89-90.

[233] Reff ME, Carner K, Chambers KS, Chinn PC, Leonard JE, Raab R, Newman RA, Hanna N,Anderson DR. Depletion of B cells in vivo by a chimeric mouse human monoclonal antibody to CD20. Blood. 1994;83:435-445.

[234] Shan D, Ledbetter JA,Press OW. Apoptosis of malignant human B cells by ligation of CD20 with monoclonal antibodies. Blood. 1998;91:1644-1652.

[235] Kanzaki M, Nie L, Shibata H,Kojima I. Activation of a calcium-permeable cation channel CD20 expressed in Balb/c 3T3 cells by insulin-like growth factor-I. J Biol Chem. 1997;272:4964-4969.

[236] Kanzaki M, Shibata H, Mogami H,Kojima I. Expression of calcium-permeable cation channel CD20 accelerates progression through the G1 phase in Balb/c 3T3 cells. J Biol Chem. 1995;270:13099-13104.

[237] Carafoli E. Calcium signaling: a tale for all seasons. Proc Natl Acad Sci U S A. 2002;99:1115-1122.

[238] Alderton JM,Steinhardt RA. Calcium influx through calcium leak channels is responsible for the elevated levels of calcium-dependent proteolysis in dystrophic myotubes. J Biol Chem. 2000;275:9452-9460.

[239] Bertorini TE, Bhattacharya SK, Palmieri GM, Chesney CM, Pifer D,Baker B. Muscle calcium and magnesium content in Duchenne muscular dystrophy. Neurology. 1982;32:1088-1092.

[240] Turner PR, Fong PY, Denetclaw WF,Steinhardt RA. Increased calcium influx in dystrophic muscle. J Cell Biol. 1991;115:1701-1712.

[241] Watkins SC, Hoffman EP, Slayter HS,Kunkel LM. Immunoelectron microscopic localization of dystrophin in myofibres. Nature. 1988;333:863-866.

[242] Brdicka T, Pavlistova D, Leo A, Bruyns E, Korinek V, Angelisova P, Scherer J, Shevchenko A, Hilgert I, Cerny J, Drbal K, Kuramitsu Y, Kornacker B, Horejsi V,Schraven B. Phosphoprotein associated with glycosphingolipid-enriched microdomains (PAG), a novel ubiquitously expressed transmembrane adaptor protein, binds the protein tyrosine kinase csk and is involved in regulation of T cell activation. J Exp Med. 2000;191:1591-1604.

[243] Kawabuchi M, Satomi Y, Takao T, Shimonishi Y, Nada S, Nagai K, Tarakhovsky A,Okada M. Transmembrane phosphoprotein Cbp regulates the activities of Src-family tyrosine kinases. Nature. 2000;404:999-1003.

[244] Moizard MP, Billard C, Toutain A, Berret F, Marmin N,Moraine C. Are Dp71 and Dp140 brain dystrophin isoforms related to cognitive impairment in Duchenne muscular dystrophy? Am J Med Genet. 1998;80:32-41.

[245] Culligan K, Glover L, Dowling P,Ohlendieck K. Brain dystrophin-glycoprotein complex: persistent expression of beta-dystroglycan, impaired oligomerization of Dp71 and up-regulation of utrophins in animal models of muscular dystrophy. BMC Cell Biol. 2001;2:2.

[246] Nico B, Paola Nicchia G, Frigeri A, Corsi P, Mangieri D, Ribatti D, Svelto M,Roncali L. Altered blood-brain barrier development in dystrophic MDX mice. Neuroscience. 2004;125:921-935.

[247] Rapaport D, Greenberg DS, Tal M, Yaffe D,Nudel U. Dp71, the nonmuscle product of the Duchenne muscular dystrophy gene is associated with the cell membrane. FEBS Lett. 1993;328:197-202.

[248] Austin RC, Fox JE, Werstuck GH, Stafford AR, Bulman DE, Dally GY, Ackerley CA, Weitz JI,Ray PN. Identification of Dp71 isoforms in the platelet membrane cytoskeleton. Potential role in thrombin-mediated platelet adhesion. J Biol Chem. 2002;277:47106-47113.

[249] Connors NC,Kofuji P. Dystrophin Dp71 is critical for the clustered localization of potassium channels in retinal glial cells. J Neurosci. 2002;22:4321-4327.

[250] Marchand E, Constantin B, Balghi H, Claudepierre MC, Cantereau A, Magaud C, Mouzou A, Raymond G, Braun S,Cognard C. Improvement of calcium handling and changes in calcium-release properties after mini- or full-length dystrophin forced expression in cultured skeletal myotubes. Exp Cell Res. 2004;297:363-379.

[251] Stashenko P, Nadler LM, Hardy R,Schlossman SF. Expression of cell surface markers after human B lymphocyte activation. Proc Natl Acad Sci U S A. 1981;78:3848-3852.

[252] Tedder TF, Boyd AW, Freedman AS, Nadler LM,Schlossman SF. The B cell surface molecule B1 is functionally linked with B cell activation and differentiation. J Immunol. 1985;135:973-979.

[253] Lyfenko AD,Dirksen RT. Differential dependence of store-operated and excitation-coupled Ca2+ entry in skeletal muscle on STIM1 and Orai1. J Physiol. 2008;586:4815-4824.

[254] Dirksen RT. Checking your SOCCs and feet: the molecular mechanisms of Ca2+ entry in skeletal muscle. J Physiol. 2009;587:3139-3147.

[255] Hopf FW, Reddy P, Hong J,Steinhardt RA. A capacitative calcium current in cultured skeletal muscle cells is mediated by the calcium-specific leak channel and inhibited by dihydropyridine compounds. J Biol Chem. 1996;271:22358-22367.

[256] Ju YK, Wu MJ, Chaulet H, Marciniec T, Graham RM,Allen DG. IGF-1 enhances a store-operated Ca2+ channel in skeletal muscle myoblasts: involvement of a CD20-like protein. J Cell Physiol. 2003;197:53-60.

[257] Janas E, Priest R, Wilde JI, White JH,Malhotra R. Rituxan (anti-CD20 antibody)-induced translocation of CD20 into lipid rafts is crucial for calcium influx and apoptosis. Clin Exp Immunol. 2005;139:439-446.

[258] Shan D, Ledbetter JA,Press OW. Signaling events involved in anti-CD20-induced apoptosis of malignant human B cells. Cancer Immunol Immunother. 2000;48:673-683.

[259] Walshe CA, Beers SA, French RR, Chan CH, Johnson PW, Packham GK, Glennie MJ,Cragg MS. Induction of cytosolic calcium flux by CD20 is dependent upon B Cell antigen receptor signaling. J Biol Chem. 2008;283:16971-16984.